Institut für Technische Chemie
der Technischen Universität München
Lehrstuhl II

Reaction Mechanism and Deactivation Pathways in Zeolite catalyzed Isobutane/2-Butene Alkylation

Andreas Feller

Vollständiger Abdruck der von der Fakultät für Chemie der Technischen Universität München zur Erlangung des akademischen Grades eines

Doktors der Naturwissenschaften

genehmigten Dissertation.

Vorsitzender: Univ.-Prof. (Komm.) Dr. Walter Nitsch, em.

Prüfer der Dissertation:

1. Univ.-Prof. Dr. Johannes A. Lercher
2. Univ.-Prof. Dr. Thomas Bein, Ludwig-Maximilians-Universität München
3. Univ.-Prof. Dr. Klaus Köhler

Die Dissertation wurde am 27.11.2002 bei der Technischen Universität München eingereicht und durch die Fakultät für Chemie am 17.01.2003 angenommen.

Thank you!

The experimental work of this dissertation was carried out in the time span from January 99 until July 2002 at the Institut für Technische Chemie, Lehrstuhl II under the supervision of Prof. Johannes A. Lercher.

I am very much indebted to Johannes for trusting me with this important project, for making things possible that otherwise would have been impossible, for giving us the chance to meet a lot of scientists from all over the world, and for fruitful discussions (scientific and political). I learned a lot in this time; to not blame circumstances being not the least of it.

I am grateful for the funding by Süd-Chemie AG via the EUROFUEL project, and also for preparing and supplying of catalyst samples by Marcus Breuninger.

I'd like to say thank you to the Twente-crew, who gave me a warm welcome, especially Gautam, who introduced me into the secrets (and "Voodoo") of alkylation.
Thank you to Cristina and Hilton, my friends of the early München days; it was great fun to share the office with you!
Thanks to Stefan for performing the diploma thesis in a tough period of the project.
Thank you Alex and Iker, you helped me a lot and you introduced Spanish/Colombian rhythm into the alkylation group.
Thank you to all my colleagues, Bavarian, German and from the "rest of the world". It has been a great experience to meet people from all over the world. I enjoyed being with you.
Thank you to the technical crew, Martin, Andreas and Xaver; without you, no setup in this group would work!

Danke an Annette, Denise und Agnes für das Aushalten meiner Launen während der Höhen und Tiefen dieser Zeit.

Danke Marzena für Dein Da sein.

1 General introduction

Alkylation of iso-butane with C_3-C_5 alkenes in the presence of strong acids leads to the formation of a complex mixture of branched alkanes, called alkylate, which is an excellent blending component for gasoline. Alkylate has a high octane number, low Reid vapor pressure (RVP) and it is free of aromatics, alkenes and contains nearly no sulfur. The clean air regulations in the E.U. and the U.S.A., concerning the contents of alkenes, sulfur and aromatics, particularly benzene, in the gasoline will become increasingly strict. Table 1-1 gives a summary about important reformulated gasoline (RFG) specifications. Regarding these specifications, it is obvious that alkylate is an ideal component of RFG.

Table 1-1: Development of RFG specifications in the European Union.

	1999	2000	2005
Sulfur, max. ppm wt.	500	150	50 (10)*
Aromatics, max. vol.%	No spec.	42	35
Benzene, max. vol.%	5	1	1
Alkenes, max. vol.%	No spec.	18	18
Octane, RON min	95/98	95/98	95/98
RVP, max. kPa	80	60	60

* Potentially to be available in 2005, possibly mandatory in 2007/2008

Refiners have the choice of blending different product streams to meet the specifications. This is shown exemplary for sulfur in Table 1-2. Concerning the sulfur contents, reformate would be an ideal blendstock, however, it contains mainly aromatic compounds; therefore its usage cannot be considerably increased. Methyl-tertiary-butyl ether (MTBE), which is a high octane oxygenate, has been found to cause drinking water to be malodorous already in ppb concentrations (leaking out from underground storage tanks into the ground water). As a consequence, it will be phased out in several countries (1). Alcohols such as ethanol that could conceivably replace the ethers as oxygenate source suffer from a very high blending vapor pressure when mixed into gasoline, thus, limiting their usefulness. The only way to

clean-burning, high-octane gasoline with no limitations imposed by the specifications is to utilize branched alkanes.

Table 1-2: Sulfur sources in gasoline.

Blending component	Sulfur, ppm	Typical % of Gasoline	% Contribution to sulfur
FCC Gasoline	800	30-50	90
LSR Gasoline	150	3	5
Alkylate	16	10	2
MTBE	20	5	1
Butanes	10	5	<1
Reformate	0	20-40	0
Isomerate	3	5	<1

Three ways to produce isoalkanes are currently employed: (i) Isomerization of n-pentane and n-hexane from crude distillation (light straight run, LSR) to the corresponding isoalkanes (RON ca. 80). (ii) Dimerization plus hydrogenation (sometimes also called indirect alkylation), which converts isobutene to trimethylpentanes (RON 100). In case of mixed butene feed (which is the typical situation) octane numbers are substantially lower (RON ca. 80) due to production of lower value dimethylhexanes. (iii) Alkylation of C_3-C_5 alkenes with isobutane to give C_5-C_{12} isoalkanes with a RON of 92-96. Isomerization and alkylation are key processes to upgrade gasoline feedstock, while dimerization most likely will be limited to special refinery scenarios. Due to the moderate RON and relatively high RVP of isomerate, alkylate is superior. Therefore, it is expected, that the demand for alkylation catalysts will increase by 5%/year up to the year 2003, with an estimated total catalyst value for 2003 of 340 million $ (2). The worldwide installed alkylation production capacity as of the end of 2001 was approx. 74 million tons/year (3).

The alkylation unit is situated down-stream of the fluid catalytic cracking units (FCCU). The C_4 cut from the FCCU contains linear butenes, isobutene, n-butane and iso-butane. In some refineries, the isobutene is converted with methanol to MTBE. A typical modern refinery flow-scheme showing the position of the alkylation together with an acid

regeneration unit is displayed in Figure 1-1.

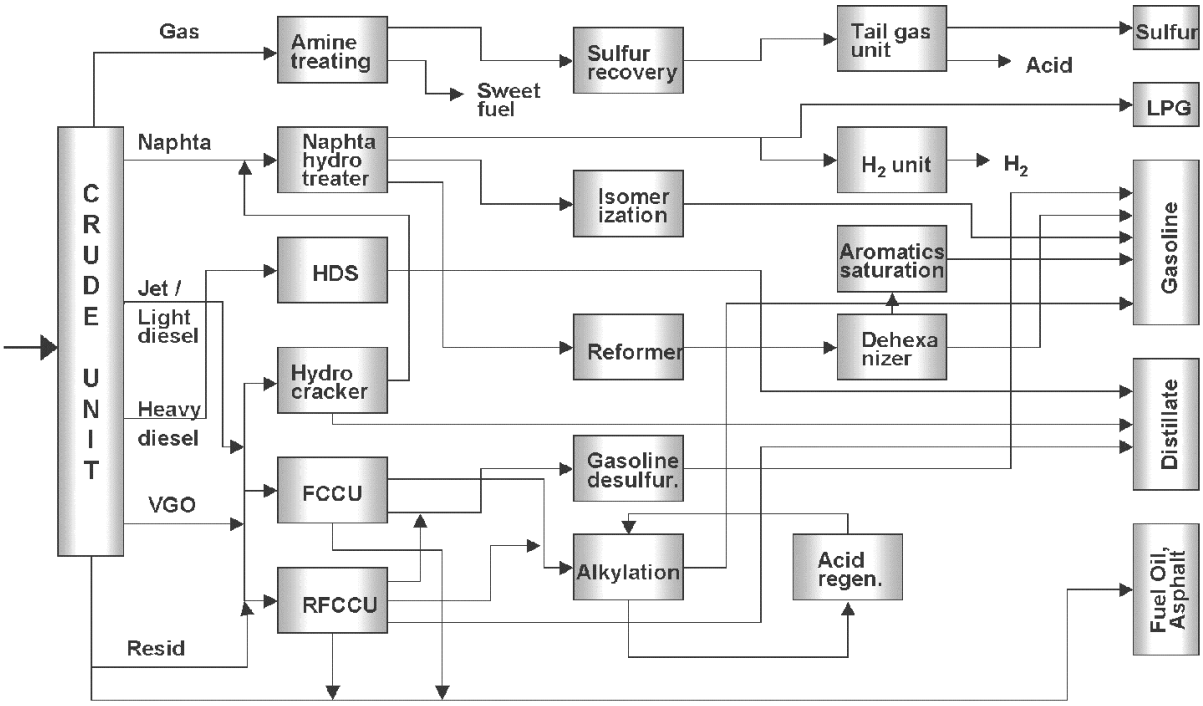

Figure 1-1: Process units in a modern refinery.

While the products from alkylation are perfect gasoline components, the catalysts are far from being ideal. The only catalysts industrially employed are sulfuric and anhydrous hydrofluoric acid. Both acids are toxic and corrosive, with HF being the substantially more dangerous compound due to its high volatility. Sulfuric acid processes mainly suffer from a high acid consumption. Numerous alternative catalysts, most of them solid acids, have been examined. The main obstacle, which has to be overcome for a successful competitive process, is the rapid catalyst deactivation. A considerable number of research projects in industry and academia are focused on this set of problems.

1.1 Scope of this thesis

Since 1995, zeolite catalyzed isobutane/butene alkylation is a research topic in Prof. Lercher's group. Started at the University Twente, a CSTR-type slurry reactor was build, which allows studying the alkylation reaction under industrially relevant conditions with a relatively slow deactivation rate. Initial mechanistic studies were performed on zeolite H-

BEA (4-6). From both industrial and scientific viewpoints however, faujasites are materials that are more attractive. They are less expensive as BEA and they potentially contain more acid sites due to a higher aluminum content in the framework. Therefore, the studies presented in this thesis were carried out with faujasites. Some of the results are compared to data obtained with zeolite BEA.

Alkylation on liquid and solid acids has been reviewed in the past by Corma and Martinez (7) and by Weitkamp and Traa (8). A substantial number of contributions regarding the chemistry and technology of alkylation have been published since the time the two reviews were published in 1993 and 1997, respectively. Therefore, a state of the art review combining the recent findings with older information was seen necessary for successful research. In Chapter 2 of this thesis, an up to date and in-depth overview about alkylation on both liquid and solid acids is given. Special attention is paid to the mechanism and the physico-chemical properties of the individual acids; from them the way in which reaction parameters influence the catalytic performance is deduced. In a final section, existing processes and new developments are briefly described.

Among the solid acids having the potential to replace sulfuric and hydrofluoric acid as alkylation catalysts, large pore zeolites are prominent. They were the first materials to be tested and at least one of the newly developed processes is based on a zeolitic catalyst. Zeolite acidity cannot be expressed by a simple number; acidic zeolites contain both Lewis and Brønsted acid sites with a wide distribution of strength, the impact of which on the alkylation mechanism still remained to be clarified. Therefore, the influence of the acidity on the alkylation performance has been examined with a range of faujasitic zeolites exhibiting a wide distribution of acid site densities and acid strengths. Furthermore, typical reaction parameters were varied in order to shed some light on their influence on the reaction mechanism. The results of this study are compiled in Chapter 3.

Due to the relatively high costs of zeolitic catalysts (compared to the commodity chemical sulfuric acid), a regeneration of deactivated catalysts in a future zeolite based alkylation process is indispensable. It is of vital importance for both successful regeneration and prolonged single cycle operation to understand the principles underlying the routes to catalyst deactivation. Only little and contradicting data about this topic is available. In Chapter 4 a detailed study on the characterization of deactivated zeolitic alkylation catalysts and of the free deposits recovered from these catalysts is presented.

1.2 References

1. Anonymous, *Oil Gas J.* **98 (13)** (2000).
2. Anonymous, *Oil Gas J.* **98 (9)** (2000).
3. Stell, J., *Oil Gas J.* **99 (52)**, 74 (2001).
4. Nivarthy, G. S., Feller, A., Seshan, K., and Lercher, J. A., *Microp. Mesop. Mater.* **35-36**, 75 (2000).
5. Nivarthy, G. S., Seshan, K., and Lercher, J. A., *Microp. & Mesop. Mater.* **22**, 379 (1998).
6. Nivarthy, G. S., He, Y., Seshan, K., and Lercher, J. A., *J. Catal.* **176**, 192 (1998).
7. Corma, A. and Martinez, A., *Catal. Rev.-Sci. Eng.* **35**, 483 (1993).
8. Weitkamp, J. and Traa, Y., *in* "Handbook of Heterogeneous Catalysis" (G. Ertl, H. Knözinger, and J. Weitkamp, Eds.), Vol. 4, p. 2039. VCH, Weinheim, 1997.

Chapter 2

The chemistry and technology of liquid and solid acid catalyzed isobutane/alkene alkylation

Abstract

This chapter gives an in depth review about chemical and technological aspects of the alkylation of iso-butane with light alkenes. Special attention is paid to the mechanism, which is operative with both liquid and solid acid catalysts. The differences in importance of the individual mechanistic steps are discussed in terms of the physico-chemical properties of the specific catalysts. The impact of important process parameters on the alkylation performance is derived from the mechanism. In a final section, the established industrial processes based on liquid acids and recent process developments based on solid acids are briefly described.

2.1 **Introduction**

In the 1930s, Ipatieff's group at UOP discovered that iso-alkanes react with alkenes in the presence of strong acids to give saturated hydrocarbons under relatively mild conditions. The initially tested acids were $AlCl_3$/HCl and BF_3/HF (1). Soon, the first processes were commercialized (2). The early alkylation plants utilized sulfuric acid, but the need for high-octane aviation gasoline spurred by World War II led to the construction of plants based on HF as catalyst, which are more flexible regarding the feed alkenes. The first HF alkylation process units were built 1942 by Phillips as wartime emergency units (3). The importance of alkylate steeply increased then. The daily production of alkylate at that time reached 5 million gallons, during the Korean War in 1952 it was already 14 million gallons and in the beginning of the 1980's, with the lead phase-out in the US, the estimated daily production amounted to 50 million gallons (4). Between the 1960s to around 1986, the relative importance of plants using HF increased as compared with those using H_2SO_4 (5). Nowadays, nearly equal amounts of alkylate are produced on a worldwide basis by each of the sulfuric acid and hydrofluoric acid catalyzed processes (6).

Both of these materials suffer from certain drawbacks. Anhydrous hydrofluoric acid is a corrosive and highly toxic liquid with a boiling point close to room temperature. Tests in the Nevada desert showed that, if released into the atmosphere, HF forms stable aerosols, which drift downwind on ground level for several kilometers. In 1987, the accidental release of gaseous HF in Texas City resulted in emergency treatment for several hundred people (7). For that reason, refineries with HF alkylation plants are under pressure to install expensive mitigation systems minimizing the dangers of HF leaks. Moreover, authorities in many industrialized countries cease to license new HF alkylation plants.

Sulfuric acid also is a corrosive liquid but not volatile, making its handling easier. Its major disadvantage is the high acid consumption, which can be as high as 70-100 kg acid / ton alkylate. The spent acid contains water and heavy hydrocarbons and has to be regenerated, usually by burning. The cost of such a regenerated acid is about two to three times the market price for sulfuric acid (8). About one third of the total operating costs of alkylation units using H_2SO_4 can be attributed to acid consumption (9). The sulfuric acid catalyzed process is more sensitive towards the fed alkenes; C_3 and C_5 alkenes generally lead to higher acid consumption and lower octane numbers (10). Equipment corrosion, transport and handling hazards and environmental liability associated with the disposal of spent acid

are disadvantages of both processes.

For more than 30 years now, these problems are the driving force for research in industry and academia to find suitable replacements for the existing liquid acid catalysts. Zeolites, being noncorrosive, nontoxic, and rather inexpensive, seemed to be promising candidates, especially after they were successfully installed as cracking catalysts. In the late 1960's two groups, Garwood and Venuto of Mobil Oil (11) and Kirsch, Potts and Barmby of Sun Oil (12) did pioneering work on rare earth exchanged faujasitic zeolites. Later, other zeolites were also examined. In general, all large pore zeolites are active alkylation catalysts, with product distributions similar to those of the liquid acids, but their unacceptably rapid deactivation was and still is the obstacle to commercialization.

Other materials studied are sulfated zirconia, Brønsted and Lewis acids promoted on various supports, heteropolyacids and organic resins, both supported and unsupported. On the whole, these materials also deactivate rapidly and some of them additionally exhibit environmental and health hazards.

The technology and chemistry of isoalkane-alkene alkylation has been thoroughly reviewed in the past for both liquid and solid acid catalysts (13) and for solid acid catalysts alone (14). The intention of this review is to give an up to date overview about the alkylation reaction with both liquid and solid acids as catalysts. Focus will be on the similarities and differences between the liquid acid catalysts on the one side and solid acid catalysts, especially zeolites, on the other. In this way, the reaction mechanism, the physical properties of the individual catalysts and the consequences of these factors for a successful operation will be reviewed. In a final section, an overview on existing processes and on new process developments utilizing solid acids will be given.

2.2 Alkylation mechanism

Since the discovery of alkylation, the elucidation of its mechanism attracted great interest. The early findings are connected to Schmerling (15-17), who successfully applied a carbenium ion mechanism with a set of consecutive and simultaneous reaction steps to describe the observed reaction kinetics. Later, most of the mechanistic information on sulfuric acid catalyzed processes was provided by Albright. Much less information is available on hydrofluoric acid as catalyst. In the following, a consolidated view on the alkylation mechanism will be discussed. Similarities and dissimilarities between zeolites as

representatives of solid acid alkylation catalysts and HF and H_2SO_4 as liquid catalysts will be highlighted. Experimental data will be compared with quantum-chemical calculations of the individual reaction steps in different media.

2.2.1 Overall product distribution

Table 2-1 gives the composition of alkylates produced with different acidic catalysts. It can be seen that the product distribution is similar within a variety of acidic catalysts, both solid and liquid, and over a wide range of process conditions. Typically, alkylate is a mixture of methyl-branched alkanes with a high fraction of isooctanes. Almost all the compounds have tertiary carbon atoms; only very few exhibit quaternary carbon atoms or are non-branched. Alkylate does not only contain the primary products, trimethylpentanes, but also dimethylhexanes, sometimes methylheptanes and a considerable amount of isopentane, isohexanes, isoheptanes and hydrocarbons with nine and more carbon atoms. The complexity of the product illustrates that no simple and straightforward single step mechanism is operative, but a set of parallel and consecutive reaction steps, with the importance of the individual steps markedly differing between catalysts. To arrive at this complex product distribution from two simple molecules such as iso-butane and butene, reaction steps like isomerization, oligomerization, β-scission and hydride transfer have to be involved.

Table 2-1: RON values for various alkanes and the C_{5+} composition of iso-butane/butene alkylates produced with different acids in lab scale/pilot-plant scale reactors. Taken from references (18) for H_2SO_4, (19) for HF, (20) for sulfated zirconia, RE-FAU unpublished data

Component (wt.-%)	Research Octane Number	H_2SO_4 T = -15°C P/O = 5	HF T = ? P/O = 12	RE-FAU T = 75°C P/O = 7	Sulfated Zirconia T = 2°C P/O = 15
Isopentane	93.0	1.2	1.8	6.8	24.0
n-Pentane	61.8	0	0.1	0	0
2,2-Dimethylbutane	91.8	0	0	0	0.8
2,3-Dimethylbutane	104.3	1.5	1.4	4.8	4.3
2-Methylpentane	73.4	0.2			3.5

3-Methylpentane	74.5	0.1	0.1	0.7	1.7
n-Hexane	24.8	0	0	0	0
2,2-Dimethylpentane	92.8	0	1.3	0	0.1
2,4-Dimethylpentane	83.1	0.6		3.5	5.5
2,2,3-Trimethylbutane	112.1	0.1	0	0.2	0.3
3,3-Dimethylpentane	80.8	0	0	0	0.3
2,3-Dimethylpentane	91.1	0.6	0.6	1.7	1.8
2-Methylhexane	42.4	0	0.1		1.0
3-Methylhexane	52.0	0	0.2	0.3	0.7
2,2,4-Trimethylpentane	100	30.2	48.7	23.8	25.5
n-Heptane	0	0	0	0	0
2,2-Dimethylhexane	72.5	0	0	0	0.4
2,4-Dimethylhexane	65.2	1.2	2.9	1.1	0.8
2,5-Dimethylhexane	55.5	2.0	2.1	10.1	0
2,2,3-Trimethylpentane	109.6	0.8	1.1		11.0
2,3,4-Trimethylpentane	102.7	33.9	21.4	13.6	5.0
2,3-Dimethylhexane	71.3	1.7	2.1	3.0	0.9
2-Methylheptane	21.7	0	0	0	0
2,3,3-Trimethylpentane	106.1	20.4	12.9	21.8	7.4
3,4-Dimethylhexane	76.3	0.2	0.2	1.0	0.4
3-Methylheptane	26.8	0	0	0	0
Octenes	> 90	0	0	0.3	1.3
C_{9+}	≈ 80-85	5.4	2.9	7.5	3.3

The distributions of products within a certain carbon number fraction are far from equilibrium. In the C_8-fraction, for example, the dimethylhexanes would be favored over the trimethylpentanes. The distribution within the trimethylpentanes is also not equilibrated. 2,2,4-TMP would prevail over the other TMPs with 60-70%, depending on the temperature. In addition, 2,2,3-TMP as the primary product is found in less than equilibrium amounts. Qualitatively, the same is valid for the other carbon number distributions. Products with a

tertiary carbon atom on the 2-position dominate over other isomers in all fractions.

The overall reaction is highly exothermic. Depending on the product composition, 82 to 93 kJ per mole of reacted iso-butane are liberated (21).

2.2.2 Initiation steps

The alkylation reaction is initiated by the activation of the alkene. With liquid acids, the alkene will form the equivalent ester. This reaction follows Markovnikov's rule, so that the acid will be added to the most substituted carbon atom. With H_2SO_4 mono- and di-alkyl sulfates and with HF alkyl fluorides are produced. Triflic acid (CF_3SO_2OH) behaves in the same way and forms alkyl triflates (22). These esters are stable at low temperatures and low acid/hydrocarbon ratios. With a large excess of acid, the esters may be also stabilized in the form of free carbenium ions and anions (Reaction 1).

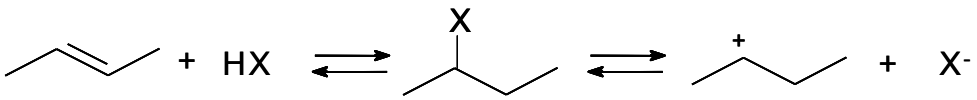

(1)

The esters differ in stability. To decompose the isopropyl ester, higher temperatures and higher acid strengths are needed than for the decomposition of the sec-butyl ester. It is claimed, that the resulting carbenium ions are stabilized by solvation through the acid (23-25). Branched alkenes do not form esters. It is believed that they easily protonate and polymerize (26).

In zeolites, the adsorption of an alkene will lead to a surface alkoxide and not to a free carbenium ion. The alkene will be "solvated" by the basic surface oxygen atoms, similar to the solvation through water in aqueous solutions. Depending on the basicity of the surface oxygen, proton transfer to adsorbed alkenes results in the formation of more or less covalent surface alkoxides rather than carbenium ions (27, 28). Ab initio quantum chemical calculations on a cluster representing the zeolitic acid site (27, 29) showed, that the alkene first forms a π-complex with the acid site. This will transform *via* a carbenium ion transition state into the alkoxide. The transition state has a much higher positive charge than the alkoxide and it forms a cycle with both oxygen atoms and the aluminum atom. The final alkoxide will not bind to the oxygen to which the hydrogen was connected but to one neighboring it. The involvement of both oxygen atoms and the "switching" between them is characteristic for hydrocarbon transformations on zeolitic acid sites (30). The exemplary

energy diagram of the isobutene protonation is depicted in Figure 2-1.

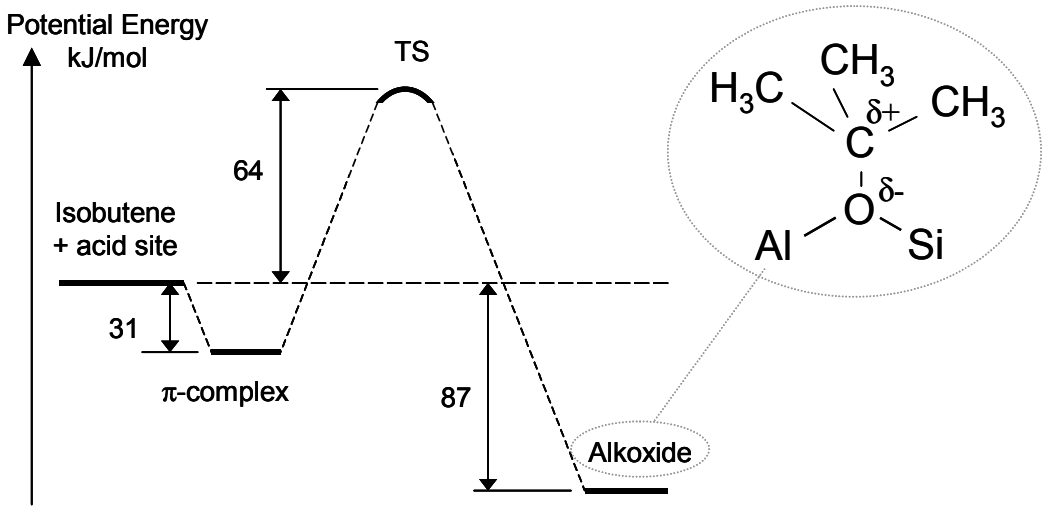

Figure 2-1: Potential energy profile and structure of final alkoxide for the adsorption of isobutene on a high silica zeolite according to (27).

More recent calculations on propene chemisorption, however, showed the sensitivity of the studied system with respect to the surrounding zeolite structure. The calculated energies depended very much on the relaxation of the unit cell size and its shape (31). Experimentally, monomeric alkoxides are difficult to study. Due to their high reactivity, alkenes tend to oligomerize, so that mainly dimerized species were detected upon adsorption of isobutene and n-butenes on zeolites (32, 33).

Engelhardt and Hall (34) found in their experiments with perdeuterioiso-butane on different zeolites the carbenium ions to be metastable reaction intermediates. The lifetime of the intermediates was concluded to depend on the acid strength.

The direct protonation of iso-butane, *via* a pentacoordinated carbonium ion, is not likely under typical alkylation conditions. This reaction would give either a tertiary butyl carbenium ion and hydrogen, or a secondary propyl carbenium ion and methane (35-37). With zeolites, this reaction starts to be significant only at temperatures higher than 200°C. At lower temperatures, the reaction has to be initiated by an alkene (38). In general, all hydrocarbon transformations at low temperatures start with the adsorption of the much more reactive alkenes, while alkanes enter the reaction cycles through hydride transfer exclusively (see chapter 2.2.4).

When n-butenes are used, the initiation will produce a secondary carbenium

ion/butoxide. This species may isomerize *via* a methyl-shift (reaction 2) or receive a hydride from iso-butane to form the tertiary butyl (reaction 3). Isobutene will directly form the tertiary cation.

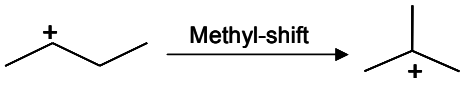

(2)

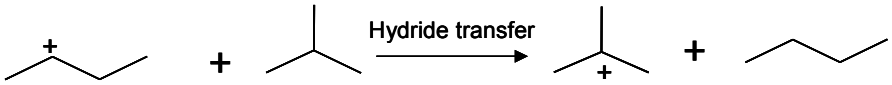

(3)

The skeletal rearrangement needed in reaction 2 has to go through a transition state, which resembles a primary carbenium ion, for which an activation energy of about 130 kJ/mol has been calculated (39). In zeolites and presumably also in the liquid acids, this reaction does not proceed under alkylation conditions. Another possibility is the addition of a butene to the secondary butyl, giving a 3,4-dimethylhexyl cation, which can be freed *via* hydride transfer from iso-butane and form the tertiary butyl in this way. This route seems to play only a minor role, as no significantly higher dimethylhexane selectivities during the initial reaction phase have been reported. At the same time, n-butane is formed in substantial amounts in this stage confirming the importance of this initiating step.

Using sulfuric acid with n-butenes or propene, only minor amounts of n-butane or propane are observed. Only little iso-butane is consumed in the initial phase, whereas the alkenes react immediately (40). Here, the alkenes first oligomerize to form conjunct polymers. These polymers are also called acid-soluble oil (ASO) or red oil, because they are found in the acid-phase and exhibit a dark red color. This oil is a complex mixture of highly branched hydrocarbons with single and conjugated double bonds and rings containing five and six carbon atoms. The individual compounds have molecular weights in the range of 265-360 (41). They can abstract a hydride from iso-butane, in this way forming the tertiary carbenium ion (5, 42). When starting the reaction with sulfuric acid, which contains already some percent of ASO, a better alkylate is produced than with fresh acid (43) and the initiation period with low yield and product quality is markedly reduced (44). The importance of the conjunct polymers will be discussed below.

2.2.3 Alkene addition and isomerization

Once the tertiary cations have been formed, they can undergo electrophilic addition to

further alkene molecules (reaction 4). The addition is exothermic and it contributes most of all the reaction steps to the overall heat of reaction. It has been proposed (22) that instead of the alkenes the corresponding esters are added to the carbenium ions, restoring the acid in this way (reaction 5). The products of both potential steps are the same.

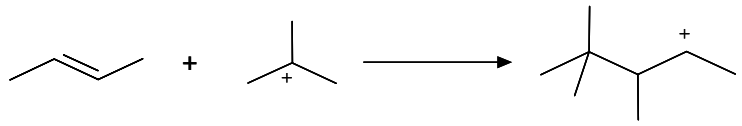

(4)

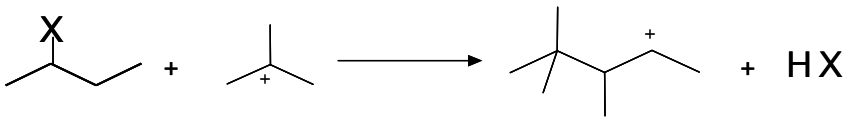

(5)

In the case of the butene isomers, the addition will lead to different isooctyl cations depending on the isomer and the type of carbenium ion (see Figure 2-2). The reactions involving sec-butyl ions are most likely negligible for liquid acid catalysts and of minor importance for zeolites.

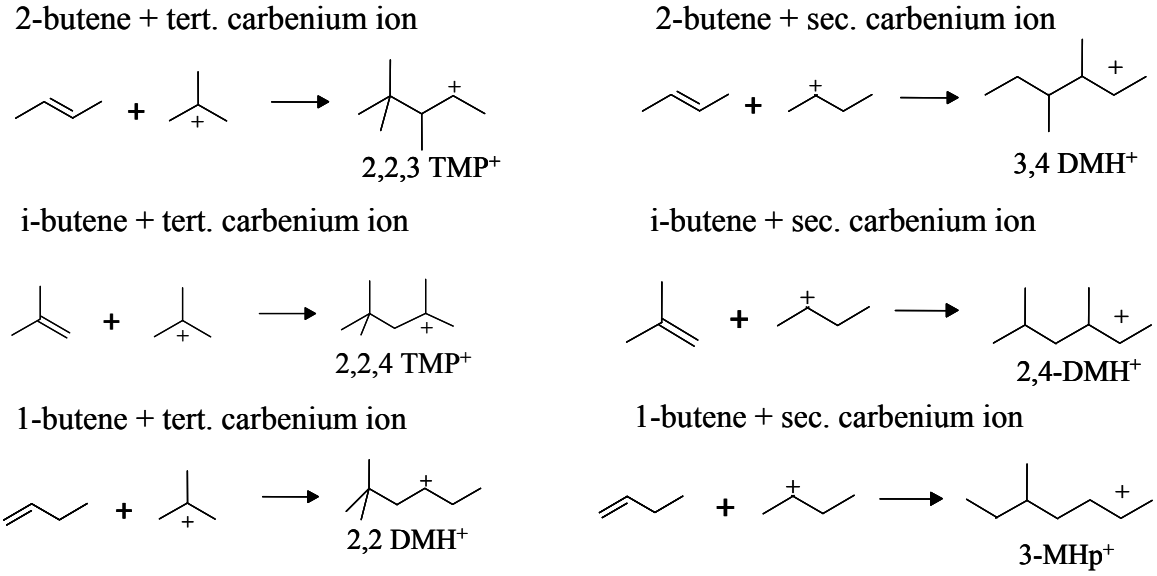

Figure 2-2: Primary products of the addition of the different butene isomers to sec.- and tert.- butyl ions.

2-Butene as feed alkene would thus give after hydride transfer 2,2,3-TMP as primary product. However, with nearly all the examined acids, this isomer is seen only in very small amounts. Usually the main components of the TMP-fraction are 2,3,3-, 2,3,4-, and 2,2,4-TMP with changing selectivities, depending on the catalyst and the reaction conditions.

Consequently, a fast isomerization of the primary TMP-cation has to occur. Isomerization through hydride- and methyl-shifts is a facile reaction. Although the equilibrium composition is not reached, long residence times favor these rearrangements (45). The isomerization pathways for the TMP isomers are schematized in Figure 2-3.

Using 1-butene as the feed alkene in most cases does not lead to dimethylhexanes as expected, but also to a mixture of TMPs. This is due to a rapid isomerization of the linear butenes almost to equilibrium compositions, in which the 2-butenes are strongly favored. On the other hand, some of the DMH-isomers produced in 2-butene alkylation also stem from a rapid isomerization of the feed.

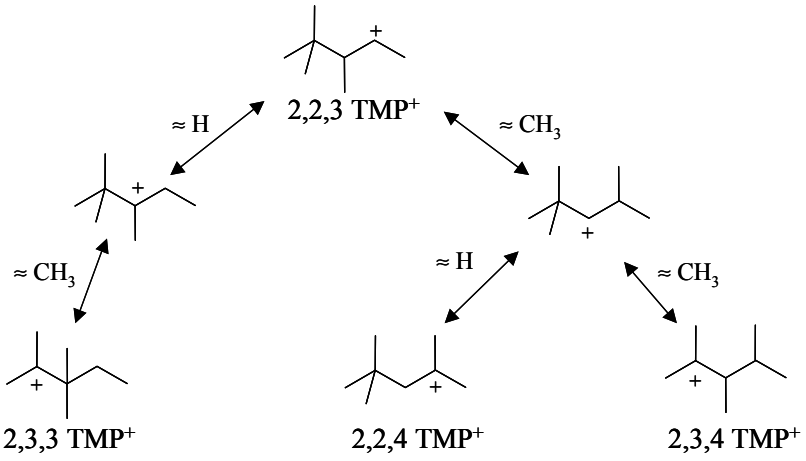

Figure 2-3: Possible hydride- and methyl-shifts between the individual TMP-isomers.

Not all acids are equally active isomerization catalysts. With zeolite H-BEA, nearly identical selectivities are achieved, when using 1-butene instead of 2-butene (46). In general, even mildly acidic zeolites are excellent catalysts for double-bond shift isomerization. Sulfuric acid also produces nearly identical alkylates with 1-and 2-butene (43, 47). Hydrofluoric acid on the other hand is known to produce substantial amounts of DMHs with 1-butene (19, 48). Aluminum chloride also shows slow rates of butene isomerization (16, 49). It seems unlikely that under the mild alkylation conditions skeletal rearrangements, which could isomerize TMP-cations into DMH-cations (and methylheptyl cations), occur to a large extent. This type of isomerization has a much higher true activation energy than hydride and methyl shifts.

Theoretically, also the direct alkylation of carbenium ions with iso-butane is feasible. The reaction of iso-butane with a tert-butyl carbenium ion would lead to 2,2,3,3-tetramethylbutane as the primary product. With liquid super acids under controlled conditions, this has been experimentally observed (50), but under typical alkylation conditions 2,2,3,3-TMB is not produced. Kazansky *et al.* proposed the direct alkylation of

isopentane with propene in a two-step alkylation process. In this process, the alkene first forms the ester, which in the second step is reacted with the isoalkane. The isopentane was found to add directly to the isopropyl ester *via* intermediate formation of non-classical carbonium ions. In this way, the carbenium ions are freed as the corresponding alkanes without hydride transfer (see chapter 2.2.4) (24, 25). This was concluded from the virtual absence of propane in the product mixture. Whether this reaction path is of significance in conventional alkylation processes is unclear at present. HF produces substantial amounts of propane in iso-butane/propene alkylation. The lack of 2,2,4-TMP in the product, which is formed in almost all alkylates regardless of the feed (51), implies that the mechanism in the two-step alkylation process is different from conventional alkylation.

2.2.4 Hydride transfer

Intermolecular hydride transfer (reaction 6), typically from iso-butane to an alkyl-carbenium ion, transforms the ions into the corresponding alkanes and regenerates the tert-butyl cation to continue the chain sequence in liquid acids and zeolites respectively.

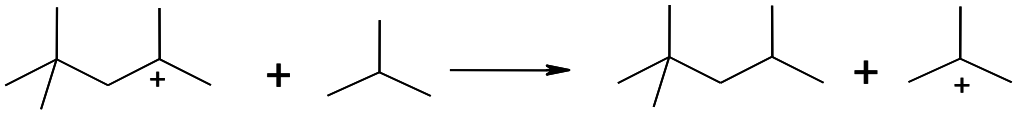

(6)

Hydride transfer is the crucial step in the reaction sequence. It ensures the perpetuation of the catalytic cycle and leads to the exclusive desorption of saturated compounds. In general, the hydride transfer between alkanes and alkyl-carbenium ions is the elementary step responsible for chain propagation of acid-catalyzed transformations of hydrocarbons (52). Hydride transfer between tertiary carbon atoms is much faster than between secondary carbons. Although hydride transfers involving secondary alkyl cations take place in aluminum halide systems (53), they are too slow to be observed in sulfuric acid (54). In general, hydride transfer is accelerated by neighboring groups, which encourage the stabilization of the resulting ion (55).

Studies on hydride transfer in the gas-phase (56-59) showed that the reaction proceeds without activation energy. Its reaction rate was found to exhibit two regimes, i.e., fast kinetics at low temperatures and slow kinetics at high temperatures. This behavior was explained by a consecutive mechanism proceeding through two reaction steps. It involved the formation of a loose complex between the ion and the neutral alkane, which reacts to form a tight complex

having a bridging hydride between the two fragments. The rates of different hydride transfer reactions between different carbenium ions and different alkanes were found to depend on the reaction enthalpy and steric factors involving van der Waals interactions between the approaching ion and hydrogen and methyl groups on the adjacent carbon atom next to the tertiary carbon. Steric hindrance in tertiary-tertiary hydride transfer reactions was also established in the liquid phase employing super-acidic catalysts (60). These steric restrictions presumably are responsible for the low selectivity to the primary product 2,2,3-TMP seen with all acids. Hydride- or methyl shifts are much more likely than hydride transfer to a difficult to access carbon atom bearing the positive charge center. Note that the precursor carbenium ions of the most abundant TMPs have their charge center next to the chain end at a tertiary carbon atom (see Figure 2-3).

There are substantial differences between gas-phase and liquid-phase hydride transfer reactions. In the latter, the hydride transfer occurs with a small activation energy of 13-17 kJ/mol and no carbonium ions have been detected as intermediates, when secondary or tertiary carbenium ions were present (23). These differences were explained by solvation effects in the liquid phase. The carbenium ions are more efficiently stabilized by solvation than carbonium ions, because the former have unsaturated trivalent carbon atoms. In this way, the energy barrier between the two states increases.

In zeolites, this barrier is even higher. As discussed in Chapter 2.2.2, the lower acid strength and the interaction between the zeolitic oxygen atoms and the hydrocarbon fragments lead to the formation of alkoxides rather than carbenium ions. Thus, extra energy is needed to transform these esters into carbonium ion-like transition states. Quantum-chemical calculations of hydride transfer between C_2-C_4 adsorbed alkenes and free alkanes on clusters representing zeolitic acid sites led to activation energies of approximately 200 kJ/mol for iso-butane/*tert*-butoxide (27), 230-305 kJ/mol for propane/*sec*-propoxide and 240 kJ/mol for iso-butane/tert-butoxide (30), 130-150 kJ/mol for ethane/ethene (61), 95-105 kJ/mol for propane/propene, 88-109 kJ/mol for iso-butane/isobutene and 110-118 kJ/mol for propane/isobutene (62). In the two last references, the carbonium ions were not found to be transition states but energetically high lying reaction intermediates. The authors claim that these carbonium ions exist as intermediates when the charge is delocalized and not accessible to framework oxygen. The carbonium ions decompose directly into the alkene and alkane, without forming alkoxides. Thus, the activation energies are about a 100 kJ/mol lower than

calculated in the other mentioned references, because covalent bonds have not to be broken to reach the transition state. Note that the activation energy is lowest in tertiary-tertiary hydride transfer. In a study by Nowak *et al.* activation energies for hydride transfer between iso-butane and tertiary and secondary acceptor cations were compared with activation energies of isomerization steps between tertiary carbenium ion species. The energy for tertiary/tertiary hydride transfer was comparable to the energy of the isomerization, while the energy for tertiary/secondary hydride transfer was almost twice as high (63).

Another study of ethane/ethene hydride transfer was performed in order to investigate the influence of the Si/Al ratio and different levels of coverage of the acid sites (64). The zeolite was modeled to represent the chabazite structure. It was found that the electrostatic effects increase with decreasing Si/Al ratio, but are only important when the interaction between the zeolite and the adsorbed species are clearly ionic. High coverage exhibited a destabilizing effect on the carbonium ions due to repulsion of the molecules. The authors assume that the electrostatic forces are just one of many effects being of importance in zeolite-catalyzed hydrocarbon reactions. Figure 2-4 summarizes the different calculated potential energy profiles for the hydride transfer reaction in different media.

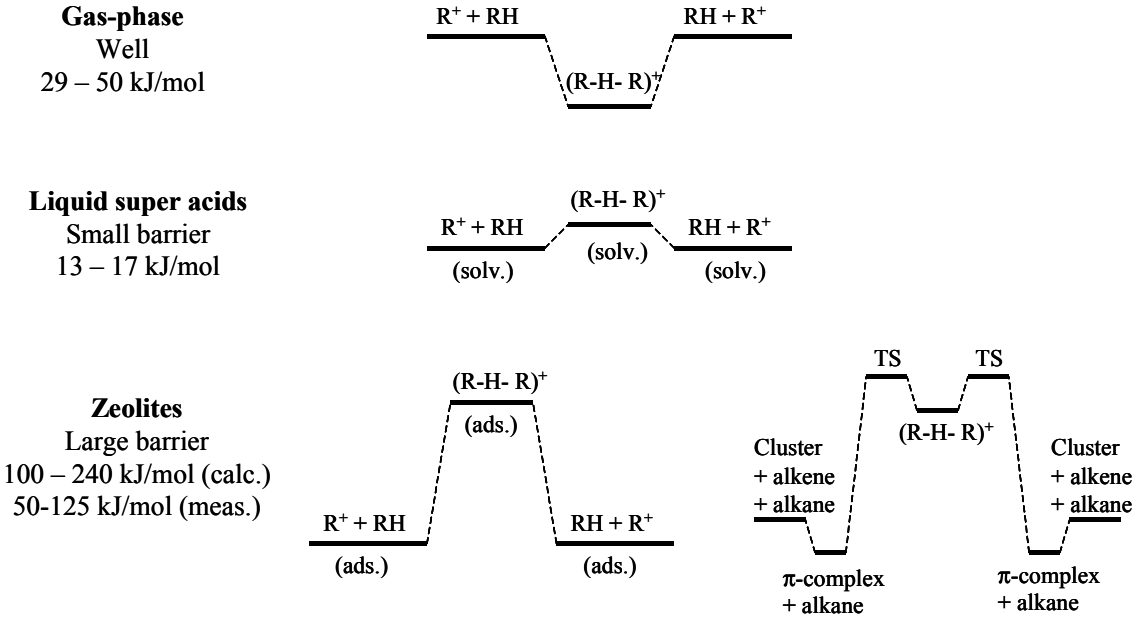

Figure 2-4: Potential energy profiles for the iso-butane/tert-butyl hydride transfer reaction in different media. Taken from references (23, 62)

Experimental data on hydride transfer in zeolites is scarce as it is a secondary reaction,

which cannot be observed directly. Data from kinetic measurements of cracking reactions of 2,2,4-TMP on USY zeolite gave values for the apparent energies of activation of 47 kJ/mol lumped for all occurring hydride transfer reactions (65). A more detailed study of iso-butane cracking gave values of 64 kJ/mol for iso-butane/propyl, 76 kJ/mol for iso-butane/n-butyl and 62 kJ/mol for iso-butane/isopentyl hydride transfer (38). An earlier study of the same group lead to higher values of 81 kJ/mol for iso-butane/propyl, 67 kJ/mol for iso-butane/n-butyl and 125 kJ/mol for iso-butane/isopentyl hydride transfer (66). Even when adding average heats of adsorption (ca. 40 kJ/mol) to the measured apparent energies to get the true activation energies the numbers are lower than the calculated values. Clearly, the theoretical calculations overestimate the energy barrier. This is speculated to be due to incorrect modeling of the acid strength (deprotonation energy, basicity of the lattice oxygen atoms) in the zeolitic cluster used for the calculation.

It has been proposed that hydride transfer in zeolites requires the presence of two adjacent Brønsted acid sites (67). In the light of the abovementioned theoretical examinations and also from adsorption isotherms of 1-butene and n-butane measured on USY-zeolites with different aluminum content (68), this seems unlikely.

The reaction enthalpy of the hydride transfer step usually has a low absolute value. Whether hydride transfer is exo- or endothermic depends on the stability (evidenced by the heat of formation) of the involved carbenium ions. Branched carbenium ions are more stable than linear ions. Longer carbenium ions are more stable than short ions. Replacement of an ion with a longer chain than the incoming alkane is endothermic. This is for example the case, when iso-butane transfers the hydride to C_8 carbenium ions.

With both liquid acid catalysts, but presumably to a higher degree with sulfuric acid, hydrides are not exclusively transferred from iso-butane, but also from the conjunct polymers to the carbenium ions (42, 44, 69). Sulfuric acid containing 4-6 wt.-% of conjunct polymers produces a much higher quality alkylate than acids without acid-soluble oils (43). Cyclic and unsaturated compounds, which are both present in conjunct polymers, are known to be hydride donors (70). As already mentioned in Chapter 2.2.2, these species can abstract a hydride from iso-butane to form the tert-butyl carbenium ion, and they can give a hydride to a carbenium ion, producing the corresponding alkane, for example the TMPs, as shown in reactions 7 and 8.

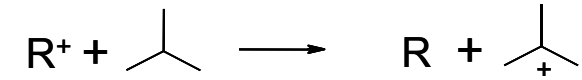

(7)

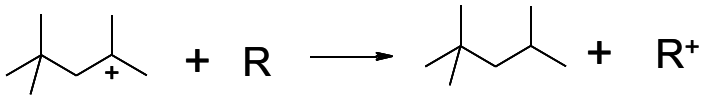

(8)

In this way, the conjunct polymers serve as a reservoir of hydride ions. Under some conditions, the polymers are a source of hydride ions, but accept these ions under other conditions. Substantial amounts of the saturated products are supposedly formed *via* this route with sulfuric acid. In zeolites, species similar to conjunct polymers also form. The heavy hydrocarbon molecules, which deactivate the catalyst by pore- or by site-blocking, are generally termed soft coke or low-temperature coke, because of the absence of aromatic species. Only scarce information is available about the influence of coke formation on the alkylation mechanism. It has been proposed, that similar to the conjunct polymers in liquid acids, heavy unsaturated molecules participate in hydride transfer reactions. However, no direct evidence was given (67). In another study, the hydride transfer from unsaturated cyclic hydrocarbons was deduced from an initiation period in the activity of NaHY zeolites. Complete butene-conversion was achieved only after sufficient formation of such compounds (71). In a series of studies on the cracking of alkanes and alkenes on Y zeolites (72, 73), the effect of coke formation on the conversion was examined. The formed coke was found to exhibit considerable hydride transfer activity. This activity can compensate for a while the deactivating effect of the coke molecules. From dimerization and cracking experiments with labeled 1-butene on zeolite Y (74) it is known, that substantial amounts of alkanes are formed, which are saturated by hydride transfer from surface polymers. In both types of

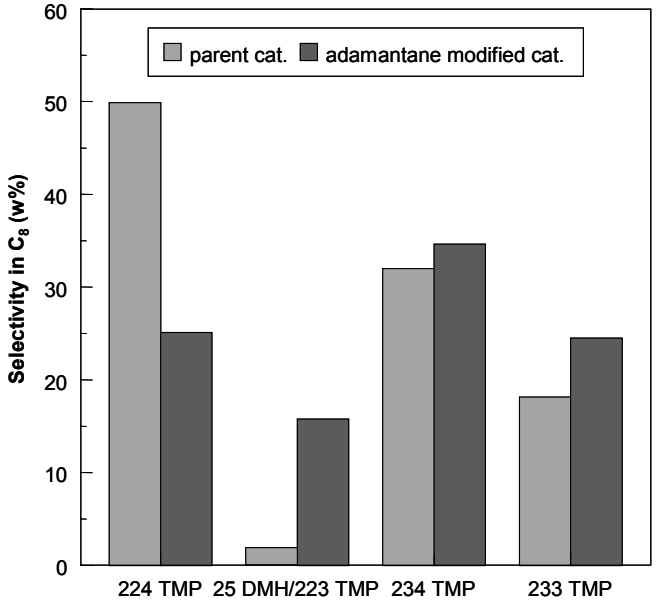

Figure 2-5: Changes in TMP selectivities with the use of adamantane (5 wt.-%) as additive in a H-BEA catalyst at 30 min TOS (P/O = 10, OSV = 0.2 h^{-1}, T = 75°C). Taken from reference (78).

catalysts, liquid and solid acids, hydride transfer from iso-alkanes larger than iso-butane may occur, especially from isopentane, which sometimes is used as feedstock. However, no data are available about the significance of hydride transfer reactions with higher hydrocarbons.

Hydride transfer from olefins was also proposed to occur during sulfuric acid catalyzed alkylation modified with anthracene (75). Here, the butene loses a hydride and forms a cyclic carbocation intermediate, yielding on reaction with iso-butane trimethylpentyl cations. This was concluded from a sharp decrease in 2,2,3-TMP selectivity upon addition of anthracene to the acid.

Fast hydride transfer reduces the lifetimes of the isooctyl carbenium ions. The molecules have less time to isomerize and, consequently, the observed product spectrum should be closer to the primary products and further away from equilibrium. This has indeed been observed when adamantane, an efficient hydride donor, was admixed to zeolite H-BEA as catalyst (76). Using 2-butene/iso-butane feed, the increased hydride transfer activity led to considerably higher 2,2,3-TMP and lower 2,2,4-TMP selectivities, as shown in Figure 2-5.

2.2.5 Oligomerization and cracking

The overall product distribution is governed by the relative rates of alkene addition and hydride transfer. With all acids, alkene addition is a much more facile reaction than hydride transfer. With sulfuric acid, n-butene oligomerization was found to be four times faster than hydride transfer (77). With zeolites, de Jong *et al*. reported oligomerization to be two orders of magnitude faster than hydride transfer (78), while Simpson *et al.* reported even higher values of three orders of magnitude (79). With too low internal paraffin/olefin ratios the alkenes will oligomerize before they can be removed *via* hydride transfer. This is the key problem in solid acid catalyzed alkylation. A polymer will build up, which will finally block the acid sites. With liquid acids, the conjunct polymers help in maintaining a high hydride transfer activity. However, when the concentration reaches a critical level, the acid strength will be too low for producing high quality alkylate. For this reason, in a continuous process, a stream of used acid has to be constantly replaced by fresh acid to maintain the optimum level of acid strength. The route to oligomerization products (sometimes also called multiple alkylate) is depicted in Figure 2-6.

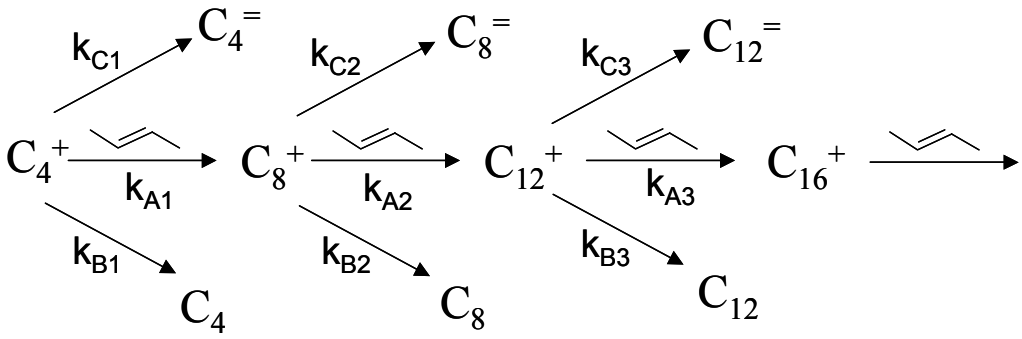

Figure 2-6: Pathway to oligomerization products with the corresponding rate constants. Adapted from (79)

The rate constant k_A defines the rate of alkene addition, k_B defines the hydride transfer rate and k_C the rate of deprotonation. The rate ratio $r_B/(r_A+r_C)$ is the critical parameter that determines whether the catalyst will effectively catalyze alkylation or deactivate quickly through multiple alkylation/oligomerization reactions. High ratios can be achieved with low alkene concentrations (backmixed reactor) and maximized hydride transfer rates (catalyst property).

Hydrocarbons with up to16 carbon atoms are detected in a typical alkylate (80). With the liquid acids it was found, that the oligomerization rate is higher for iso-alkenes in comparison to linear alkenes (47). The same is true for solid acids (12, 81). Due to their tertiary carbon atoms, iso-butene and iso-pentene obviously react more easily with carbenium ions. This can be concluded from the reverse reaction, β-scission (see below), which is fastest for tertiary-tertiary cleavages. In oligomerization experiments the following reactivity for alkenes has been found: iso-butene >> n-butenes > propene > ethene. This order can be readily explained by the relative stabilities of the alkyl-carbenium ions involved (82).

Not only products with carbon numbers, which are multiples of four, are produced, but also C_5-C_7 and C_9, C_{10} and higher hydrocarbons. Cracking is invariably connected to oligomerization. The heavy cations formed by oligomerization have the tendency to fragment, forming C_4-C_{16} cations and alkenes, according to the β-scission rule. This is schematically depicted in reaction 9 with a dodecyl carbenium ion cracking into an iso-pentene and a heptyl carbenium ion.

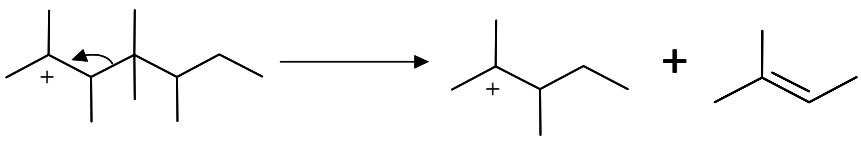

(9)

The produced iso-pentene either will be protonated or added to another carbenium ion. With a butyl, this would lead to a nonyl carbenium ion. The formed carbenium ion fragment can receive a hydride and leave the reaction as a heptane, or possibly add a butene to form a C_{11} carbenium. With hydride transfer, another alkane with an odd carbon number is produced. This small example shows the huge variety of possible reactions. By means of GC-analysis Albright and Wood (80) found about 100-200 peaks in the C_9-C_{16} region, regardless of the alkene and acid employed. A similar magnitude of products can be observed for solid acid catalyzed alkylation. In general, oligomerization and cracking products exhibit lower octane numbers than the TMPs. Average RON values of 92-93 for C_5-C_7 and of 80-85 for C_9-C_{16} have been reported (5). Parts of the octane fraction also stem from oligomerization/cracking reactions. It is believed, that substantial amounts of the dimethylhexanes are produced *via* this route (77), especially when using isobutene as the feed alkene (69). Iso-butene tends to oligomerize quickly. Hence, it produces higher amounts of light and heavy ends and it cannot isomerize to 1-butene to produce DMHs in this way. Some of the TMPs also will be produced through oligomerization/cracking pathways (18). Concentrations of more than 20 wt.-% of TMPs in the C_{6+} fraction have been observed in isopentane/2-pentene alkylation (51). The TMPs cannot be produced *via* simple alkylation or self-alkylation with this feed. It has been proposed, that oligomerization/cracking constitutes the *main* route to alkylation products (14), but this theory fails to explain the usually high selectivity to the TMPs. To form trimethylpentanes, certain specific precursors would have to build up in high concentrations, which is rather unlikely.

Hydrocracking experiments under ideal conditions provided kinetic information on the β-scission step. Based on this work, a classification of different types of β-scission has been introduced (83). Fragmentations starting from a tertiary carbenium ion and giving a tertiary ion (type A) are very rapid. Fragmentations involving secondary and tertiary ions (type B) are slower than tertiary-tertiary β-scissions, but faster than secondary-secondary β-scissions (type C). The slowest mode is the cracking of a secondary ion to give a primary ion (type D). From the typical low reaction temperatures and the product composition of a typical alkylate, which consists almost exclusively of branched hydrocarbons, it can be concluded, that only type A β-scissions occur. Furthermore, protolytic cracking of alkanes *via* a carbonium ion mechanism is very unlikely under typical alkylation conditions. Hydrogen or methane as characteristic products are not found in the alkylate. At low temperatures, the cracking of

alkanes is initiated by traces of alkenes in the feed (see also Chapter 2.2.2).

In general, oligomerization is an exothermic and therefore β-scission an endothermic reaction. Quantum-chemical calculations of the β-scission step on a zeolitic cluster were performed to calculate activation energies. For tertiary-secondary fragmentations, values in the order of 234-284 kJ/mol and for secondary-secondary 288-314 kJ/mol (30) and 217-275 kJ/mol (84) were calculated. Here, the activation energy of the reverse reaction was reported to be 71 kJ/mol less. Evaluation of alkane conversion experiments on USY zeolites in general provided much lower values. Average apparent activation energies for secondary-tertiary and secondary-secondary β-scission steps were estimated to be approximately 115 kJ/mol (38, 65). The values for tertiary-tertiary β-scission differed between 66 and 102 kJ/mol. In an older study of the same authors (66) values for β-scission and oligomerization were given. Tertiary-tertiary β-scission had an activation energy of 184 kJ/mol; 105 kJ/mol the reverse. Tertiary-secondary β-scission had an activation energy of 84 kJ/mol, 71 kJ/mol the reverse. Secondary-secondary β-scission had an activation energy of 130 kJ/mol, the reverse 33 kJ/mol. Similar to hydride transfer, the calculated values are significantly higher than the measured values (plus heat of adsorption), presumably due to an underestimation of the acid strength.

2.2.6 Self-alkylation

With hydrofluoric acid (21, 48) and to a lesser degree also with zeolites (12, 79, 85-87) a significant fraction of the product stems from self-alkylation, which is sometimes also termed hydrogen transfer. The importance of this mechanism depends on the acid, the alkene and the reaction temperature. Self-alkylation activity increases with molecular weight and increased branching of the feed alkene (88).

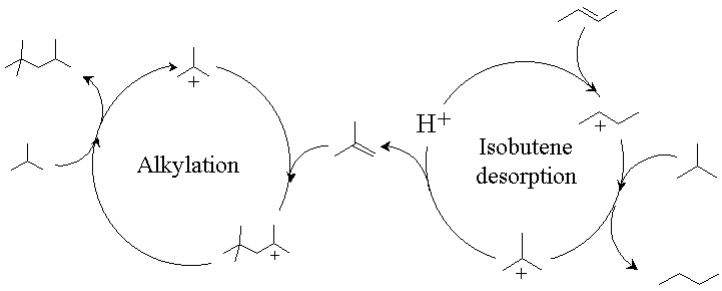

Figure 2-7: Self-alkylation mechanism, depicted with 2-butene as the feed alkene.

Generally, sulfuric acid is less active for self-alkylation than hydrofluoric acid. Only when using pentenes or higher alkenes, self-alkylation activity is significant with sulfuric acid (47, 89). In Figure 2-7, the mechanism is displayed with an exemplary iso-butane/2-butene feed.

The crucial step in self-alkylation is decomposition of the butoxy group into a free Brønsted acid site and iso-butene (proton transfer from the tert-butyl carbenium ion to the zeolite). Iso-Butene will react with another tert-butyl ion to form an isooctyl ion. At the same time, a feed alkene repeats the initiation step to form a sec-alkyl ion, which after receiving a hydride gives the tert-butyl ion and an n-alkane. The overall reaction with a linear alkene C_nH_{2n} as feed is summarized in reaction 10:

$$2\ i\text{-}C_4H_{10} + C_nH_{2n} \rightarrow i\text{-}C_8H_{18} + C_nH_{2n+2} \qquad (10)$$

With propene, n-butene and n-pentene the formed alkanes are propane, n-butane and n-pentane (plus isopentane), respectively. The production of considerable amounts of light n-alkanes is a disadvantage of this reaction route. Furthermore, the yield of the desired alkylate product is reduced relative to iso-butane and alkene consumption (5). For example, propene alkylation with HF can give more than 15 vol.-% yield of propane (19). Aluminum chloride-ether complexes also catalyze self-alkylation. However, when the acidity is moderated with metal chlorides, the self-alkylation activity is drastically reduced. Intuitively, the formation of isobutene *via* proton transfer from an isobutyl ion should be more pronounced at a weaker acidity, but the opposite has been found (90). Other factors besides the acidity may contribute to the self-alkylation activity. Earlier publications on zeolites claimed this mechanism to be a source of hydrogen for saturating cracking- or dimerization-products (67, 91). However, as shown in reaction 10, only the feed alkene will be saturated and dehydrogenation does not take place.

2.2.7 Product and acid degradation

It has been found that C_7-C_9 iso-alkanes react with strong acids and produce a low quality alkylate and conjunct polymers (92). In the presence of conjunct polymers, highly branched iso-alkanes might reenter the reaction cycle by the reverse of reaction 8.

Oligomerization/cracking will then lead to inferior products. This problem affects both HF and H_2SO_4. It is unclear whether this side reaction is of importance with zeolites under alkylation conditions. On H-FAU at temperatures as low as 100°C, 2,2,4-TMP undergoes cracking into iso-butane and isobutene, with significant "coke" formation (93).

A problem that is characteristic for sulfuric acid is its capability to oxidize hydrocarbons. H_2SO_4 decomposes in the presence of iso-alkanes to form water, SO_2 and alkenes. This is a slow process, so it predominantly occurs in situations where the acid is in contact with hydrocarbons for a longer period. Higher temperatures favor the formation of SO_2 (8). Some irreversible reactions between acid and hydrocarbons take place also during alkylation. Sulfone, sulfonic acid and hydroxy groups have been detected in conjunct polymers produced with H_2SO_4 as catalyst (5, 94). Kramer reported that 2,3,4-TMP after an induction period is converted to a mixture of lower alkanes, with a high fraction of iso-butane, and isomerized octanes. The reaction was initiated by the reduction of sulfuric acid to SO_2 with the formation of carbenium ions (95). In a subsequent paper by Kramer more information on the reaction of selected branched alkanes with sulfuric acid was given. It was concluded that SO_2 is only produced during the initiation reaction. All subsequent reactions are conventional carbenium ion type reactions. Alkanes with a higher degree of branching show higher rates of degradation (96). Pure iso-butane was found to react with sulfuric acid at 25°C. The acid was slowly reduced to SO_2, with iso-butane forming carbenium ions undergoing subsequent reactions. With traces of olefins in the feed, however, acid reduction was not observed (97).

2.2.8 Pathways to allylic and cyclic compounds

The conjunct polymers formed during the liquid-phase alkylation contain single and conjugated double bonds and five- and six-rings. The residue on zeolitic catalysts is highly branched, contains double bonds and conjugated double bonds and possibly also five- and six-rings (71, 86, 98). The H/C ratio is about 1.8 (99), similar to the conjunct polymers. In general, it is believed that at temperatures below 200°C, coking of acidic catalysts mainly involves condensation and rearrangement steps. Aromatic compounds are usually not formed under such mild conditions (93). Transferring this to the reaction conditions typical for alkylation, several alkene molecules will oligomerize and crack or deprotonate to form a large and branched alkene. This might transfer a hydride to another carbenium ion and, thus, form an alkenyl carbenium ion, which can desorb *via* proton transfer as a diene (Reaction

11). Further hydride transfer leads to a dienylic cation, which easily rearranges into an alkyl-substituted ring (Reaction 12) *via* a 1,5-cyclization and subsequent hydride and methyl shifts.

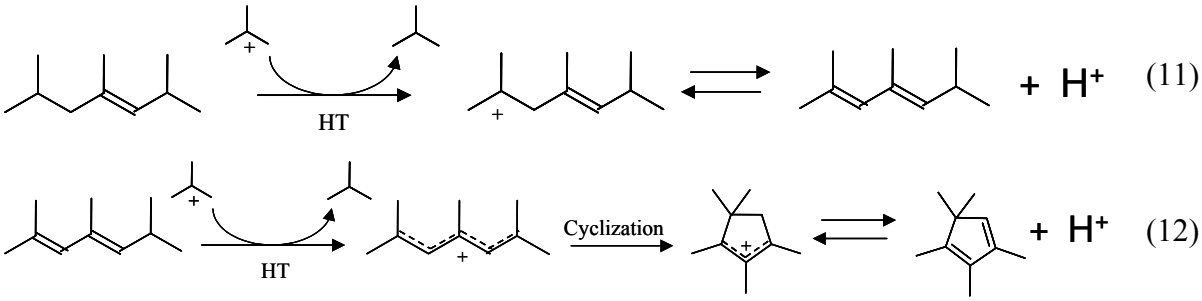

The formed cycloalkenyl carbenium ions, especially the cyclopentenyl cations, are very stable (100, 101) and can even be observed as free cations in zeolites (102, 103). These ions can oligomerize further and, within zeolites, irreversibly block the acidic hydroxyls. With liquid acids, the oligomers will dilute the acid and, thus, lower its acid strength.

2.2.9 Summary

Figure 2-8 summarizes the main reactions occurring during alkylation. Dimerization and oligomerization reactions are more important with zeolitic catalysts on acid sites with lower acid strength (see Chapter 2.3.2.2) or with severely diluted liquid acids (see Chapter 2.3.1). Hydride transfer from conjunct polymers is more important with sulfuric acid, while self-alkylation activity is more significant with hydrofluoric acid. Repeatedly going through the alkylation cycle without hydride transfer (multiple alkylation) and through the dimerization cycle without proton transfer (oligomerization) leads to the formation of heavy compounds, which will react further *via* cracking, hydride or proton transfer and cyclization. As long as the catalyst shows sufficient hydride transfer activity, all alkenes will react and only saturated products will leave the reaction cycles.

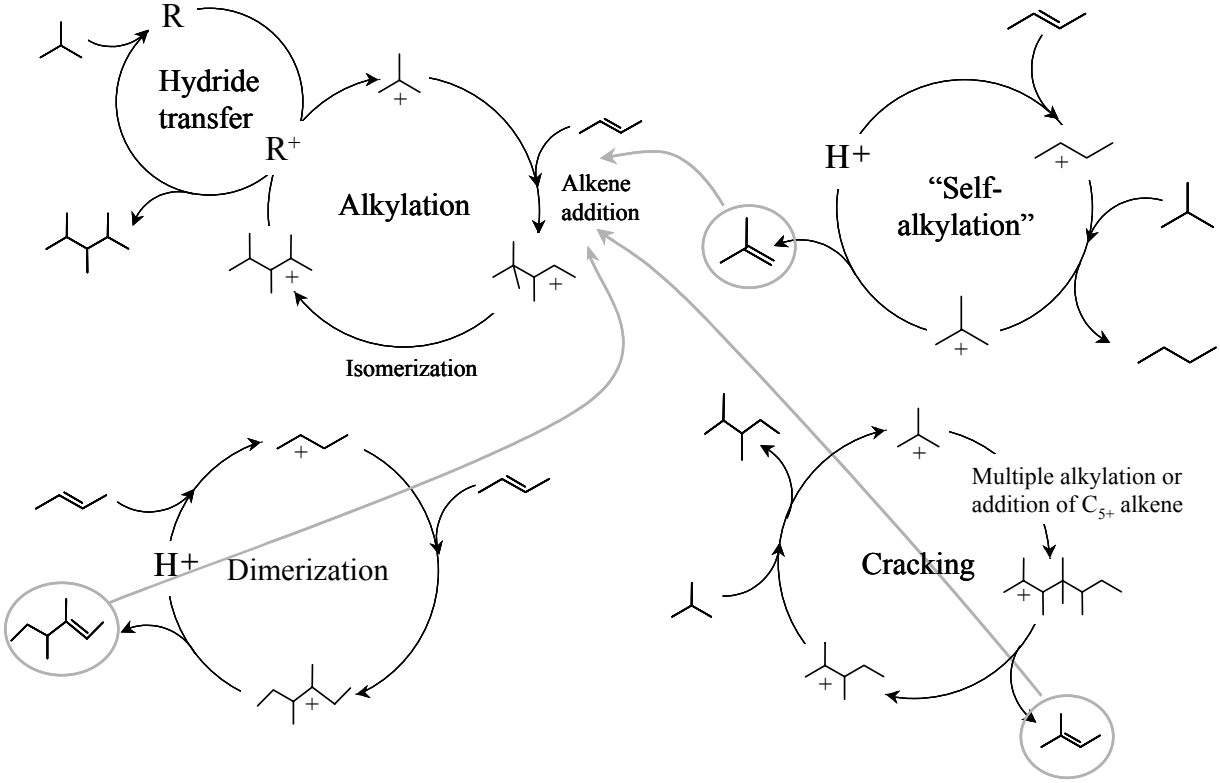

Figure 2-8: Concerted alkylation mechanism including alkylation, "self-alkylation", cracking, dimerization and hydride transfer *via* iso-butane and *via* conjunct polymers.

2.3 Physico-chemical phenomena influencing the reaction

As has been pointed out in the chapters above, the chemistry of the alkylation reaction can be explained by a set of various mechanistic steps, which are similar and in some cases the same for all the different acids examined. However, the importance of each single step varies with the catalyst and the reaction conditions chosen. The understanding of these parameters is, thus, of utmost importance. This is especially true for the solid acids. They can be synthesized and modified in a nearly infinite number of ways, all of them influencing in a complex and subtle manner the alkylation performance. In this chapter, the chemical and physical properties of the individual alkylation catalysts and how they affect the mechanism will be reviewed. Next to this, also the influence of process parameters, such as temperature, paraffin/olefin ratio and residence time on the reaction will be discussed.

2.3.1 Properties of liquid acid alkylation catalysts

In the liquid acid catalyzed processes, the hydrocarbon phase is dispersed as droplets in

the continuous acid phase. The reaction takes place at or close to the interface between the hydrocarbon and the acid phase. The overall reaction rate will depend on the area of the interface. Larger interfacial areas promote more rapid alkylation reactions and generally result in higher-quality products. The alkene diffuses through the hydrocarbon phase to the interface and upon contact with the acid forms an acid-soluble ester, which slowly decomposes in the acid phase to a solvated carbenium ion or to the alkene. Iso-butane can react at the interface or diffuse into the acid phase and react there. The most important parameters determining the ease of formation of a large reaction zone are the viscosity and the solubility of hydrocarbons in the acid. Comparing sulfuric and hydrofluoric acid, these properties differ substantially. Under typical alkylation conditions, the viscosity of sulfuric acid is two orders of magnitude higher than that of hydrofluoric acid, while the solubility of iso-butane is approx. 30 times lower. High solubility of iso-butane together with a high interfacial area ensures high iso-butane/alkene ratios in the acid and, thus, high hydride transfer rates, decreasing the selectivity to undesired products from oligomerization/cracking and isomerization and the formation of conjunct polymers. Consequently, sulfuric acid/hydrocarbon phases have to be mixed much more vigorously in order to obtain a high quality alkylate. For the same reason, hydrofluoric acid catalyzed processes can operate at lower residence times and higher temperatures. Using sulfuric acid with iso-butane/2-butene in a laboratory reactor, Li *et al.* (104) found that increasing the agitator speed from 1000 to 3000 rpm increased the product RON from 86 to 94. Albright discerned a minimum of four types of droplets in acid/hydrocarbon dispersions. They differ in size and in the concentrations of reactants and products (9). The formation (and the separation) of acid/hydrocarbon emulsions depends on the temperature, the composition of the acid and the acid/hydrocarbon ratio (105).

Sulfuric acid is a somewhat stronger acid than hydrofluoric acid. The H_0 values for the water-free acids are -14.1 for H_2SO_4 and -12.1 for HF. It is, however, interesting to note that the maximum alkylate quality employing sulfuric acid is not achieved with the highest acidity, but with acid containing 1 – 1.5% water and 4 – 5 % acid soluble oils (94). Water reduces the acidity to a greater extend than hydrocarbon diluents. Besides their hydride transfer capabilities, the acid soluble oils act as surfactants, increasing the interfacial area. When the concentration of diluents exceeds a certain level, the acid strength is too low to produce a high quality alkylate. Sulfuric acid of 60-80% concentration catalyzes only alkene

oligomerization. The acid strength is too low to catalyze the more demanding reactions hydride transfer and β-scission (25). A relatively sharp transition between oligomerization and alkylation activity has been measured with sulfuric acid at H_0 values between -8.0 and -8.5 (106). If such low acidity values occur in an alkylation reactor, oligomerization reactions become so predominant that the acid strength cannot be maintained and the plant is said to be in an acid runaway condition.

The same acidity principles can be applied to hydrofluoric acid. However, HF alkylation is more sensitive towards water, so that the feed must be thoroughly dried before entering the reactor. In addition, the acid dilution through hydrocarbons is greater due to their higher solubility in HF (13). Employing triflic acid modified with water or trifluoroacetic acid, Olah *et al.* found the best alkylation conditions at an acid strength of about H_0 = -10.7 for both systems. Pure triflic acid with H_0 = -14.1 produced mainly cracked compounds. Diluted triflic acid with H_0 > -10.7 favored oligomerization (107). The same group tested different liquid acids diluted with liquid carbon dioxide. While very strong acids such as triflic acid produce higher quality alkylate upon dilution with CO_2, sulfuric acid (being less acidic than triflic acid) performed better without CO_2 (108). The different H_0 values for the transition from alkylation to oligomerization with sulfuric and triflic acid suggest that the acid strength is not the only factor determining the reactivity of the carbenium ions.

2.3.2 Properties of zeolitic alkylation catalysts

Zeolites are widely used as solid acid catalysts or catalyst components in areas ranging from petroleum refining to the synthesis of intermediates and fine chemicals (109, 110). The reason for the widespread use is the flexibility regarding their tailoring with respect to the concentration and nature of catalytically active sites and their immediate environment. It should be noted at this point that discrimination between chemical and structural aspects works well at a conceptual level, but faces quite severe limitations as soon as one tries to separate the contributions of the two effects. This is because the chemical properties of a particular molecular sieve are interconnected with its framework density.

2.3.2.1 Adsorption and diffusion of hydrocarbons

One of the major differences between acidic zeolites and the liquid acids is their selective and strong chemisorption of unsaturated compounds. Due to the high polarity of the zeolitic

surface, especially in aluminum rich zeolites, polar molecules will be preferentially adsorbed. This is clearly seen in the high water uptake capacity of zeolite X which exceeds 25 wt.-%. Furthermore, the electrostatic field in the zeolite pores enhances the adsorption of polarizable molecules (111). Thus, although the concentration of alkenes in the liquid phase might be low, they will preferentially adsorb in the zeolite pores, so that in the pore system the alkene concentration will be considerably higher. This results in much higher relative rates of oligomerization *vs.* hydride transfer, as already discussed in Chapter 2.2.5. That is the major reason why zeolites deactivate rapidly, if no special measurements are taken to minimize the alkene concentration close to the acid sites. Nevertheless, the adsorption of alkenes can differ substantially even in the same type of zeolite, depending on the concentration of framework aluminum and the modification procedure (68).

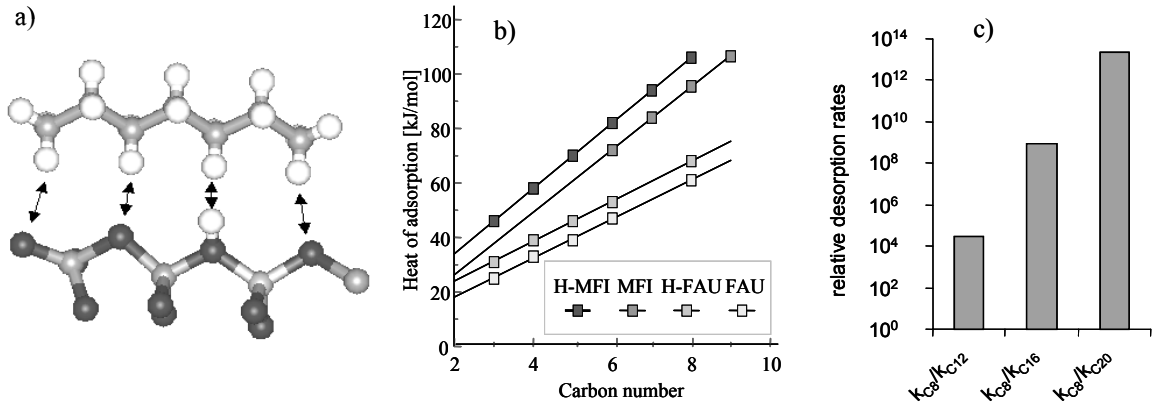

Figure 2-9: Effect of the chain length of hydrocarbons on the adsorption enthalpy and rates of desorption. A) Hydrocarbon in interaction with zeolite framework. B) Heat of adsorption as a function of carbon number for zeolites MFI and FAU in the acidic and non-acidic form. C) Relative desorption rates of a C_{12}, C_{16} and C_{20} alkane compared to octane.

Also typical for molecular sieves is the increasing heat of adsorption of hydrocarbons with increasing chain length (112). Each C-atom contributes equally to the total heat of adsorption. This value depends on the pore size and shape, so that in different zeolites different adsorption enthalpies are measured. Increasing framework density (number of T-atoms per volume) leads to increased heats of adsorption (113, 114). Protons add another constant value, which depends on the chemical composition, to the overall heat of adsorption. This is represented in Figure 2-9 a) and b). This phenomenon is responsible for different

apparent activation energies for a given reaction found with hydrocarbons of different chain length. The actual intrinsic activation energies (as well as the corresponding pre-exponential factors) are nearly constant (115). Assuming the relation between chain length and adsorption enthalpy to be linear over a wide range, relative desorption rates for different hydrocarbons can be calculated for a given temperature. Thus, using the data for H-FAU and a temperature of 75°C, the desorption of a C_{12} molecule is four orders of magnitude slower than an C_8 molecule, a C_{16} is eight and a C_{20} is twelve orders of magnitude slower (Figure 2-9 c). These huge differences give a feeling for the difficulties of removing heavy products from the zeolite surface using purely adsorption/desorption arguments. Once such a heavy molecule has formed, it is unlikely to desorb.

2.3.2.2 Brønsted acid sites

Zeolites exhibit a considerably lower proton (acid site) concentration than liquid acids. For example, 1g of H_2SO_4 contain $20 \cdot 10^{-3}$ moles of protons, whereas 1g of zeolite HY, with Si/Al ratio of five, contain no more than $3 \cdot 10^{-3}$ moles of protons. Note that this is a crude approximation of the acidic protons available for catalysis, because it assumes that with both materials all protons are available and catalytically active. Additionally, 1g of H_2SO_4 occupies far less volume (i.e., 0.5 cm^3) than the equivalent mass of zeolites (4-6 cm^3).

Fundamentally different to liquid acids, zeolites encompass different populations of sites differing substantially in their nature and strength. Liquid acids with a certain composition have a well-defined acid strength. This is not the case for zeolites. Depending on the type of zeolite, its aluminum content and the exchange procedure, Brønsted and Lewis acid sites with a wide range of strength and concentration are present. To summarize the effects of all parameters influencing the acidity of zeolites is beyond the scope of this review.

The different reaction steps in alkylation require different minimum acid strengths to be effectively catalyzed. Double bond isomerization is catalyzed already by weak acid sites. Even a fully deactivated zeolite retains some activity for isomerizing butenes (116, 117). Dimerization/oligomerization also does not require strong acidity. This was concluded from a study of a series of USY zeolites with different unit cell sizes. Correlations between the acidity and the alkylation performance revealed that the acid strength required performing the different reactions occurring during alkylation decreases in the order: cracking > alkylation (addition of butene to a tertiary butyl) > dimerization (addition of a butene to a secondary

butyl) (118). A comparison between the iso-structural H-SAPO-37 and H-FAU as alkylation catalysts showed that the H-FAU has a much higher relative concentration of strong acid sites than the H-SAPO-37. For this reason, the H-SAPO-37 mainly catalyzed dimerization, with a small amount of 3,4-DMH as the most abundant saturated compound. The H-FAU produced mainly TMPs (119).

The lifetime of zeolitic alkylation catalysts depends on the concentration of Brønsted acid sites. This has been shown by Nivarthy *et al.*, using a series of zeolite H-BEA with increasing concentration of back-exchanged sodium. The sodium decreased the concentration of Brønsted centers, which led to a concomitant decrease in the measured catalyst lifetime during alkylation (76).

However, different opinions exist about the acid strength required for optimum alkylation performance with zeolites. Hydride transfer is the step that determines the product quality and the catalyst lifetime. Thus, it is crucial to know which conditions favor a high hydride transfer rate. From the above-presented studies, it can be concluded that stronger sites are necessary to effectively catalyze hydride transfer. Stöcker *et al.* synthesized and tested EMT and FAU samples with enhanced Si/Al ratios of 3.5 utilizing crown ethers. They explained the better performance of H-EMT with the higher ratio of strong-to-weak Brønsted acid sites as compared to H-FAU (120). Dealumination of the H-FAU led to better results because of additional small numbers of very strong acid sites. No direct proof was given to support this opinion (121). La-exchange of H-EMT led to a slightly better performance than H-EMT. This was also attributed to a higher ratio of strong-to-weak Brønsted acid sites (122). A similar conclusion was derived by Corma *et al.*, who compared USY, MOR, BEA, ZSM-5 and MCM-22. The relative decrease of activity for the formation of TMPs during time on stream was seen to depend on the concentration of strong Brønsted acid sites in the fresh zeolite (123). Diaz-Mendoza *et al.*, studied commercial REY, USY and BEA samples. In contradiction to the aforementioned groups, they found Brønsted sites with intermediate strength to be the appropriate sites for maintaining good alkylation performance (124).

It is well established, that with time on stream the sites strong enough for catalyzing hydride transfer deactivate first. In the first phase, the catalyst produces a mixture of saturated iso-alkanes usually with (near-) complete butene conversion, while in the second phase alkenes, mainly octenes, are produced at a substantially lower butene conversion. The product in this second phase resembles the product of the weakly acidic H-SAPO-37. The

mixture of butene-isomers found in the product stream in the second phase is close to the equilibrium composition. A typical example is depicted in Figure 2-10.

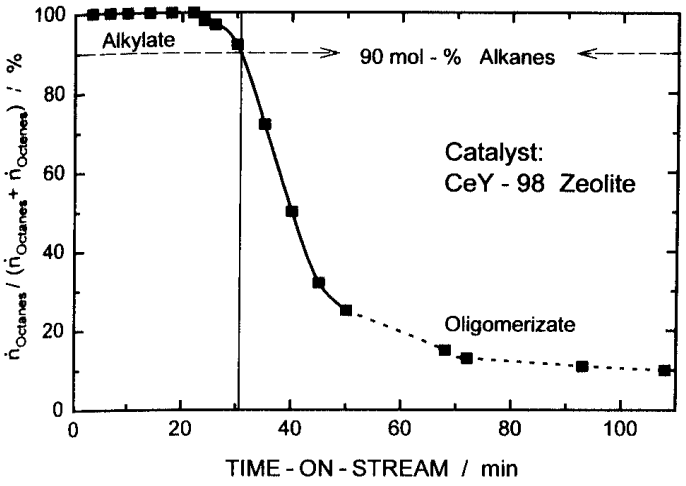

Figure 2-10: Typical time on stream behavior of a Ce-Y zeolite alkylated in a fixed bed reactor. Taken from reference (133).

Several studies in zeolite and other solid acid catalyzed alkylation obviously have been performed in the oligomerization regime (125-130). Due to insufficient acidity or wrong choice of reaction conditions, the catalysts examined in these studies produced mainly oligomerization products and only small amounts of true alkylate. Unequivocal conclusions can be drawn neither on the alkylation mechanism nor on the true alkylation activity of the tested materials under these circumstances.

The characterization method employed in nearly all abovementioned studies for measuring the strength of acid sites was pyridine adsorption/desorption monitored by IR. Pyridine forms the pyridinium ion on Brønsted acid sites and binds coordinately to Lewis acid sites. Heating the sample with the adsorbed pyridine gives a characteristic desorption curve for pyridine bound to Brønsted and Lewis centers respectively. From this set of data, Brønsted/Lewis ratios at a given temperature and "strong"-to-"weak" acid site ratios can be calculated and correlated to the catalytic performance. "Strong" and "weak" acid sites here are defined by the amount of pyridine adsorbed at a certain temperature. These temperatures are chosen in a rather arbitrary manner, the upper limit of which is typically restricted by the IR-cell and the zeolite itself (400°C – 550°C). The "strong" acid sites are not of uniform strength, but also most likely exhibit a broad distribution, up to a minute amount of "very strong" acid sites, which are hard to detect due to their low concentration. Whether such very strong sites are responsible for an enhanced alkylation activity is not proven yet.

2.3.2.3 Lewis acid sites / extra-framework aluminum

Lewis acid sites in zeolites originate from a partial destruction of the framework. During

the modification procedure, which is necessary to transform the parent material into its acidic form, part of the aluminum present in the framework is removed from its position (usually during calcination in a water-containing atmosphere, i.e. high-temperature hydrolysis of Si-O-Al bonds) to give extra-framework aluminum species (EFAL). Some of the species formed in this way exhibit Lewis-type acidity. Another source of Lewis acid sites are metal ions on ion-exchange positions. However, most of these metals exhibit weaker Lewis-acidity than aluminum species. Lewis acid sites do not catalyze the alkylation reaction, but their presence undoubtedly influences the alkylation performance of zeolitic catalysts. It has been claimed that the presence of strong Lewis acid sites promotes the formation of unsaturated compounds (124). The favored production of unsaturated carbenium ions with increased Lewis-acidity was also evidenced by Flego *et al.*, studying the deactivation of a La-H-FAU zeolite in iso-butane/1-butene alkylation. Increasing catalyst activation temperatures led to higher Lewis acid site concentrations, which increased the formation of mono- and dienylic carbenium ions (98). Besides the ability to increase the rate of formation of unsaturated compounds, Lewis acid sites have been claimed to increase the paraffin/olefin ratio close to the Brønsted acid sites, through the adsorption/desorption equilibrium of the alkenes on the Lewis acid sites. The increased alkene concentration accelerates oligomerization and leads to premature deactivation (76). EFAL species also influence the acidity of neighboring Brønsted acid sites. Corma *et al.* examined zeolite H-BEA, which they exposed to several post-synthesis treatments, in order to change the framework and extra-framework composition. From the combined reaction and characterization data the authors concluded, that some cationic EFAL-species compensate the framework charge and other condensed EFAL-species block a fraction of the Brønsted acid sites, thus, lowering their concentration. On the other hand, they suggested a combined synergistic effect of dispersed cationic EFAL-species with framework hydroxyls to form Brønsted acid sites of enhanced acid strength (131). A further study of the same group showed that in samples with a high framework aluminum concentration, the removal of EFAL was detrimental to the catalytic performance, while in the samples with low framework aluminum content the catalyst activity increased after the removal of EFAL (132). The fact that mild steaming enhances the strength of Brønsted acid sites is known from other hydrocarbon reactions, such as alkane cracking and isomerization and toluene disproportionation. Selective poisoning of Brønsted acid sites with cesium has shown that only a minute amount of very strong sites is present in mildly steamed samples.

However, these sites are responsible for a drastic increase in activity (115). Residual sodium also exhibits a poisoning effect on "very strong" Brønsted acid sites. Small amounts of sodium were found to eliminate highly acidic centers created by the interaction of EFAL with protonic sites (133).

2.3.2.4 Silicon/aluminum ratio

The influence of the Si/Al ratio on the catalytic performance is mainly discussed in terms of changing concentration and acid strength of the protonic sites. The electrostatic forces induced by the presence of framework-aluminum are often neglected. With increasing aluminum concentration in the framework (i.e., with lower Si/Al ratio), the total concentration of acid sites in the protonic form increases. On the other hand, it is believed that the strength of the acid sites decreases with increasing aluminum concentration. At high aluminum concentrations also the thermal stability of the zeolites in their protonic forms is reduced, facilitating the formation of extraframework species (134). Examining a series of ultrastable Y zeolites, Corma *et al.* found the catalyst with the lowest Si/Al ratio to be best in time-on-stream behavior and TMP-selectivity. With decreasing Si/Al the ratio of stronger to weaker acid sites increased. This correlated to the alkylation/oligomerization ratio measured with the samples (118). The same trend was found by de Jong *et al.*, also testing a series of ultrastable Y zeolites in a semi-batch reactor (78). The authors also tested a zeolite BEA with a Si/Al ratio of 15 that performed better than the Y zeolites. They postulated that a decrease of the Si/Al ratio in BEA also should lead to a superior catalyst through a higher Brønsted acid site concentration. Weitkamp and Traa also accentuated this hypothesis (135). Some studies have been devoted to the influence of the Si/Al ratio in zeolite BEA. Corma *et al.* used different BEA samples synthesized with different Si/Al ratios and found a higher thermal stability towards dealumination with increasing Si/Al ratio. The most stable catalyst was also the most active (136). Weitkamp *et al.* compared the selectivities of four different H-BEA samples with Si/Al ratios ranging from 12 to 90. The octane-selectivities ran through a maximum at a Si/Al ratio of 19, while the TMP/DMH ratio decreased continuously with the Si/Al ratio (137). Loenders *et al.* tested BEA samples with a range of framework Si/Al ratios from 13 to 77. The authors report that the individual acid sites perform an identical number of catalytic turnovers before deactivation, independent of the acid site density. They claim that the only way to enhance the activity and stability of zeolite BEA for iso-butane alkylation is

by increasing the aluminum content of BEA nanoparticles (138). The only study at present on zeolite BEA with a Si/Al ratio lower than 9 was performed by Yoo and Smirniotis, utilizing H-BEA synthesized with Si/Al ratios between 6 and 30 (139). In contrast to what was postulated earlier, the zeolites exhibited a maximum in the catalytic lifetime between a Si/Al ratio of 8.5 and 15. The hydrogen transfer activities measured separately with n-hexane were comparable for all the samples up to a Si/Al ratio of 15. The authors conclude that the BEA with the highest aluminum content performed worse than the other samples with the same hydride transfer activity due to lower crystallinity and micropore volume, which was inherent to the synthesis procedure for aluminum rich zeolite BEA. In a patent assigned to Mobil Oil, three BEA samples with Si/Al ratios of 7.3, 16.0 and 18.5 have been compared. The only detail given on the alkylation performance was the TMP/(C_8-TMP) ratio. This was seen to increase with decreasing Si/Al ratio, which is suggesting the superiority of the low Si/Al material (140).

Despite some obviously contradictory results published in the open literature, the above-presented data can be summarized as follows: The general trend is that high aluminum contents are beneficial for the alkylation performance. This opinion is supported by results from cracking experiments over zeolites with various Si/Al ratios. The bimolecular hydride transfer step is favored in low Si/Al ratio materials (52, 141, 142). Thus, low Si/Al ratio zeolites should exhibit better time-on-stream behavior.

Zeolite X is the large pore zeolite with the highest aluminum content possible. The first studies in zeolite-catalyzed alkylation were done on this material (11, 143). Weitkamp, comparing highly cerium-exchanged Y and X zeolites, found the Ce-X to exhibit a two times higher lifetime than the Ce-Y due to a higher concentration of acid sites (144). In the light of these findings, it is surprising that only a small number of studies were devoted to this material. As the purely protonic form of zeolite X is unstable, polyvalent metal cations have to be introduced to induce acidity (see Chapter 2.3.2.5). A variety of di- and trivalent metals has been examined, with and without additional ammonium-exchange (145-147). Rare earth elements, especially lanthanum, obviously are suited best, producing highly acidic and thermally stable catalysts. La-Ca-X has also been proposed as an excellent iso-butane/ethene alkylation catalyst (148, 149). Falsely, the authors attribute this to super-acid centers with a narrow acidity distribution.

2.3.2.5 Metal cations on ion-exchange positions

Rare earth exchanged faujasites (REHY and REUSY) are widely used in the fluid catalytic cracking process (134). Aqueous ion exchange with rare earth salts in faujasites leads to removal of ions in the supercage only. This is due to a bulky hydration sphere around the ions, which is larger than the 6-membered ring of the sodalite cage. Calcination removes the hydrate and the naked ion is able to move into the sodalite cage forming cationic polynuclear hydroxy complexes (150-152). These species impart thermal and hydrothermal stability to the material. Rare earth exchanged zeolites exhibit considerable Brønsted acidity due to a hydrolysis of the hydrated rare earth ions (153, 154). This principle works with most polyvalent metals, but rare earth elements induce the highest acidity and best stability (155-157).

Besides zeolite X (discussed in Chapter 2.3.2.4), mainly zeolite Y was subject to metal-ion exchange. The researchers at Sun Oil extensively explored rare earth exchanged Y zeolites (12). From their work described in a number of patents (147, 158-162), it can be concluded that partially rare earth exchanged faujasites are more active catalysts than the purely protonic form. The importance to remove the sodium from the zeolite quantitatively was demonstrated. Chu and Chester compared different modified Y zeolites. REHY gave the highest yield and the best product quality. Dealumination of REHY did not improve the performance. USY and REUSY both showed low conversion and yield, without significant differences. In their work on EMT and FAU zeolites, the SINTEF group compared H- and La-exchanged samples. It could be shown, that a partially La-exchanged catalyst is superior to both fully La-exchanged and pure H-form samples. H-EMT contains the highest total number of Brønsted acid sites as measured with pyridine adsorbed at 150°C. The partially La-exchanged sample (51% exchange degree) has a two times higher concentration of strong Brønsted acid sites as measured with pyridine retained at 550°C and also has a lower concentration of Lewis acid sites (122, 163). The increase in acid strength has been rationalized by a withdrawal of electrons from the Lewis-base framework oxygens through polyvalent La-cations in the sodalite cages similar to EFAL species in steamed zeolites. The abstraction of electrons weakens the O-H bond and, thus, increases the acid strength of the proton (152). In a patent assigned to Mobil Oil, rare earth exchange in zeolite ZSM-20 (intergrowth between FAU and EMT) has been claimed to improve conversion and selectivities to TMPs. REZSM-20 was also claimed to perform better than REHY (164). In

another Mobil patent REY and REUSY were compared. The REY exhibited a slightly higher alkylate quality, while the REUSY had a slightly higher conversion (165). The subtle differences in the reports are, however, difficult to evaluate as the detailed characterization of the materials is lacking most of the times. In the light of the strong influence of the concentration of Brønsted and Lewis acid sites a judgment, which of the materials has the best properties, is not possible.

2.3.2.6 Structure types of zeolites

Only large pore zeolites exhibit sufficient activity and selectivity for the alkylation reaction. Chu and Chester found ZSM-5 as a typical medium pore zeolite to be inactive under typical alkylation conditions (116). This was explained by diffusion limitations in the pores. Corma *et al.* tested H-ZSM-5 and H-MCM-22 samples at 50 °C. The ZSM-5 exhibited a very low activity with a rapid and complete deactivation and produced mainly dimethylhexanes and dimethylhexenes. The authors claim that alkylation takes place mainly at the external surface, while dimerization, which is less sterically demanding, proceeds in the pore system. At temperatures above 150°C Weitkamp and Jacobs found ZSM-5 and ZSM-11to be active (166). The product distribution was very different from a typical alkylate; it contained much more cracked products, trimethylpentanes were absent and considerable amounts of monomethyl-isomers, n-alkanes and cyclic hydrocarbons were formed. This behavior was explained by steric restrictions preventing the formation of highly branched carbenium ions. Reactions with the less branched or non-branched carbenium ions require higher activation energies, so that higher temperatures are necessary.

MCM-22, with larger pore void space than ZSM-5, revealed a behavior in between large and medium pore size zeolites (123). Unverricht *et al.* also examined MCM-22. At 80°C and 120°C, it was found to produce mainly cracked products and dimethylhexanes and deactivated rapidly (137). MCM-36 gained considerable interest in the patent-literature (167-170). MCM-36 is a pillared zeolite based on the structure of MCM-22. Ideally, it should contain mesopores between layers of MCM-22 crystallites. This structure was found to be much more active and stable than MCM-22 (171). Alkane cracking experiments on zeolites with different pore dimensions evidenced the preference of monomolecular over sterically more demanding bimolecular pathways, such as hydride transfer, in small and medium pore zeolites (142).

Unlike in medium pore zeolites, the product distributions in large pore zeolites resemble typical alkylates. However, within the distribution, significant changes are observed. It is very difficult to separate the influence of the structure from other properties, mainly the acid site strength and concentration, on the alkylation reaction. Undisputable results may only be achieved if all other parameters stay constant. Yoo *et al.* compared USY, BEA, MOR, LTL and ZSM-12 zeolites with a Si/Al ratio between 20 and 34 (achieved either by direct synthesis or by various leaching techniques) and acid site densities between 0.4 and 0.7 mmol/g. These structure types were chosen because they represent 3-, 2- and 1-dimensional zeolites. The authors claim that most other factors influencing the performance besides the structure have been minimized. Zeolite BEA exhibited the best time-on-stream behavior with respect to lifetime and TMP selectivity. ZSM-12 also showed a long lifetime, but catalyzed oligomerization instead of alkylation. USY, MOR and LTL were found to deactivate quickly, with LTL retaining a surprisingly stable TMP selectivity also at low conversion levels. No heavy coke molecules were found in zeolite BEA and ZSM-12. The authors conclude that zeolites without periodic expansions do not allow extensive coke formation and hence deactivate at a slower rate (172). Unfortunately, no details about the concentration and strength of the acid sites on the samples were given. The finding that zeolite BEA does not produce significant amounts of coke is at variance with results of other research groups. For example, Nivarthy *et al.* calculated values of about 14 wt.-% of deposit formed over H-BEA zeolites (46). In the already mentioned study by Corma *et al.*, USY, BEA and MOR were compared next to ZSM-5 and MCM-22. The three large pore zeolites exhibited similar C_8-selectivities but different TOS-behavior. This was attributed to differences in the acidity of the samples (123). In a comparative study on the acidity of low Si/Al ratio zeolites BEA, ZSM-20, Y and dealuminated USY the acid strength was derived in the following order: H-BEA > H-USY > H-ZSM-20 > H-Y (173)

In another article by Corma *et al.* ITQ-7, a three-dimensional large pore zeolite, was tested as alkylation catalyst and compared to a BEA sample of comparable Si/Al ratio and crystal size. The ratio of the selectivities to 2,2,4-TMP and 2,2,3-TMP, which have the largest kinetic diameter of the TMPs, and 2,3,3-TMP and 2,3,4-TMP, which have the lowest kinetic diameter, was used as a measure for the influence of the pore structure. Lower (2,2,4-TMP + 2,2,3-TMP)/(2,3,3-TMP + 2,3,4-TMP) ratios in ITQ-7 were attributed to its smaller pore diameter. The bulky isomers have more spacious transition states so that their formation will

be hindered in narrow pores. Moreover, their diffusion will be slower. The hydride transfer activity, estimated by the dimethylhexane/dimethylhexene ratio, was found to be lower in ITQ-7 than in H-BEA. This was also explained by the smaller pore diameter, because the acidity of the two different zeolites was found to be similar (174). Nivarthy *et al.* compared the three large pore zeolites H-BEA, H-FAU and H-EMT. The lifetimes of the zeolites were found to depend on the Brønsted acid site concentration; H-BEA with the lowest Brønsted acid site concentration gave the shortest and H-EMT with the highest concentration the longest lifetime. Significant differences were seen in the TMP distribution. H-BEA exhibited a very high 2,2,4-TMP selectivity, which was attributed to a lower rate of hydride transfer vs. isomerization of the precursor carbenium ions (175). An exceptionally high 2,2,4-TMP selectivity is characteristic for zeolite BEA. While with most other zeolites the selectivities vary depending on the conditions employed, BEA always produces high amounts of 2,2,4-TMP.

The research group at SINTEF dedicated a series of papers to the examination of FAU and EMT zeolites comparing them in their H- and La-exchanged form with and without dealumination. EMT was always superior to FAU. The alkylate yield, expressed as mass alkylate produced divided by the catalyst mass, was higher for the EMT samples. EMT also produced a higher amount of trimethylpentanes as compared to the FAU samples. The differences between the two materials were discussed in terms of the slightly larger supercage in EMT, which is claimed to reduce the steric constraints on the bulky transition states for hydride transfer, and in terms of acidity, with EMT samples exhibiting a higher concentration of Brønsted acid sites retaining pyridine at high temperatures (120, 121, 176). A comparison of La-EMT, La-FAU and La-BEA revealed that the La-BEA performed worse than the two other materials, both in alkylate yield and selectivity (163), but the lack of information on the acidity of the samples prevents a detailed evaluation of this report.

Recently, mesoporous aluminosilicates with strong acidity and high hydrothermal stability have been synthesized via self-assembly of aluminosilicate nanoclusters with templating micelles. The materials were found to contain both micro- and mesopores and the pore walls consist of primary and secondary building units, which might be responsible for the acidity and stability. These materials were tested in iso-butane/n-butene alkylation at 25°C and showed a similar time-on-stream behavior than zeolite BEA. No details on the product distribution were given (177).

The patent literature discloses alkylation performances of several additional structure types. A Mobil patent describes the use of VTM-A, a pillared titanosilicate of the MCM-27 family. The catalyst produced about 80 wt.-% of octanes under relatively mild conditions (OSV = 0.05h^{-1}, P/O ratio = 20) (178). A number of patents describe the use of MCM-36. MCM-49, which is closely related to MCM-22, has also been tested as alkylation catalyst. In general, these materials require a higher reaction temperature to be sufficiently active, which inevitably leads to high cracking and high DMH selectivities (168, 179-183).

2.3.3 Other solid acids

2.3.3.1 Sulfated zirconia and related materials

Besides zeolites, a variety of solid acids has been tested as alkylation catalysts. Sulfated zirconia and related materials received considerable interest because of their super-acidic nature and ability to isomerize short linear alkanes at temperatures below 150°C. Corma *et al.* compared sulfated zirconia and zeolite BEA at reaction temperatures of 0°C and 50°C in iso-butane/2-butene alkylation. While BEA catalyzed mainly dimerization at 0°C, the sulfated zirconia exhibited a high selectivity to TMPs. At 50°C, on the other hand, zeolite BEA produced more TMPs than sulfated zirconia, which under these conditions produced mainly cracked products with 65 wt.-% selectivity. The TMP/DMH ratio was always higher for the sulfated zirconia sample. These distinctive differences in the product distribution were attributed to the much stronger acid sites in sulfated zirconia as compared to zeolite BEA. The strong sites preferentially catalyzed cracking reactions, and allowed hydride transfer at lower temperatures than the zeolitic acid sites. The time-on-stream behavior was more favorable for BEA, which deactivated at a slower rate than sulfated zirconia. Whether differences in the adsorption of the feed and product molecules influenced the performance was not discussed (184). In a subsequent publication, two sulfated zirconia samples with different sulfuric acid loading were tested as alkylation catalysts with iso-butane/2-butene feed at temperatures between –10°C and 50°C. The sample with the higher sulfur loading was slightly more active in the initial reaction phase, while for both catalysts deactivation was comparably rapid. The alkylation/cracking ratio increased when decreasing the reaction temperature. 2,2,4-TMP was the dominating octane isomer under all conditions, less dimethylhexanes and octenes were produced as compared to zeolitic catalysts (20). In another

study by the same authors sulfate-doped ZrO_2, TiO_2 and SnO_2 were prepared utilizing various sulfation and activation procedures. The acidity decreased in the order $SO_4^{2-}/ZrO_2 > SO_4^{2-}/TiO_2 > SO_4^{2-}/SnO_2$, which was reflected in the cracking activity of the samples. All oxides showed considerable sensitivity towards the modification procedure, each with a different optimum. All samples rapidly deactivated and additionally lost significant fractions of the originally present sulfur (185). Satoh *et al.* also compared several sulfated metal oxides. The samples were tested in the gas-phase at 0°C (186). This is an inappropriate procedure, because most of the products are liquid under these conditions and will stay in the catalyst pores. The authors of a pulsed gas-phase alkylation study over sulfated zirconia also concluded that below 50°C the TMPs could not desorb from the pores. Raising the temperature to 100°C led already to dehydrogenation of iso-butane (187, 188). Other gas-phase alkylation studies on sulfated zirconia were reported by Das and Chakrabarty (189) and Guo et al. (190, 191). Working in the liquid phase and employing relatively mild conditions, Xiao *et al.* could extend the lifetime of a sulfated zirconia catalyst to over 70 hrs. In the initial phase, the catalyst produced 80 wt.-% cracked products, which fell below 20 wt.-% after 30 hrs TOS with an increase in TMP-selectivity to over 60 wt.-%. Within the TMPs, 2,2,4-TMP reached selectivities higher than 60 wt.-%. Platinum promoted sulfated zirconia and tungstated zirconia were much less active alkylation catalysts (192). An interesting variation on sulfated metal oxide type catalysts has been presented by Sun *et al.* The authors impregnated a dealuminated zeolite BEA with Ti and Fe salts and subsequently sulfated the material. The samples exhibited a better time-on-stream behavior in the iso-butane/1-butene alkylation (reaction temperature not given) than H-BEA and a mixture of sulfated zirconia and H-BEA. The product distribution was also better for the sulfated metal oxide impregnated BEA samples. These results were explained with the higher concentration of strong Brønsted acid sites of the composite materials as compared to H-BEA (193).

2.3.3.2 Heteropolyacids

Heteropolyacids are strongly acidic nonporous solids. Salts of these acids containing large cations, such as Cs^+, K^+, Rb^+, and NH_4^+, exhibit surface areas in the order of 150 $m^2\ g^{-1}$. Supporting heteropolyacids on highly porous carriers is another way to increase the surface area. This was done by Blasco *et al.*, who supported 12-tungstophosphoric acid on silica, on a high surface area amorphous aluminosilicate and on all-silica mesoporous MCM-41. These

materials were tested in iso-butane/2-butene alkylation at 33°C. The acid supported on silica performed best, with high initial activity and selectivity to trimethylpentanes. Heteropolyacids supported on the aluminosilicate strongly interacted with the support, which decreased the acidity, thus, leading to lower activity and selectivity. Heteropolyacids on MCM-41 were seen to block the pores of the support partly, so that a fraction of the acid was inaccessible to the reactants. This could be decreased by using a MCM-41 with larger pore diameter. All materials rapidly deactivated (194). Potassium salts of 12-tungstophosphoric acid have been tested with various potassium loadings to modify acidity and porosity by Gayraud *et al*. The samples were tested at sub-and supercritical conditions. Samples with high potassium content exhibited better time-on-stream behavior and selectivities. The authors claimed that high acid site density was detrimental for the alkylation reaction, leading to increased oligomerization activity. This is in contradiction to the generally accepted theory that high acid site densities enhance the alkylation activity. The results can be better explained by the decrease in surface area with decreasing potassium content, which was found to decrease from 156 to 50 m^2 g^{-1} (195). Cesium salts of 12-tungstophosphoric acid have been compared to the pure acid and to a sulfated zirconia sample with iso-butane/1-butene at room temperature. The salt was much more active than both the acid and the sulfated zirconia (196). Heteropolyacids have also been supported on sulfated zirconia catalysts. The combination was found to be superior to heteropolyacid supported on pure zirconia and on zirconia and other supports treated with a variety of mineral acids (197). Solutions of heteropolyacids (containing phosphorous or silicon) in acetic acid have been tested as alkylation catalysts at 50°C by Zhao *et al*. The system was sensitive towards the ratio of heteropoly acid/acetic acid and the amount of crystal water. Similar to conventional liquid acids a polymer was formed, which enhanced the catalytic activity (198).

2.3.3.3 Acidic organic polymers

Nafion-H, a perfluorinated sulfonic acid resin, is another strongly acidic solid with H_0 comparable to sulfuric acid. Rørvik *et al.* examined unsupported Nafion-H with a surface area of 0.2 m^2 g^{-1} in iso-butane/2-butene alkylation at 80°C and compared it with a Ce-Y zeolite. The zeolite gave a better alkylate and higher conversion than Nafion-H, which produced significant amounts of octenes and heavy-end products. The low surface area of the resin probably makes the comparison inadequate (199). To increase the insufficiently small

surface area, the resin can be supported on porous carriers, or it can directly be incorporated into silica using a sol-gel technique. Both methods have been utilized by Botella *et al.,* who compared several composite nafion/silica samples with varying surface area and Nafion loading in iso-butane/2-butene alkylation at 80°C. In addition, supported and unsupported Nafion samples were used. Like above, the unsupported resin with its low surface area performed only poorly. Interestingly, the composite materials showed a maximum of performance at intermediate surface areas. This was explained by an interaction between the sulfonic groups of the resin with the silanol groups of the silica, decreasing the acid strength of the resin. The supported resin showed similar activity and selectivity than the composite material of the same Nafion content. Temperature variations from 32°C to 80°C showed that the material produces oligomers at low temperatures and saturated products at higher, indicating in this way an acid strength in the range of zeolite BEA and lower than sulfated zirconia (200).

2.3.3.4 Supported metal halides

Supported metal halides gained considerable attention, which is reflected in at least three companies having tested such catalysts in pilot plants (201). Chlorinated alumina, obtained by reacting alumina with hydrogen chloride, is a highly Brønsted-acidic and porous solid. This material is related to the Friedel-Crafts catalyst aluminum chloride, which was one of the first compounds tested in alkylation. Similar catalysts are used in commercial isomerization plants. A series of chlorinated alumina samples modified with Li^+ and Na^+ cations was prepared and tested by Clet *et al.* in iso-butane/2-butene alkylation at 0°C. Cation modification was performed to moderate the acidity of the material. It could be shown that in this way excessive cracking is prevented and the time-on-stream behavior is superior to the unmodified sample. This was attributed to a selective annihilation of very strong acid sites by the basic cations. The degradation of 2,2,4-TMP on these catalysts at 0°C was also studied. 2,2,4-TMP was surprisingly reactive under these conditions and gave a product resembling an alkylate but with more dimethylhexanes, light- and heavy-end products. While emphasis was put on the explanation of the rearrangement steps for producing dimethylhexanes and cracked products, the initiation of the 2,2,4-TMP degradation was not discussed (202). These catalysts are also described in a patent application assigned to Total (203).

A similar type of catalyst including a supported noble metal for regeneration, its use and

preparation has been extensively described in a series of patents assigned to UOP. The catalysts were prepared by the sublimation of metal halides, especially aluminum chloride and boron trifluoride, onto an alumina carrier modified with alkaline or earth-alkaline metal cations. The noble metal was preferably deposited in an eggshell concentration profile (204-209). An earlier patent assigned to Texaco describes the use of chlorinated alumina in the iso-butane alkylation with higher olefins, especially hexenes. TMPs were supposed to form *via* self-alkylation (210). Fluorinated alumina and silica samples were also tested in iso-butane alkylation, but were found to produce mainly heavy-end products under the employed conditions (211).

Patents assigned to Mobil describe the use of boron trifluoride supported on several porous carriers. BF_3 supported on silica was found to exhibit a slightly higher performance with added water in the alkylation of a mixed alkene feed at 0°C. It was also shown that self-alkylation activity was considerably lower than with HF as catalyst (212). Another patent describes the use of a pillared layered silicate, labeled MCM-25, promoted with BF_3 to give a high quality alkylate at around 0°C (213). BF_3 was also supported on zeolite BEA, with adsorbed water still present. This composite catalyst exhibited low butene isomerization activity, which was evident from the inferior results obtained with 1-butene. At very low reaction temperatures the product quality was superior to HF alkylate (214). Triflic acid has also been supported on a porous silica carrier. Emphasis was put on a strong interaction between the acid and the support, to prevent leaching of the acid. In pulsed liquid-phase iso-butane/1-butene alkylation experiments at 25°C, the catalysts produced a very high quality alkylate nearly exclusively made up of isooctanes. With silanol groups on the silica surface or with added water triflic acid was found to form a monohydrate firmly grafted on the silica surface (215).

2.3.4 The influence of process conditions

The choice of appropriate reaction conditions is crucial for optimized performance in alkylation. The most important parameters are the reaction temperature, the feed paraffin/olefin ratio, the olefin space velocity, the olefin feed composition and the reactor design. Changing these parameters will induce similar effects independent of the chosen catalyst. Nevertheless, the sensitivity towards changes is different for the individual catalysts.

Table 2-2 summarizes the most important parameters employed in industrial operations for different acids. The values given for zeolites represent best estimates of data available from laboratory and pilot scale experiments.

Two points should be marked here: (i) Zeolites can be successfully operated at the same or higher severity (with respect to P/O and OSV) than the liquid acids. (ii) The catalyst productivity of zeolites is in the same order of magnitude as of sulfuric acid. Comparing the intrinsic activity of zeolites (0.5-3 mmol acid sites per gram acid) with that of sulfuric acid (20 mmol acid sites per gram acid), zeolites outperform sulfuric acid. Nevertheless, the price of a zeolitic catalyst and the high costs for effective regeneration sets high hurdles for a competition with sulfuric acid catalyzed processes.

Table 2-2: Typical values of important process parameters. The numbers for the liquid acids are taken from references (10, 21, 216). As zeolites are not used industrially so far, the given values represent the view of the authors extracted from laboratory and pilot scale data in a slurry reactor.

	HF	H_2SO_4	Zeolites
Reaction temperature (°C)	16-40	4-18	50-100
Feed paraffin/olefin ratio (mol/mol)	11-14	7-10	6-15
Olefin space velocity (kg_{Olefin}/kg_{Acid} hr)	0.1-0.6	0.03-0.2	0.2-1.0
Exit acid strength (wt.-%)	83-92	89-93	-
Acid per reaction volume (vol.-%)	25-80	40-60	20-30
Catalyst productivity ($kg_{Alkylate}/kg_{Acid}$)	1000-2500	6-18	4-10

2.3.4.1 Reaction temperature

The reaction temperature affects both the chemistry of alkylation through the activation energies of the individual reaction steps and the solubility/adsorption and diffusion of products and reactants. With sulfuric acid, also the viscosity is strongly influenced by the temperature. Dispersion effects are, thus, setting the lower temperature limit with sulfuric acid. Temperatures below 4°C inhibit the separation of acid from the hydrocarbon phase and lead to acid carryover from the acid settler. At temperatures exceeding 18°C, polymerization reactions dominate, which leads to increased acid consumption and low octane numbers (10).

The higher solubility of iso-butane in HF and its lower viscosity allow higher iso-butane consumption rates to be applied with HF. For this reason, HF can be operated at higher temperatures resulting in higher reaction rates. This also reduces the refrigeration costs. Instead of a true refrigeration system, cooling water can be used. Nevertheless, the product quality is higher when operating at the lower temperature limit. With increasing temperature the significance of side reactions increases. Oligomerization/cracking is of higher importance at higher temperatures, reducing the selectivity to trimethylpentanes.

Zeolites in principle operate at significantly higher reaction temperatures. This is due to the lower acid strength of zeolites or the lack of solvation resulting in higher activation energies for the individual reaction steps. Efficient mobility in the zeolitic micropores also requires higher temperatures. The temperature optimum is in the range of 50 to 100°C, the exact value depending most likely on the individual sample. This problem is very often overlooked, when testing and comparing different catalysts. Testing catalysts at sub-optimum temperatures leads to false conclusions about the true alkylation performance. Nivarthy *et al.* found a temperature optimum for zeolite H-BEA at 75°C, at which the highest octane-selectivity and the highest TMP/DMH ratio was achieved. At lower temperatures oligomerization and at higher temperatures cracking reactions dominated (46). Kirsch *et al.* tested various rare earth exchanged Y zeolites at temperatures from 25 to 100°C. A sample with 0.2 wt.-% residual sodium had a temperature optimum around 40°C, while a sample with 1.0 wt.-% sodium performed best at 80°C (12). Taylor and Sherwood examined the influence of several process parameters on the performance of a USY zeolite. The catalyst was tested at 38, 66 and 94°C. While the TMP-selectivity steadily decreased with increasing temperature, the highest lifetime was achieved at 66°C (217). Pronounced effects on the product selectivities were also seen by Corma *et al.*, using a H-BEA at 50 and at 80°C. At the higher temperature, the activity was higher, as seen in the increased conversion. The selectivity to cracked products increased drastically, also the C_{9+}-selectivity increased. Within the TMP-fraction, 2,2,4-TMP increased considerably with the temperature (136). Feller *et al.* performed a detailed study on the influence of the reaction temperature in the range 40 to 130°C on a La-X zeolite. The catalyst-lifetime strongly depended on the reaction temperature with an optimum at 75°C. The product quality was highest at low temperatures; with increasing temperatures, increasingly more cracked and heavy compounds are produced. The TMP/DMH ratio constantly declined with temperature (87). The selectivity phenomena can

be explained by the relative rates of the individual reaction steps. β-Scission and presumably also alkene addition require higher activation energies than hydride transfer. Increase in temperature consequently leads to higher relative rates of secondary products from multiple alkylation and cracking. Cracked products are favored over multiple alkylation products, because the activation energy is higher for β-scission than for alkene addition, which is the (exothermic) reverse reaction. The bad performance of zeolites at low reaction temperatures is most likely due to the hindered diffusion of bulky molecules under such conditions. The catalyst will prematurely deactivate by pore blocking.

These diffusion problems are the reason why several research groups tried to overcome a buildup of heavy molecules in the catalyst pores by employing super-critical conditions. A super-critical reaction medium should combine liquid-like density with high oligomer solubilities and gas-like transport properties. Under such conditions, the bulky molecules that otherwise would deactivate the catalyst are supposedly more efficiently removed from the catalyst pores. The feed itself can be employed as supercritical medium, but the critical point of iso-butane is at 135°C and 36.5 bar. Performing the alkylation reaction under these conditions leads to excessive cracking. The catalyst stays active for longer TOS as compared to conventional operation, but produces cracked and especially substantial amounts of olefinic products (126, 127). To overcome the problems connected with the high critical temperature of iso-butane, carbon dioxide has been used as a diluent to reduce the critical temperature. The results presented by Clark and Subramaniam show that a stable conversion can indeed be maintained with a ten-fold excess of carbon dioxide at 50°C and 155 bar. However, the conversion was very low (<20 wt.-%) and the product contained only minor amounts of trimethylpentanes (218). Similar results were reported by Santana and Akgerman (219). Ginosar et al., testing a variety of super-critical solvents on a variety of different solid acids came to the conclusion, that working under super-critical conditions generally does not improve the alkylation performance (220). A temperature programmed oxidation analysis of samples coked under supercritical conditions revealed that the carbonaceous deposits are very similar in concentration and oxidizability as compared to coke produced under liquid-phase conditions. The slight changes were related to a smaller amount of coke on the outer surface of the zeolite (221).

2.3.4.2 Paraffin/olefin ratio and olefin space velocity

While the temperature influences the reaction rates *via* the activation energies, the feed composition determines the concentration term of the rate expressions. The crucial parameter that determines a high alkylate quality and a low acid consumption is the ratio of the hydride transfer and oligomerization rates. This ratio should be as high as possible. With high iso-butane concentrations the carbenium ion has a higher probability to react with an iso-butane molecule to form the desired product *via* hydride transfer rather than undergoing oligomerization with other alkenes, thus minimizing undesired reactions and acid consumption. Two process parameters influence the hydride transfer/oligomerization ratio: the feed paraffin/olefin (P/O) ratio and the olefin space velocity (OSV, which is the reciprocal of the residence time). The P/O ratio determines the concentration of iso-butane in the reactor, which in turn determines the rate of hydride transfer. Moreover, the significance of product degradation reactions depends on the product concentration.

Another point might be of importance although no quantitative data is available. Ideally, feed entering the reactor should be instantaneously mixed with the acid. The conversion of the alkene is generally complete, so that the internal P/O ratio might be 1000:1 and higher. In case of non-ideal mixing, the alkene concentration will be higher and consequently lead to higher rates of oligomerization and acid consumption. With high feed P/O ratios this problem will be minimized. Thus, increasing the P/O ratio increases alkylate quality and yield and decreases acid consumption. On the other hand, at high P/O ratios more iso-butane has to be recycled, which leads to increased separation costs. A balance has to be found in order to optimize the economical performance of the unit. The OSV determines the production rate of alkylate, so that high OSV would be economically favored. This is limited by high acid consumption, low octane and high heavy-end product formation at high OSV. In the case of sulfuric acid more esters are introduced into the products, which are corrosive to down-stream equipment (216). As first approximation for sulfuric acid catalyzed n-butene alkylation, an increase in OSV of 0.1 vol/(vol hr) leads to a decrease in RON of about 1, while an increase in the P/O from 8 to 9 leads to an increase in RON of 0.15 (10). The abovementioned higher solubility of iso-butane in HF allows higher space velocities in HF plants, although they are usually operated at higher P/O ratios.

In principle, the same rules hold true for zeolitic alkylation catalysts. A detailed study about the influence of PO and OSV on the performance of zeolite H-BEA in a CSTR has

been reported by de Jong *et al.* The authors developed a simple kinetic model, which was able to predict catalyst lifetimes as a function of P/O and OSV. Catalyst lifetimes (which is equivalent to the catalyst productivity, the reciprocal of acid consumption) increased with increasing P/O ratio and decreasing OSV. Additionally, the authors impressively demonstrate the superiority of CSTR- over PFR-technology (78). Qualitatively similar results were obtained by Taylor and Sherwood employing a USY zeolite in a CSTR. The authors stress the detrimental effect of unreacted alkene on lifetime and product quality (217). Feller *et al.* testing La-X zeolites in a CSTR found the catalyst productivity to be nearly independent of the OSV within the examined OSV-range. At higher OSV, the catalyst lifetime was shorter, but in this shorter time the same total amount of product was produced. The P/O ratio had only a moderate influence on the catalytic performance (87).

2.3.4.3 Olefin feed composition

Propene, 1-butene, 2-butene, isobutene, normal- and iso-pentenes can be used as feedstock in alkylation. Depending on the catalyst, they will give different alkylate quality and yield with differing acid consumption. Only linear butenes give a fairly low acid consumption in sulfuric acid catalyzed processes. All other alkenes lead to an up to three times higher acid consumption (10). Hydrofluoric acid consumption is nearly independent of the employed feed alkene (222). The low double bond isomerization activity of HF leads to higher production of dimethylhexanes, when using 1-butene. The high self-alkylation activity of HF is responsible for a high fraction of TMPs in the alkylate when employing alkenes other than butenes. Table 2-3 compares alkylate compositions for both liquid acid catalyzed reactions with different feed alkenes. It can be seen that H_2SO_4 produces a better alkylate with 1-butene, while HF gives better results with propene and isobutene. The product from 2-butene and also from pentenes (not shown in Table 2-3) is comparable with both acids.

Zeolites also have been tested with feed alkenes other than butenes. Daage and Fajula performed an iso-butane/propene alkylation study on a Ce-Y zeolite with ^{13}C-labeled feed molecules. The products could be grouped into three classes: dimerization leading to C_6 products, alkylation leading to C_7 and self-alkylation leading to C_8 and also to C_7 products (223). Studies by Guisnet *et al.* comparing 2-butene and propene as feed alkenes on a USY zeolite gave similar results. Self-alkylation was slower by a factor of two than the alkylation of iso-butane with propene and faster by a factor of two than the dimerization of propene.

The conversion in iso-butane/propene alkylation was considerably lower than in iso-butane/2-butene alkylation (67, 91).

Table 2-3: Compositions of alkylates with different feed alkenes and different acids as catalyst. Taken from references (48, 224).

	Alkene							
	Propene		Isobutene		2-butene		1-butene	
Component, wt.-%	HF	H_2SO_4	HF	H_2SO_4	HF	H_2SO_4	HF	H_2SO_4
C_5								
Isopentane	1.0	3.8	0.5	10.0	0.3	4.2	1.0	4.7
C_6								
Dimethylbutanes	0.3	4.2	0.8	5.2	0.7	4.6	0.8	4.4
Methylheptanes	0		0.2		0.2		0.3	
C_7								
2,3-Dimethylpentane	29.5	50.4	2.0	2.6	1.5	1.4	1.2	1.5
2,4-Dimethylpentane	14.3	20.8	0	3.9	0	2.4	0	2.6
C_8								
2,2,4-Trimethylpentane	36.3	4.4	66.2	28.7	48.6	30.6	38.5	30.5
2,2,3-Trimethylpentane	0		0		1.9		0.9	
2,3,4-Trimethylpentane	7.5	3.7	12.8	23.1	22.2	41.6	19.1	39.1
2,3,3-Trimethylpentane	4.0		7.1		12.9		9.7	
Dimethylhexanes	3.2	1.7	3.4	9.5	6.9	9.0	22.1	11.0
C_{9+} products	3.7	11.0	5.3	17.1	4.1	6.3	5.7	6.2

A comparative study on zeolite H-BEA catalyzed alkylation of iso-butane with 2-butene, propene and ethene was published by Nivarthy *et al.* The reactivity of the alkenes was decreasing in the order 2-butene > propene > ethene. Here, the products also can be grouped into dimerization, alkylation and self-alkylation products. Dimerization is especially

important with ethene, forming n-butenes, which react in the normal way to octanes. The distribution within the C_8-fraction was almost identical, when using ethene instead of 2-butene. Ethene exhibits such a low reactivity, because it can only form primary carbenium ions, the formation of which requires high activation energies (225). Ethene is reactive with $AlCl_3$/HCl, but not with sulfuric and hydrofluoric acid. Iso-butane/ethene alkylation has been examined also independently of iso-butane/butene alkylation. Early studies on zeolite REHX tested ethene as feed alkene (11). At 27°C, the product was mainly made up of hexanes, while at temperatures as high as 149°C, isopentane dominated, with hexanes and octanes being the main other products. KTI developed a process, which utilizes ethene from FCC off-gases to produce alkylate on a zeolitic catalyst with a "dimerization function" (226). The catalyst as disclosed consists of a RE-Ca-X zeolite impregnated with palladium as the "dimerization function" (148). Operated at 50-70°C the catalyst produces a very high amount of octanes, and nearly no hexanes (149, 227, 228). As a non-zeolitic catalyst, chlorided alumina was also tested in iso-butane/ethene alkylation between 0 and 100°C. Catalyst stability was better at low temperatures. Hexanes constituted the main product fraction, especially at high P/O ratios (229). Thermodynamically, hexanes should be strongly favored over octanes and higher products (230).

2.4 Industrial processes and process developments

In this chapter, the alkylation process technology will be reviewed. The liquid acid based processes, which are all mature technologies, will be briefly described. Additionally, information on process developments based on solid acids will be given.

2.4.1 Liquid acid catalyzed processes

As already discussed in chapter 2.3.1, all processes require intensive mixing of acid and hydrocarbon phases to form emulsions. The droplets have to be small enough to give a sufficiently large phase boundary area, but they also have to ensure a quick separation in the settler to prevent degradation reactions. Due to its higher viscosity, mixing is more of a problem with sulfuric acid than with HF. In all sulfuric acid catalyzed processes impellers have to be employed. In HF based processes the hydrocarbons are typically injected through nozzles, which are sufficient for effective dispersion.

Due to the exothermic nature of the alkylation reaction, a considerable amount of process

heat has to be removed. As HF catalyzed processes operate at temperatures between 16 and 40°C, they can be cooled with cooling water. Sulfuric acid catalyzed processes operate at temperatures between 4 and 18°C (see Table 2-2) requiring, therefore, a more complex cooling system, which typically utilizes the process hydrocarbon stream itself.

The feed hydrocarbons, which come from the FCC or from the etherification unit, usually have to be treated before entering the alkylation unit. They contain water, butadienes, sulfur and nitrogen compounds and – when coming from an etherification unit – traces of oxygenates.

The general treatment of the hydrocarbon stream leaving the reactor is similar in all processes. First, the acid and hydrocarbon phases have to be separated in a settler. The hydrocarbon stream is fractionated in one or more columns to separate the alkylate from recycle iso-butane as well as from propane, n-butane and (sometimes) isopentane. Because HF plants operate at higher iso-butane/alkene ratios, a larger separation unit is required. All hydrocarbon streams have to be treated in order to remove impurities of acid and acid esters.

2.4.1.1 Sulfuric acid catalyzed processes

Two licensors are offering sulfuric acid alkylation units. The one with the highest market share is Stratco with its Effluent Refrigerated Sulfuric Acid Alkylation Process (10). The reactor is a horizontal pressure vessel called Contactor™ containing an inner circulation tube, a heat exchanger tube bundle to remove the heat of reaction and a mixing impeller in one end. The hydrocarbon feed and recycle acid enter on the suction side of the impeller inside the circulation tube. This ensures the formation of a fine acid-continuous emulsion. The high circulation rate prevents significant temperature differentials within the reactor. The reactor is shown in Figure 2-11.

A portion of the emulsion flows to the settler, where the hydrocarbon phase is separated from the acid phase. The hydrocarbon phase is expanded and partially evaporated. The cold two-phase hydrocarbon effluent is passed through the cooling coils of the contactor reactor and takes up the heat of reaction by further evaporation. To increase the efficiency of the cooling system, propane is co-fed to the system. The gaseous hydrocarbons are sent to a refrigerant compressor and separated from excess propane in a depropanizer column. The acid leaving the settler is recycled into the reactor, with a small stream of fresh acid continuously replacing the equivalent stream of spent acid. To increase product quality and

reduce acid consumption, the reaction can be staged with respect to the acid flow. The acid can be passed through up to four contactor reactors with each reactor being fed with fresh hydrocarbons.

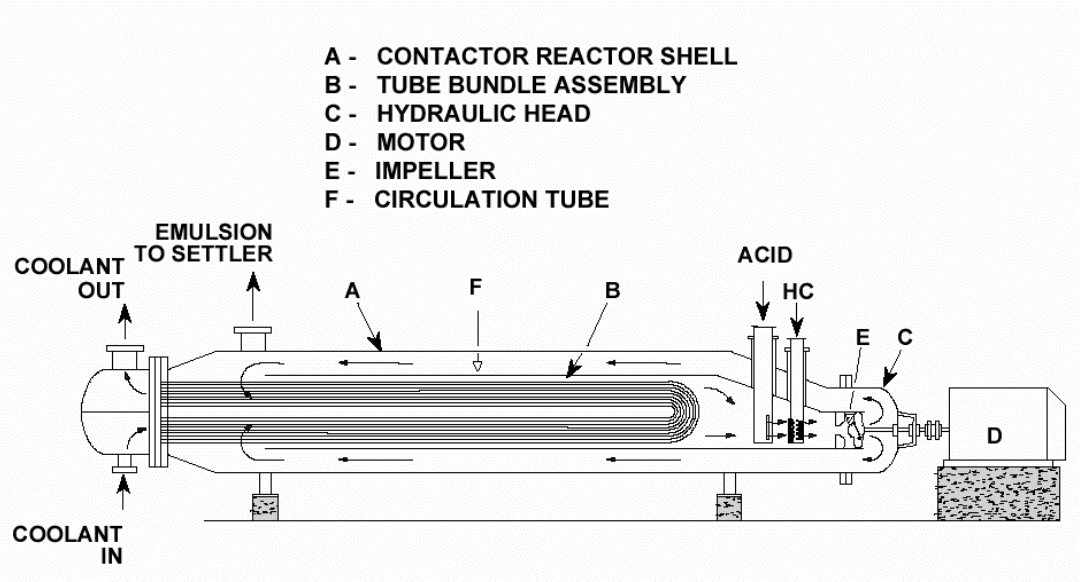

Figure 2-11: Stratco® Contactor™ reactor used in sulfuric acid catalyzed alkylation.

The spent acid strength is maintained at about 90 wt.-% H_2SO_4. The iso-butane/alkene feed ratio ranges from 7:1 to 10:1. Typical operating alkene space velocities (LHSV) range from 0.2 to 0.6 hr^{-1} (corresponding to WHSVs from 0.06 to 0.19 hr^{-1}). The optimum reaction temperatures range from 6 – 10°C, but some units are operated at temperatures up to 18°C.

The second licensor for sulfuric acid catalyzed alkylation processes is ExxonMobil with the stirred auto-refrigerated process (216), a technology formerly licensed by Kellogg. Here, the reactor consists of a large horizontal vessel divided into a series of reaction zones, each of them equipped with a stirrer, shown in Figure 2-12. The alkene feed is premixed with recycle iso-butane and fed in parallel to all mixing zones, while the acid and additional iso-butane enter only the first zone and cascade internally to the other zones. The heat of reaction is removed by evaporating iso-butane plus added propane from the reaction zones. Thus, no cooling coils are necessary in this type of process. To minimize an increase in temperature along the reaction zones, the vessel is divided into two pressure stages, with the second stage operating at a lower pressure to decrease the boiling point of the hydrocarbon mixture. The vapors are sent to the refrigeration section, where they are compressed, condensed and returned to the reactor as recycle refrigerant. To prevent a buildup of propane in the

refrigeration section, a slipstream has to be withdrawn and separated in a depropanizer. The liquid stream is separated in a settler, from which the acid phase is recycled into the reactor.

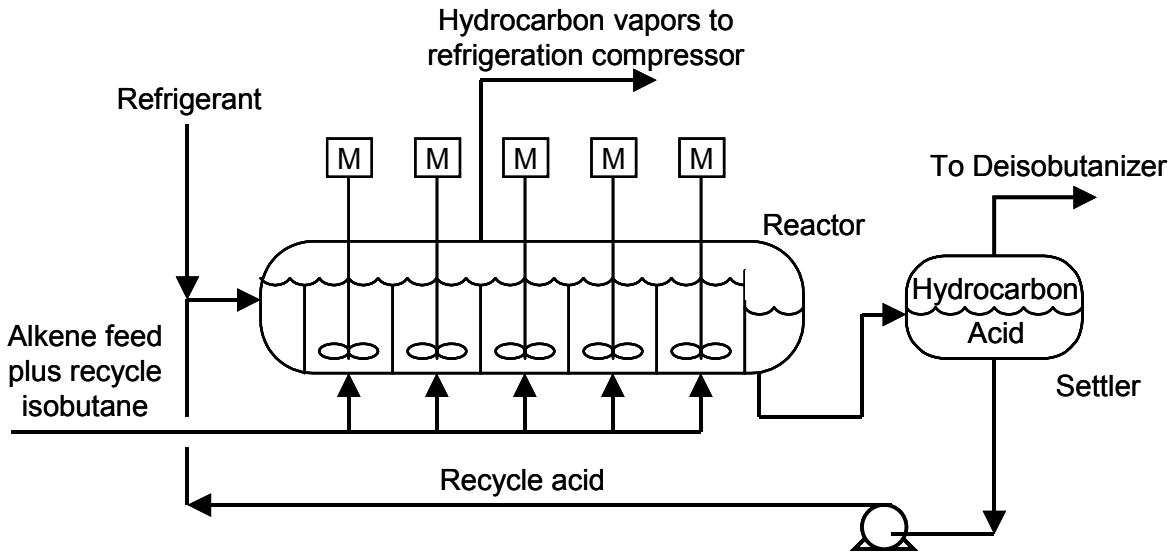

Figure 2-12: ExxonMobil auto-refrigerated alkylation process.

Due to a large reactor volume, the auto-refrigerated process can operate at very low alkene space velocities of about 0.1 hr^{-1} LHSV (WHSV ≈ 0.03 hr^{-1}). This helps in increasing the octane number and lowering acid consumption. The reaction temperature is maintained at around 5°C to minimize side reactions. Spent acid is withdrawn at 90 to 92 wt.-%. The iso-butane concentration in the hydrocarbon phase is kept between 50 – 70 vol.-%.

Stratco offers a process called Alkysafe™, proposes the conversion of an existing HF alkylation unit to use H_2SO_4 for approximately the same cost as installing an effective HF mitigation system. The process reuses the reaction and distillation sections from the existing unit. Refrigeration is carried out with a closed-loop packaged propane refrigeration section. The process flow of the converted unit is similar to the time tank units built between 1938 and 1958. Emulsion pumps and static mixers have to be installed to provide the required mixing. Stratco claims the production of similar or even increased quality alkylate as compared to the former HF plant.

2.4.1.2 Hydrofluoric catalyzed processes

Phillips Petroleum offers a process utilizing a non-cooled riser-type reactor, see Figure 2-13. The hydrocarbon mixture is introduced through nozzles at the bottom and along the length of the riser. The acid is injected at the bottom. The reactor contains perforated trays,

which help in maintaining a high dispersion of the hydrocarbons in the acid phase. The reaction mixture enters the settler, from where the acid is withdrawn at the bottom and cooled in a heat exchanger with cooling water to remove the reaction heat.

The cold acid is then fed again into the reactor. The acid flow is driven by gravity. The hydrocarbons in the settler are routed to the fractionation section, with a top stream of propane and HF, a side stream of iso-butane, another side stream of n-butane and a bottom stream of alkylate leaving the section. The HF is separated from propane in a HF stripper. The acid is regenerated by distillation to remove ASO and water. Typical process

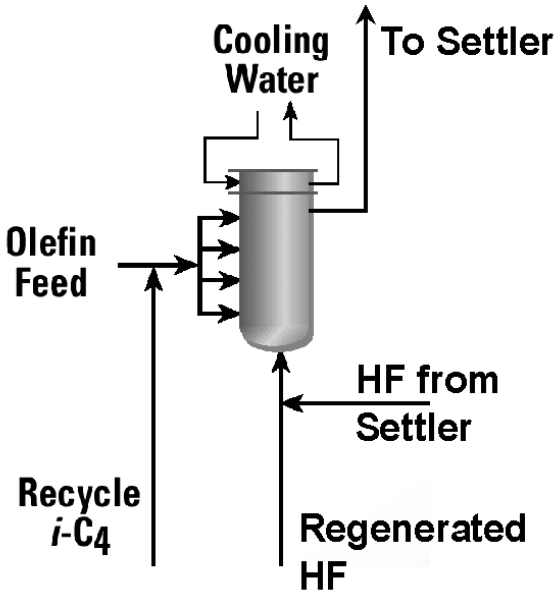

Figure 2-14: UOP HF alkylation reactor.

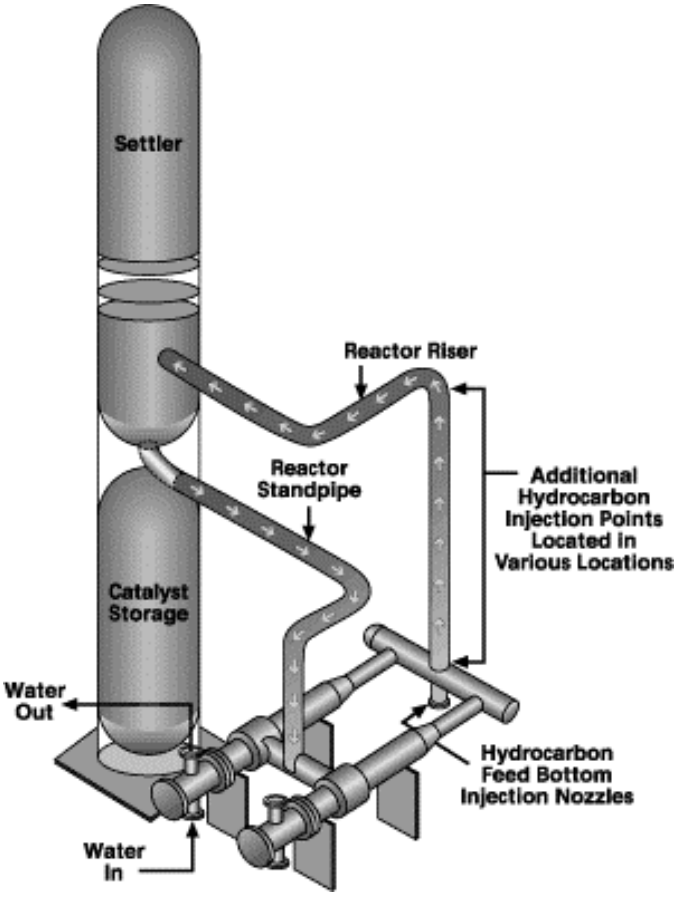

Figure 2-13: Phillips HF alkylation reactor.

parameters are temperatures in the order of 24°C, iso-butane/alkene ratios of about 14-15, and acid concentrations of 86-92 wt.-%.

At the heart of the UOP HF alkylation unit is a vertical reactor-heat exchanger, shown in Figure 2-14. The iso-butane-alkene mixture enters the shell of the reactor through several nozzles, while HF enters at the bottom of the reactor. The reaction heat is removed by cooling water, which is flowing through cooling coils inside the reactor. After phase separation in the settler the acid is recycled to the reactor. The hydrocarbon phase together with a slipstream of used acid and makeup iso-

butane is sent to the “isostripper”, where the alkylate product, n-butane and iso-butane are separated. The iso-butane is recycled to the reactor. During normal operation, the acid is distilled with the product, so that no external regeneration is necessary. An additional acid regeneration column is still needed, though, for startup, or when feed contamination occurs.

As a reaction to the pressure posed on refiners operating HF based processes, licensors developed safety systems to reduce the inherent risks. Among the mitigation systems are high volume water sprays to “knock down” an acid cloud, a low acid inventory and a rapid acid de-inventory system. HF modifiers, which reduce the volatility and the aerosol-forming tendency of HF, are additionally offered. Phillips together with Mobil developed a HF modifier technology named ReVap™ to reduce the volatility of the acid. It is claimed, that a 60 to 90% reduction in airborne acid release over unmodified acid is achieved. The modifier does not undergo a chemical reaction with the acid. The additive is separated from the alkylate by extraction and recycled within the alkylation unit. In addition, the ASO has to be separated from the additive. The additive most likely is based upon sulfones. Phillips claims that when using the additive the acid concentration can be lowered to 60%. UOP in a joint venture with ChevronTexaco developed an additive technology named Alkad™. The additive is based on HF salts of amines, which form liquid “onium” poly hydrogen fluoride complexes with HF, reducing the vapor pressure of the catalyst. 65 to over 80% aerosol reduction are claimed to be achieved with this additive. Similar to the ReVap technology, additional separation columns have to be installed. Both additives are claimed to increase the product octane especially when propene, isobutene and pentenes are employed as feedstock.

2.4.2 Solid acid catalyzed processes

Processes based on solid acids are not operated on industrial scale. However, several companies are developing processes or already offer technology for licensing. The overall process scheme is similar to the liquid acid based process schemes, except for the regeneration section, which is necessary with all solid acid catalysts. In principle, three regeneration methods have been closely examined.

(1) Like in fluid catalytic cracking, the hydrocarbons can be burned off the catalyst surface. This requires a catalyst with extreme temperature stability, which only ultrastable zeolites achieve. Moreover, as the alkylation process is exothermic and conducted at low to moderate temperatures, large amounts of process heat have to be removed.

(2) The catalyst can be treated with a solvent to extract hydrocarbon deposits. The most straightforward solvent is iso-butane, which could is shown to restore catalytic activity only partially. Supercritical solvents have been tested for their effectiveness, but they also lead only to partial restoration of the activity. Supercritical alkylation to remove the deposits *in situ* has been shown in Chapter 2.3.4.1 to be of low effectiveness. It is unlikely that this way of operation does lead to a competitive process.

(3) The most promising regeneration method and the one that is used in all true solid acid catalyzed process developments is a hydrogen treatment at both reaction and elevated temperature. This typically requires the incorporation of a hydrogenation function, for example a noble metal, into the catalyst. The regeneration mechanism depends on the temperature: At low (<100°C) temperatures, most likely highly unsaturated species, which block the acid sites but not the pores, are hydrogenated. At higher temperatures, hydrocracking of long-chain alkanes and other hydrocarbons, which are too bulky to leave the pores, is the predominant reaction. The fragments formed in this process easily desorb out of the pore-system.

While a substantial research was devoted to plug-flow reactors, they are not a good choice for large-scale operation. To achieve a high internal iso-butane/alkene ratio (>200), an enormous amount of iso-butane has to be recycled. Nevertheless, a plug-flow reactor remains attractive due to the simplicity of its design and operation. When the alkene feed is introduced over the whole length of the reactor, very low iso-butane/alkene ratios are avoided. However, in a true fixed bed the inlet zones would nevertheless suffer from the higher alkene concentration.

A more appropriate type of reactor would be a CSTR-type slurry reactor, with the catalyst suspended in the liquid. Such a system has, however, also obvious disadvantages, such as the more complex design necessary for suspending the solid in the liquid and for solid/liquid separation. They may be compensated for by intrinsically higher iso-butane/alkene ratios, which lower catalyst consumption. Another advantage of a slurry reactor is the possibility to withdraw spent catalyst for regeneration. In fixed bed reactors, the bed can only be regenerated as a whole, so that multiple swing reactors are necessary for uninterrupted production. In addition, isothermicity in slurry reactors is superior to the situation achieved with fixed bed reactors.

2.4.2.1 UOP Alkylene™ Process

UOP offers the Alkylene™ process (231) utilizing a vertical riser reactor. The pretreated alkene feed is mixed with recycle iso-butane and injected into the riser together with freshly reactivated catalyst. Both flow concurrently upwards in the riser, where the reaction occurs. At the top of the riser the catalyst particles are disengaged and sink downwards into the reactivation zone. The hydrocarbons flow out through the top of the reactor vessel to the fractionation section, where they are separated into alkylate, n-butane, iso-butane and light ends including hydrogen. The recycle iso-butane is cooled before re-entering the riser. The reactivation zone is a packed bed with the catalyst slowly moving downward in a low-temperature stream of iso-butane saturated with hydrogen. Unsaturated molecules on the catalyst are claimed to be hydrogenated and desorbed from the catalyst surface. The reactivation zone leads to the bottom of the riser, where the cycle starts again. The reactivation is not complete. A small slipstream of catalyst is withdrawn and directed to a reactivation vessel, in which the catalyst is regenerated semi-batch or batch wise at elevated temperature in a circulating hydrogen stream. A process scheme is shown in Figure 2-15.

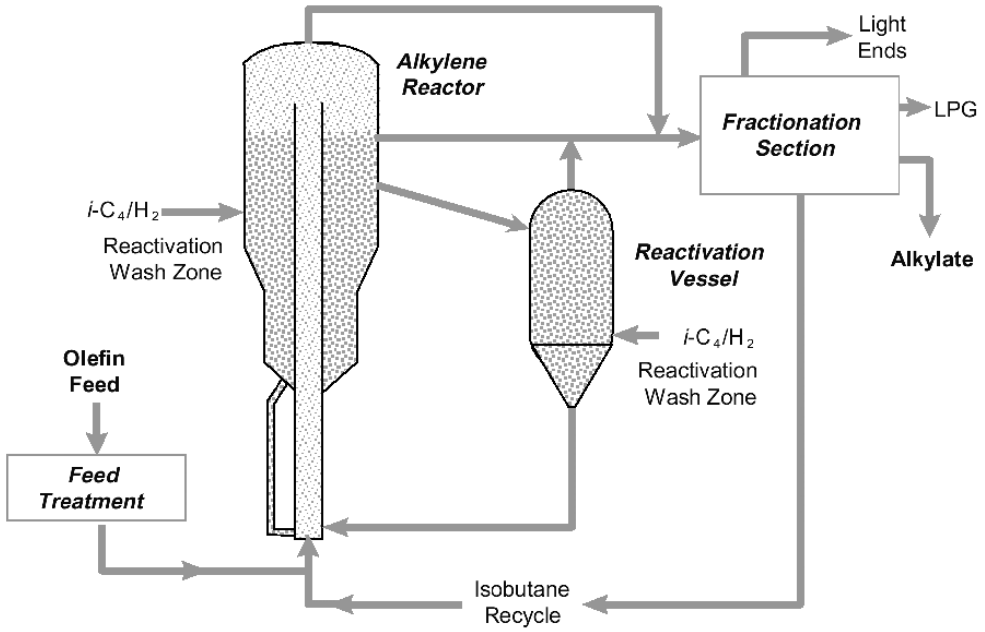

Figure 2-15: UOP Alkylene™ solid acid catalyzed alkylation process.

The composition of the catalyst, which UOP refers to as HAL-100™, has not been

disclosed. In several patents the use of an alumina supported $AlCl_3$ catalyst modified with alkaline metal cations and a Ni, Pd or Pt hydrogenation function is mentioned (see for example (209)). Obviously, traces of halogen compounds are leached out of the catalyst, because a product treatment section is necessary. This would additionally imply that a makeup halogen source is required. The alkene feed has to be extensively treated to remove di-olefins, sulfur, oxygen and nitrogen compounds. The process operates at 10-40°C and at an iso-butane/alkene ratio of 6-15. No information is available on the alkene space velocity. It is interesting to note that typical alkene conversions are between 93-100%, which most likely is a consequence of very low contact times in the riser reactor. The alkylate RON is claimed to be as high as with the existing technology.

2.4.2.2 Akzo Nobel/ABB Lummus AlkyClean™ process

Akzo Nobel and ABB Lummus recently started a solid acid catalyzed alkylation demonstration plant at a Fortum refinery in Finland (232). The reactor type used in the AlkyClean™ process has not been disclosed. However, the process utilizes serial reaction stages with distributed alkene feed injection for high internal iso-butane/alkene ratios. The reactor type is claimed to achieve a high degree of mixing to reduce alkene gradients throughout the reactor. Multiple reactors are used, which swing between reaction and regeneration. Similar to the Alkylene™ process, two regeneration phases with different severity are employed. A mild regeneration at reaction temperature and pressure with hydrogen dissolved in iso-butane is performed frequently (far before the end of the theoretical catalyst lifetime). When necessary, the catalyst is fully regenerated at 250°C in a stream of gas-phase hydrogen. Presumably, each reactor is in (mild) regeneration mode far longer than in reaction mode.

The catalyst is reported to be a “true solid acid” without halogen ion addition. In the patent describing the process, a Pt/USY with alumina binder is employed (233). It is claimed that the catalyst is rather insensitive against feed impurities and feedstock composition, so that feed pretreatment can be less stringent. The process is operated at 50-90°C, reducing cooling requirements. The iso-butane/alkene feed ratio is kept between 8 to 10. Alkene space velocities are not reported. Akzo claims that the alkylate quality is identical or higher than with the liquid acid catalyzed processes.

2.4.2.3 LURGI EUROFUEL® process

LURGI and Süd-Chemie AG are developing a solid acid catalyzed alkylation process termed LURGI EUROFUEL®. The reactor is derived from tray distillation towers. Iso-butane and suspended catalyst enter at the top of the tower and the alkene with premixed iso-butane is introduced in stages (see Figure 2-16). The evolving reaction heat is most likely dissipated by the evaporation of the reaction mixture. Thus, the temperature is being controlled by the overall pressure and the composition of the liquid. The catalyst reactant mixture is agitated by the boiling mixture of alkylate and iso-butane. At the bottom of the column, the catalyst is separated and the majority of the alkylate/iso-butane mixture is fed into the separation section. Iso-butane is recycled and mixed together with the catalyst, which is fed into the top of the reaction column. Intermittently the catalyst is exposed to hydrogen rich operating conditions in order to minimize accumulation of unsaturated compounds on the catalyst surface. Infrequent regeneration occurs in a proprietary section at elevated temperatures.

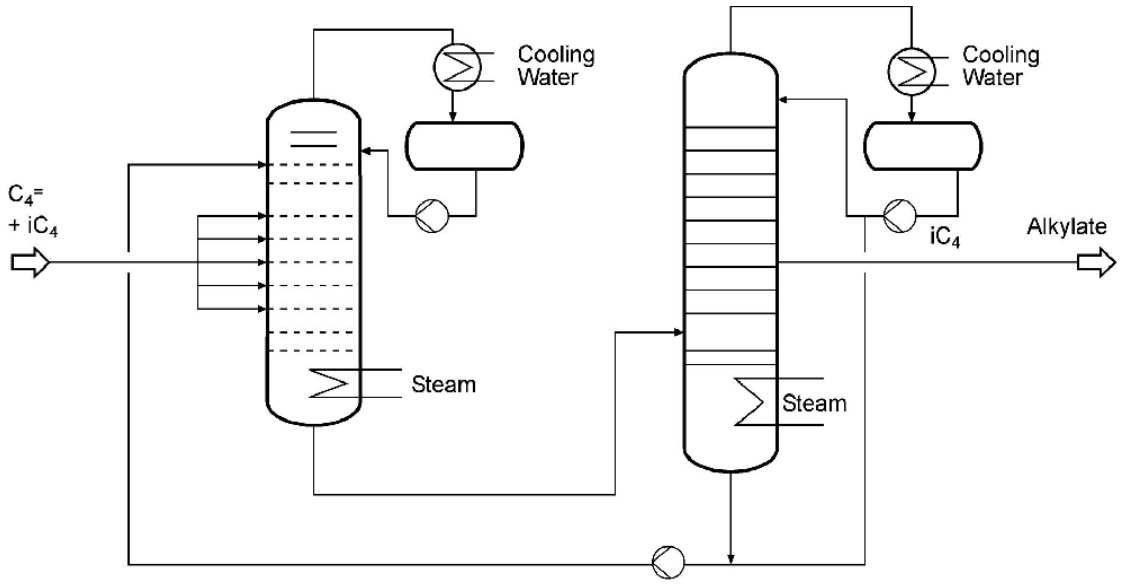

Figure 2-16: Lurgi Eurofuel® solid acid catalyzed alkylation process.

The catalyst is faujasite derived, with a high concentration of sufficiently strong Brønsted acid sites and a minimized concentration of Lewis acid sites. It additionally contains a hydrogenation function. The process operates at temperatures around 50-100°C with an iso-butane/alkene ratio between 6 to 12 and a higher alkene space velocity than in the liquid acid based processes. Preliminary details of the process concept are described in ref. (234).

2.4.2.4 Haldor Topsøe FBA™ process

The Haldor Topsøe's fixed-bed alkylation (FBA™) technology is a compromise between liquid and solid acid based processes. It applies a supported liquid phase type catalyst in which liquid triflic (trifluoromethanesulfonic) acid is supported on a porous support material (201, 235). The acid in the bed is concentrated in a well-defined catalyst zone, in which all the alkylation chemistry takes place. At the upstream end of the catalyst zone, ester intermediates are formed, which are soluble in the hydrocarbons and are transported into the acid zone. Here, they react to form the products and free acid. Thus, the active zone slowly migrates through the bed in the direction of the hydrocarbon flow, as shown in Figure 2-17.

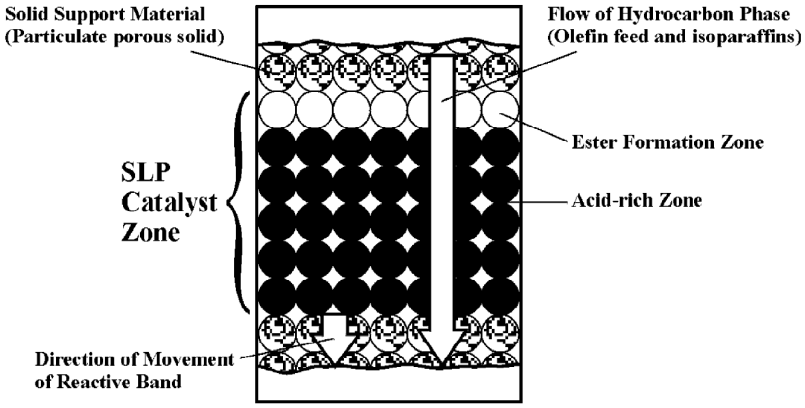

Figure 2-17: Reaction zone in Haldor Topsøe's FBA™ alkylation process.

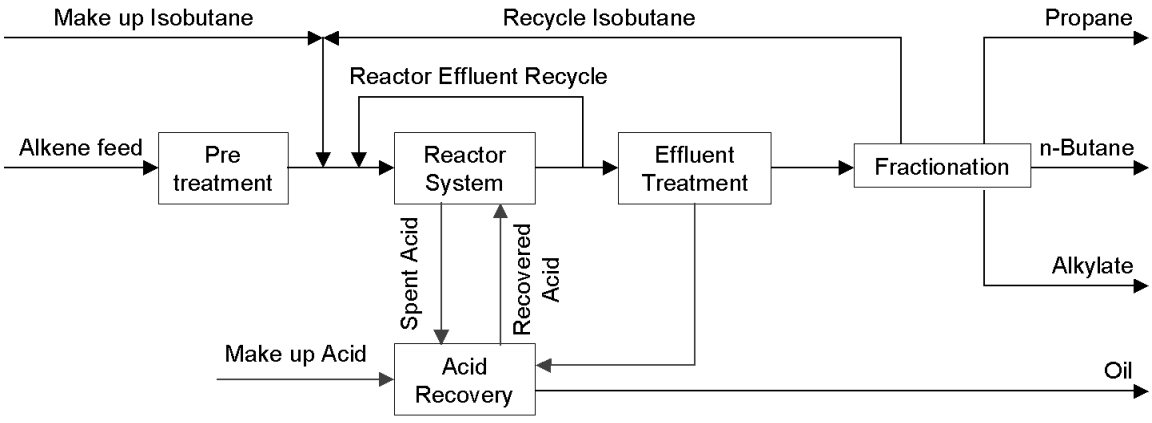

Figure 2-18: Haldor Topsøe's FBA™ alkylation process.

The spent acid can be withdrawn from the reactor without interrupting the production. The acid is regenerated in a proprietary acid-recovery unit, which produces some oil as by-

product. The products have to be treated to remove trace amounts of acid. Reaction temperature is in the range of 0-20°C. The reactor is operated adiabatically and the reaction heat is removed by a cooled reactor effluent recycle, see Figure 2-18. The process is claimed to be robust against feed impurities. Feed drying, however, is recommended.

2.5 Conclusions

The alkylation mechanism and the influence of the catalyst type and the reaction conditions have been reviewed. The principle chemistry is identical with all the examined acids, liquid and solid. Differences in the importance of individual steps originate from the variety of possible structures and acidity distributions of solid acids. Changing process parameters induces similar effects independent of the catalyst; however, the sensitivity for a particular parameter strongly depends upon the catalyst. All acids deactivate by the formation of unsaturated polymers, which are strongly bound to the acid.

Liquid acid catalyzed processes are mature technologies, which do not see dramatic changes in the near future. Solid acid catalyzed alkylation is at a point now, at which the technology can compete with the existing processes. Regeneration *via* hydrogen treatment is the method of choice in all process developments. Some of the process developments eliminate most if not all the drawbacks of the liquid acid based processes. The verdict whether or not solid acid catalyst based processes will be seen in the new future and it will be primarily determined by economic arguments.

2.6 References

1. Ipatieff, V. N. and Grosse, A. V., *J. Am. Chem. Soc.* **57**, 1616 (1935).
2. Ipatieff, V. N. and Pines, H., U.S. Patent 2,122,847 (1938).
3. Hutson Jr., T. and McCarthy, W. C., *in* "Handbook of petroleum refining processes" (R. A. Meyers, ed.), p. 1/23. McGraw-Hill, New York, 1986.
4. Pines, H., *Chemtech* **March 1982**, 150 (1982).
5. Albright, L. F., *Chemtech* **June 1998**, 40 (1998).
6. Stell, J., *Oil Gas J.* **99 (52)**, 74 (2001).
7. Albright, L. F., *Oil & Gas Journal* **Nov. 26**, 70 (1990).
8. Furimsky, E., *Catal. Today* **30**, 223 (1996).
9. Albright, L. F., *Chemtech* **July 1998**, 46 (1998).

10. Kinnear, S., in: Proceedings of the STRATCO Alkylation seminar, Phoenix, Arizona, 1998.
11. Garwood, W. E. and Venuto, P. B., *J. Catal.* **11**, 175 (1968).
12. Kirsch, F. W., Potts, J. D., and Barmby, D. S., *J. Catal.* **27**, 142 (1972).
13. Corma, A. and Martinez, A., *Catal. Rev.-Sci. Eng.* **35**, 483 (1993).
14. Weitkamp, J. and Traa, Y., *in* "Handbook of Heterogeneous Catalysis" (G. Ertl, H. Knözinger, and J. Weitkamp, Eds.), Vol. 4, p. 2039. VCH, Weinheim, 1997.
15. Schmerling, L., *J. Am. Chem. Soc.* **67**, 1778 (1945).
16. Schmerling, L., *J. Am. Chem. Soc.* **68**, 275 (1946).
17. Schmerling, L., *Ind. Eng. Chem.* **45**, 1447 (1953).
18. Albright, L. F., Spalding, M. A., Faunce, J., and Eckert, R. E., *Ind. Eng. Chem. Res.* **27**, 391 (1988).
19. Hutson Jr., T. and Logan, R. S., *Hydrocarbon Processing* **Sept. 1975**, 107 (1975).
20. Corma, A., Martinez, A., and Martinez, C., *J. Catal.* **149**, 52 (1994).
21. Gary, J. H. and Handwerk, G. E., *in* "Petroleum Refining - Technology and Economics" (L. F. Albright, R. N. Maddox, and J. J. McKetta, Eds.), p. 142. Marcel Dekker, Inc., New York, 1979.
22. Hommeltoft, S. I., Ekelund, O., and Zavilla, J., *Ind. Eng. Chem. Res.* **36**, 3491 (1997).
23. Frash, M. V., Solkan, V. N., and Kazansky, V. B., *J. Chem. Soc. Faraday Trans.* **93**, 515 (1997).
24. Kazansky, V. B., Abbenhuis, H. C. L., van Santen, R. A., and Vorstenbosch, M. L. V., *Catal. Lett.* **69**, 51 (2000).
25. Kazansky, V. B., *Catal. Rev.-Sci. Eng.* **43**, 199 (2001).
26. Albright, L. F., Spalding, M. A., Nowinski, J. A., Ybarra, R. M., and Eckert, R. E., *Ind. Eng. Chem. Res.* **27**, 381 (1988).
27. Kazansky, V. B., *Catal. Today* **51**, 419 (1999).
28. Gorte, R. J. and White, D., *Topics Catal.* **4**, 57 (1997).
29. Kazansky, V. B., *in* "Handbook of Heterogeneous Catalysis" (G. Ertl, H. Knözinger, and J. Weitkamp, Eds.), Vol. 2, p. 740. VCH, Weinheim, 1997.
30. Rigby, A. M., Kramer, G. J., and van Santen, R. A., *J. Catal.* **170**, 1 (1997).
31. Rozanska, X., Demuth, T., Hutschka, F., Hafner, J., and van Santen, R. A., *J. Phys. Chem. B* **106**, 3248 (2002).

32. Ishikawa, H., Yoda, E., Kondo, J. N., Wakabayashi, F., and Domen, K., *J. Phys. Chem. B* **103**, 5681 (1999).
33. Kondo, J. N., Ishikawa, H., Yoda, E., Wakabayashi, F., and Domen, K., *J. Phys. Chem. B* **103**, 8538 (1999).
34. Engelhardt, J. and Hall, W. K., *J. Catal.* **151**, 1 (1995).
35. Mota, C. J. A., Esteves, P. M., Ramirez-Solis, A., and Hernandez-Lamoneda, R., *J. Am. Chem. Soc.* **119**, 5193 (1997).
36. Hogeveen, H., Gaasbeek, C. J., and Bickel, A. F., *Rec. Trav. Chim.* **88**, 703 (1969).
37. Olah, G. A. and Olah, J. A., *in* "Carbonium Ions" (G. A. Olah and P. R. Schleyer, Eds.), Vol. 2, p. 715. Interscience, New York, 1970.
38. Sanchez-Castillo, M. A., Agarwal, N., Miller, C., Cortright, R. D., Madon, R. J., and Dumesic, J. A., *J. Catal.* **205**, 67 (2002).
39. Boronat, M., Viruela, P., and Corma, A., *J. Phys. Chem. A* **102**, 982 (1998).
40. Stewart, T. D. and Calkins, W. H., *J. Am. Chem. Soc.* **70**, 1006 (1948).
41. Miron, L. and Lee, R. J., *J. Chem. Eng. Data* **8**, 150 (1963).
42. Albright, L. F. and Li, K. W., *Ind. Eng. Chem. Process Des. Develop.* **9**, 447 (1970).
43. Li, K. W., Eckert, R. E., and Albright, L. F., *Ind. Eng. Chem. Process Des. Develop.* **9**, 441 (1970).
44. Hofmann, J. E. and Schriesheim, A., *J. Am. Chem. Soc.* **84**, 953 (1962).
45. Gorin, M. H., Kuhn, C. S., and Miles, C. B., *Ind. Eng. Chem.* **38**, 795 (1946).
46. Nivarthy, G. S., He, Y., Seshan, K., and Lercher, J. A., *J. Catal.* **176**, 192 (1998).
47. Albright, L. F. and Kranz, K. E., *Ind. Eng. Chem. Res.* **31**, 475 (1992).
48. Shah, B. R., *in* "Handbook of petroleum refining processes" (R. A. Meyers, ed.), p. 1/3. McGraw-Hill, New York, 1986.
49. Pines, H., Grosse, A. V., and Ipatieff, V. N., *J. Am. Chem. Soc.* **64**, 33 (1942).
50. Olah, G. A. and Prakash, G. K. S., *in* "The chemistry of alkanes and cycloalkanes" (S. Patai and Z. Rappoport, Eds.), p. 609. John Wiley & Sons Ltd, London, 1992.
51. Durrett, L. R., Taylor, L. M., Wantland, C. F., and Dvoretzky, I., *Anal. Chem.* **35**, 637 (1963).
52. Cumming, K. A. and Wojciechowski, B. W., *Catal. Rev.-Sci. Eng.* **38**, 101 (1996).
53. Bartlett, P. D., Condon, F. E., and Schneider, A., *J. Am. Chem. Soc.* **66**, 1531 (1944).
54. Deno, N. C., Peterson, H. J., and Saines, G. S., *Chem. Rev.* **60**, 7 (1960).

55. Wojciechowski, B. W. and Corma, A., *in* "Catalytic cracking - Catalysts, Chemistry, and Kinetics", p. 5. Marcel Dekker, New York, 1986.
56. Ausloos, P. and Lias, S. G., *J. Am. Chem. Soc.* **92**, 5037 (1970).
57. Meot-Ner, M. and Field, F. H., *J. Chem. Phys.* **64**, 277 (1976).
58. Meot-Ner, M., *J. Am. Chem. Soc.* **109**, 7947 (1987).
59. Sunner, J. A., Hirao, K., and Kebarle, P., *J. Phys. Chem.* **93**, 4010 (1989).
60. Olah, G. A., Mo, Y. K., and Olah, J. A., *J. Amer. Chem. Soc.* **95**, 4939 (1973).
61. Boronat, M., Viruela, P., and Corma, A., *Phys. Chem. Chem. Phys.* **2**, 3327 (2000).
62. Boronat, M., Viruela, P., and Corma, A., *J. Phys. Chem. A* **102**, 9863 (1998).
63. Nowak, A. K., Mesters, C. M. A. M., Rigby, A. M., and Schulze, D., *Preprints, Div. Petr. Chem., Am. Chem. Soc.* **41**, 668 (1996).
64. Boronat, M., Zicovich-Wilson, C. M., Corma, A., and Viruela, P., *Phys. Chem. Chem. Phys.* **1**, 537 (1999).
65. Beirnaert, H. C., Alleman, J. R., and Marin, G. B., *Ind. Eng. Chem. Res.* **40**, 1337 (2001).
66. Yaluris, G., Rekoske, J. E., Aparicio, L. M., Madon, R. J., and Dumesic, J. A., *J. Catal.* **153**, 54 (1995).
67. Guisnet, M. and Gnep, N. S., *Appl. Catal. A* **146**, 33 (1996).
68. Corma, A., Faraldos, M., Martinez, A., and Mifsud, A., *J. Catal.* **122**, 230 (1990).
69. Hofmann, J. E. and Schriesheim, A., *J. Am. Chem. Soc.* **84**, 957 (1962).
70. Nenitzescu, C. D., *in* "Carbonium ions" (G. A. Olah and P. R. Schleyer, Eds.), Vol. 2, p. 463. Interscience, New York, 1970.
71. Schöllner, R. and Hölzel, H., *Z. Chem.* **15**, 469 (1975).
72. Reyniers, M.-F., Beirnaert, H., and Marin, G. B., *Appl. Catal. A* **202**, 49 (2000).
73. Reyniers, M.-F., Tang, Y., and Marin, G. B., *Appl. Catal. A* **202**, 65 (2000).
74. Weeks, T. J., Jr. and Bolton, A. P., *J. Chem. Soc. Faraday Trans.* **170**, 1676 (1974).
75. Lutsyk, A. I. and Suikov, S. Y., *Petrol. Chem.* **35**, 412 (1995).
76. Nivarthy, G. S., Seshan, K., and Lercher, J. A., *Microp. & Mesop. Mater.* **22**, 379 (1998).
77. Lee, L. and Harriott, P., *Ind. Eng. Chem. Process Des. Develop.* **16**, 282 (1977).
78. de Jong, K. P., Mesters, C. M. A. M., Peferoen, D. G. R., van Brugge, P. T. M., and de Groot, C., *Chem. Eng. Sci.* **51**, 2053 (1996).

79. Simpson, M. F., Wei, J., and Sundaresan, S., *Ind. Eng. Chem. Res.* **35**, 3861 (1996).
80. Albright, L. F. and Wood, K. V., *Ind. Eng. Chem. Res.* **36**, 2110 (1997).
81. Schöllner, R. and Hölzel, H., *Journal f. prakt. Chemie* **317**, 694 (1975).
82. Martens, J. A. and Jacobs, P. A., *Stud. Surf. Sci. Catal.* **137**, 633 (2001).
83. Weitkamp, J. and Ernst, S., *Stud. Surf. Sci. Catal.* **38**, 367 (1988).
84. Frash, M. V. and van Santen, R. A., *Topics in Catal.* **9**, 191 (1999).
85. Daage, M. and Fajula, F., *Bull. Soc. Chim. Fr.* **5-6**, 153 (1984).
86. Pater, J., Cardona, F., Canaff, C., Gnep, N. S., Szabo, G., and Guisnet, M., *Ind. Eng. Chem. Res.* **38**, 3822 (1999).
87. Feller, A., Guzman, A., Zuazo, I., and Lercher, J. A., *see chapter 3*, (2002).
88. Hofmann, J. E., *J. Org. Chem.* **29**, 1497 (1964).
89. Graves, D. C., Kranz, K., and Millard, J., *Preprints, Div. Petr. Chem., Am. Chem. Soc.* **39**, 398 (1994).
90. Roebuck, A. K. and Evering, B. L., *Ind. Eng. Chem. Prod. Res. Develop.* **9**, 76 (1970).
91. Cardona, F., Gnep, N. S., Guisnet, M., Szabo, G., and Nascimento, P., *Appl. Catal. A* **128**, 243 (1995).
92. am Ende, D. J. and Albright, L. F., *Ind. Eng. Chem. Res.* **33**, 840 (1994).
93. Guisnet, M. and Magnoux, P., *Appl. Catal. A* **212**, 83 (2001).
94. Albright, L. F., Spalding, M. A., Kopser, C. G., and Eckert, R. E., *Ind. Eng. Chem. Res.* **27**, 386 (1988).
95. Kramer, G. M., *J. Org. Chem.* **32**, 920 (1967).
96. Kramer, G. M., *J. Org. Chem.* **32**, 1916 (1967).
97. Otvos, J. W., Stevenson, D. P., Wagner, C. D., and Beeck, O., *J. Amer. Chem. Soc.* **73**, 5741 (1951).
98. Flego, C., Kiricsi, I., Parker Jr., W. O., and Clerici, M. G., *Appl. Catal. A* **124**, 107 (1995).
99. Weitkamp, J. and Maixner, S., *Zeolites* **7**, 6 (1987).
100. Deno, N. C., *in* "Carbonium Ions" (G. A. Olah and P. R. Schleyer, Eds.), Vol. 2, p. 783. Interscience, New York, 1970.
101. Sorensen, T. S., *in* "Carbonium Ions" (G. A. Olah and P. R. Schleyer, Eds.), Vol. 2, p. 807. Interscience, New York, 1970.
102. Nicholas, J. B. and Haw, J. F., *J. Am. Chem. Soc.* **120**, 11804 (1998).

103. Yang, S., Kondo, J. N., and Domen, K., *Catal. Today* **73**, 113 (2002).
104. Li, K. W., Eckert, R. E., and Albright, L. F., *Ind. Eng. Chem. Process Des. Develop.* **9**, 434 (1970).
105. Albright, L. F., *Ind. Eng. Chem. Res.* **40**, 4032 (2001).
106. He, M. Y. and Min, E., *Catal. Today* **63**, 113 (2000).
107. Olah, G. A., Batamack, P., Deffieux, D., Török, B., Wang, Q., Molnar, A., and Surya Prakash, G. K., *Appl. Catal. A* **146**, 107 (1996).
108. Olah, G. A., Marinez, E., Török, B., and Prakash, G. K. S., *Catal. Lett.* **61**, 105 (1999).
109. Hölderich, W. and Jacobs, P. A., *Stud. Surf. Sci. Catal.* **137**, 821 (2001).
110. Corma, A. and Garcia, H., *Catal. Today* **38**, 257 (1997).
111. Ramachandran, S., Lenz, T. G., Skiff, W. M., and Rappé, A. K., *J. Phys. Chem.* **100**, 5898 (1996).
112. Eder, F. and Lercher, J. A., *Zeolites* **18**, 75 (1997).
113. Jänchen, J., Stach, H., Uytterhoeven, L., and Mortier, W. J., *J. Phys. Chem.* **100**, 12489 (1996).
114. Eder, F. and Lercher, J. A., *J. Phys. Chem.* **100**, 16460 (1996).
115. Haag, W. O., *Stud. Surf. Sci. Catal.* **84**, 1375 (1994).
116. Chu, Y. F. and Chester, A. W., *Zeolites* **6**, 195 (1986).
117. Weitkamp, J., *in* "Proc. 5th International Zeolite Conference" (L. V. C. Rees, ed.), p. 858. Heyden, London, 1980.
118. Corma, A., Martinez, A., and Martinez, C., *J. Catal.* **146**, 185 (1994).
119. Mostad, H. B., Stöcker, M., Karlsson, A., and Rørvik, T., *Appl. Catal. A* **144**, 305 (1996).
120. Stöcker, M., Mostad, H., and Rørvik, T., *Catal. Lett.* **28**, 203 (1994).
121. Stöcker, M., Mostad, H., Karlsson, A., Junggreen, H., and Hustad, B., *Catal. Lett.* **40**, 51 (1996).
122. Rørvik, T., Mostad, H. B., Karlsson, A., and Ellestad, O. H., *Appl. Catal. A* **156**, 267 (1997).
123. Corma, A., Martinez, A., and Martinez, C., *Catal. Lett.* **28**, 187 (1994).
124. Diaz-Mendoza, F. A., Pernett-Bolano, L., and Cardona-Martinez, N., *Thermochim. Acta* **312**, 47 (1998).
125. Zhuang, Y. and Ng, F. T. T., *Appl. Catal. A* **190**, 137 (2000).

126. Nakamura, I., Ishida, S., and Fujimoto, K., *Preprints, Div. Petr. Chem., Am. Chem. Soc.* **40**, 512 (1995).
127. Fan, L., Nakamura, I., Ishida, S., and Fujimoto, K., *Ind. Eng. Chem. Res.* **36**, 1458 (1997).
128. Chu, W., Zhao, Z., Sun, W., Ye, X., and Wu, Y., *Catal. Lett.* **55**, 57 (1998).
129. Baronetti, G., Thomas, H., and Querini, C. A., *Appl. Catal. A* **217**, 131 (2001).
130. Ramos-Galvan, C. E., Dominguez, J. M., Sandoval-Robles, G., Mantilla, A., and Ferrat, G., *Catal. Today* **65**, 391 (2001).
131. Corma, A., Martinez, A., Arroyo, P. A., Monteiro, J. L. F., and Sousa-Aguiar, E. F., *Appl. Catal. A* **142**, 139 (1996).
132. Corma, A., Martinez, A., and Martinez, C., *Appl. Catal. A* **134**, 169 (1996).
133. Fritz, P. O. and Lunsford, J. H., *J. Catal.* **118**, 85 (1989).
134. Scherzer, J., *Catal. Rev.-Sci. Eng.* **31**, 215 (1989).
135. Weitkamp, J. and Traa, Y., *Catal. Today* **49**, 193 (1999).
136. Corma, A., Gomez, V., and Martinez, A., *Appl. Catal. A* **119**, 83 (1994).
137. Unverricht, S., Ernst, S., and Weitkamp, J., *Stud. Surf. Sci. Catal.* **84**, 1693 (1994).
138. Loenders, R., Jacobs, P. A., and Martens, J. A., *J. Catal.* **176**, 545 (1998).
139. Yoo, K. and Smirniotis, P. G., *Appl. Catal. A* **227**, 171 (2002).
140. Agaskar, P. A. and Huang, T. J., U.S. Patent 5,824,835 (1998).
141. Corma, A. and Orchillés, A. V., *Microp. Mesop. Mater.* **35-36**, 21 (2000).
142. Wielers, A. F. H., Vaarkamp, M., and Post, M. F. M., *J. Catal.* **127**, 51 (1991).
143. Garwood, W. E., Leaman, W. K., and Plank, C. J., U.S. Patent 3,251,902 (1966).
144. Weitkamp, J., *Stud. Surf. Sci. Catal.* **5**, 65 (1980).
145. Kashkovskii, V. I., Galich, P. N., Patrilyak, K. I., and Royev, L. M., *Petrol. Chem.* **31**, 480 (1991).
146. Galich, P. N., Tsupryk, I. N., and Vasil`yev, A. N., *Petrol. Chem.* **37**, 332 (1997).
147. Kirsch, F. W., Barmby, D. S., and Potts, J. D., U.S. Patent 4,300,015 (1981).
148. Mortikov, E. S., Plakhotnic, V. A., and Dolinsky, S. E., Germany Patent DE 197 45 548 A1 (1999).
149. Dolinsky, S. E., Plakhotnik, V. A., Mortikov, E. S., and Bachurikhin, A. L., *Preprints, Div. Petr. Chem., Am. Chem. Soc.* **46**, 246 (2001).
150. Park, H. S. and Seff, K., *J. Phys. Chem. B* **104**, 2224 (2000).

151. Scherzer, J., Bass, J. L., and Hunter, F. D., *J. Phys. Chem.* **79**, 1194 (1975).
152. Carvajal, R., Chu, P. J., and Lunsford, J. H., *J. Catal.* **125**, 123 (1990).
153. Bolton, A. P., *J. Catal.* **22**, 9 (1971).
154. Cheetham, A. K., Eddy, M. M., and Thomas, J. M., *J. Chem. Soc., Chem. Commun.*, 1337 (1984).
155. Ward, J. W., *J. Catal.* **13**, 321 (1969).
156. Ward, J. W., *J. Colloid Interface Sci.* **28**, 269 (1968).
157. Ward, J. W., *J. Catal.* **14**, 365 (1969).
158. Kirsch, F. W., Barmby, D. S., and Potts, J. D., U.S. Patent 3,624,173 (1971).
159. Kirsch, F. W., Barmby, D. S., and Potts, J. D., U.S. Patent 3,706,814 (1972).
160. Kirsch, F. W., Barmby, D. S., and Potts, J. D., U.S. Patent 3,839,228 (1974).
161. Kirsch, F. W., Barmby, D. S., and Potts, J. D., U.S. Patent 3,803,256 (1974).
162. Kirsch, F. W., Barmby, D. S., and Potts, J. D., U.S. Patent 3,865,894 (1975).
163. Mostad, H., Stöcker, M., Karlsson, A., Junggreen, H., and Hustad, B., *Stud. Surf. Sci. Catal.* **105**, 1413 (1997).
164. Chester, A. W. and Chu, Y. F., U.S. Patent 4,377,721 (1983).
165. Buchanan, J. S. and Huang, T. J., World Patent WO 97/20787 (1997).
166. Weitkamp, J. and Jacobs, P. A., *in* "New Frontiers in Catalysis" (L. Guczi, F. Solymosi, and P. Tétényi, Eds.), Vol. B, p. 1735. Akadémiai Kiadó, Budapest, 1993.
167. Chu, C. T. W., Husain, A., Keville, K. M., and Lissy, D. N., U.S. Patent 5,516,962 (1996).
168. Husain, A., World Patent WO 94/03415 (1994).
169. Child, J. E., Huss Jr., A., Krambeck, F. J., Ragonese, F. P., Thomson, R. T., and Yurchak, S., U.S. Patent 5,073,665 (1991).
170. Huss Jr., A., Kirker, G. W., Keville, K. M., and Thomson, T. J., U.S. Patent 4,992,615 (1991).
171. He, J. Y., Nivarthy, G. S., Eder, F., Seshan, K., and Lercher, J. A., *Microp. Mesop. Mater.* **25**, 207 (1998).
172. Yoo, K., Burckle, E. C., and Smirniotis, P. G., *Catal. Lett.* **74**, 85 (2001).
173. Borade, R. B. and Clearfield, A., *J. Phys. Chem.* **96**, 6729 (1992).
174. Corma, A., Diaz-Cabanas, M. J., Martinez, C., and Valencia, S., in: Proceedings of the 13th International Zeolite Conference, Montpellier, 275, 2001.

175. Nivarthy, G. S., Feller, A., Seshan, K., and Lercher, J. A., *Stud. Surf. Sci. Catal.* **130**, 2561 (2000).
176. Rørvik, T., Mostad, H., Ellestad, O. H., and Stöcker, M., *Appl. Catal. A* **137**, 235 (1996).
177. Zhang, Z., Han, Y., Xiao, F. S., Qiu, S., Zhu, L., Wang, R., Yu, Y., Zhang, Z., Zou, B., Wang, Y., Sun, H., Zhao, D., and Wei, Y., *J. Am. Chem. Soc.* **123**, 5014 (2001).
178. Huang, T. J. and Kresge, C. T., U.S. Patent 5,498,817 (1996).
179. Husain, A., Huss, A., Klocke, D. J., and Timken, H. K. C., World Patent WO 93/07106 (1993).
180. Chu, C. T., Husain, A., Huss Jr., A., Kresge, C. T., and Roth, W. J., U.S. Patent 5,258,569 (1993).
181. Harandi, M. N., Beech Jr., J. H., Huss Jr., A., Ware, R. A., and Husain, A., U.S. Patent 5,625,113 (1997).
182. Husain, A., Huss Jr., A., and Rahmim, I. I., U.S. Patent 5,475,175 (1995).
183. Huss Jr., A., Le, Q. N., and Thomson, R. T., U.S. Patent 5,326,922 (1994).
184. Corma, A., Juan-Rajadell, M. I., Lopez-Nieto, J. M., Martinez, A., and Martinez, C., *Appl. Catal. A* **111**, 175 (1994).
185. Corma, A., Martinez, A., and Martinez, C., *Appl. Catal. A* **144**, 249 (1996).
186. Satoh, K., Matsuhashi, H., and Arata, K., *Appl. Catal. A* **189**, 35 (1999).
187. Gore, R. B. and Thomson, W. J., *Appl. Catal. A* **168**, 23 (1998).
188. Chellappa, A. S., Miller, R. C., and Thomson, W. J., *Appl. Catal. A* **209**, 359 (2001).
189. Das, D. and Chakrabarty, D. K., *Energy & Fuels* **12**, 109 (1998).
190. Guo, C., Yao, S., Cao, J., and Qian, Z., *Appl. Catal. A* **107**, 229 (1994).
191. Guo, C., Liao, S., Qian, Z., and Tanabe, K., *Appl. Catal. A* **107**, 239 (1994).
192. Xiao, X., Tierney, J. W., and Wender, I., *Appl. Catal. A* **183**, 209 (1999).
193. Sun, M., Sun, J., and Li, Q., *Chem. Lett.* **1998**, 519 (1998).
194. Blasco, T., Corma, A., Martinez, A., and Martinez-Escolano, P., *J. Catal.* **177**, 306 (1998).
195. Gayraud, P. Y., Stewart, I. H., Derouane-Abd Hamid, S. B., Essayem, N., Derouane, E. G., and Vedrine, J. C., *Catal. Today* **63**, 223 (2000).
196. Okuhara, T., Yamashita, M., Na, K., and Misono, M., *Chem. Lett.* **1994**, 1451 (1994).

197. de Angelis, A., Ingallina, P., Berti, D., Montanari, L., and Clerici, M. G., *Catal. Lett.* **61**, 45 (1999).
198. Zhao, Z., Sun, W., Yang, X., Ye, X., and Wu, Y., *Catal. Lett.* **65**, 115 (2000).
199. Rørvik, T., Dahl, I. M., Mostad, H. B., and Ellestad, O. H., *Catal. Lett.* **33**, 127 (1995).
200. Botella, P., Corma, A., and Lopez-Nieto, J. M., *J. Catal.* **185**, 371 (1999).
201. Hommeltoft, S. I., *Appl. Catal. A* **221**, 421 (2001).
202. Clet, G., Goupil, J. M., Szabo, G., and Cornet, D., *Appl. Catal. A* **202**, 37 (2000).
203. Nascimento, P., Szabo, G., and Milan, A., U.S. Patent 6,225,517 (2001).
204. Kojima, M. and Kocal, J. A., U.S. Patent 5,391,527 (1995).
205. Funk, G. A., Hobbs, S. A., Oroskar, A. R., Gembicki, S. A., and Kocal, J. A., U.S. Patent 5,523,503 (1996).
206. Zhang, S. Y. F., Gosling, C. D., Sechrist, P. A., and Funk, G. A., U.S. Patent 5,675,048 (1997).
207. McBride, T. K., Bricker, M. L., and Steigleder, K. Z., U.S. Patent 5,744,682 (1998).
208. Kocal, J. A. and Oroskar, A. R., U.S. Patent 5,849,977 (1998).
209. McBride, T. K., Bricker, M. L., and Steigleder, K. Z., U.S. Patent 5,883,039 (1999).
210. Herbstman, S., Cole, E. L., and Estes, J. H., U.S. Patent 4,138,444 (1979).
211. Mantilla-Ramirez, A., Ferrat-Torres, G., Dominguez, J. M., Aldana-Rivero, C., and Bernal, M., *Appl. Catal. A* **143**, 203 (1996).
212. Chou, T. S., Huss Jr., A., Kennedy, C. R., Kurtas, R. S., and Tabak, S. A., World Patent WO 90/00534 (1990).
213. Huss Jr., A. and Johnson, I. D., U.S. Patent 5,221,777 (1993).
214. Chou, T. S., Huss Jr., A., Kennedy, C. R., and Kurtas, R. S., World Patent WO 90/00533 (1990).
215. de Angelis, A., Flego, C., Ingallina, P., Montanari, L., Clerici, M. G., Carati, C., and Perego, C., *Catal. Today* **65**, 363 (2001).
216. Ackerman, S., Chitnis, G. K., and McCaffrey Jr., D. S., *Preprints, Div. Petr. Chem., Am. Chem. Soc.* **46**, 241 (2001).
217. Taylor, R. and Sherwood Jr., D. E., *Appl. Catal. A* **155**, 195 (1997).
218. Clark, M. C. and Subramaniam, B., *Ind. Eng. Chem. Res.* **37**, 4 (1998).
219. Santana, G. M. and Akgerman, A., *Ind. Eng. Chem. Res.* **40**, 3879 (2001).

220. Ginosar, D. M., Thompson, D. N., Coates, K., and Zalewski, D. J., *Ind. Eng. Chem. Res.* **41**, 2864 (2002).
221. Querini, C. A., *Catal. Today* **62**, 135 (2000).
222. Jones, E. K., *Adv. Catal.* **10**, 165 (1958).
223. Daage, M. and Fajula, F., *Bull. Soc. Chim. Fr.* **5-6**, 160 (1984).
224. Cupit, C. R., Gwyn, J. E., and Jernigan, E. C., *Petro/Chem. Eng.* **33**, 47 (1961).
225. Nivarthy, G. S., Feller, A., Seshan, K., and Lercher, J. A., *Microp. Mesop. Mater.* **35-36**, 75 (2000).
226. Schweitzer, E. J. A., Barendregt, S., and van der Oosterkamp, P. F., in: Proceedings of the Petrotech 98, Bahrein, 81, 1998.
227. Dolinsky, S. E. and Plakhotnik, V. A., in: Proceedings of the 13th International Zeolite Conference, Montpellier, 272, 2001.
228. Dolinskii, S. E., Subbotin, A. N., Lishchiner, I. I., Plakhotnik, V. A., and Mortikov, Y. S., *Petrol. Chem.* **37**, 447 (1997).
229. Cornet, D., Goupil, J. M., Szabo, G., Poirier, J. L., and Clet, G., *Appl. Catal. A* **141**, 193 (1996).
230. Goupil, J. M., Poirier, J. L., and Cornet, D., *Ind. Eng. Chem. Res.* **33**, 712 (1994).
231. Black, S. M., Gosling, C. D., Steigleder, K. Z., and Shields, D. J., in: Proceedings of the NPRA Annual Meeting, San Antonio, TX, USA, 2000.
232. D'Amico, V. J., van Broekhoven, E. H., Nat, P. J., Nousiainen, H., and Jakkula, J., in: Proceedings of the NPRA 2002 Annual Meeting, San Antonio, TX, USA, 2002.
233. van Broekhoven, E. H., Mas Cabre, F. R., Bogaard, P., Klaver, G., and Vonhof, M., U.S. Patent 5,986,158 (1999).
234. Buchold, H., Dropsch, H., and Eberhardt, J., in: Proceedings of the World Petroleum Congress 2002, Rio de Janeiro, in print, 2002.
235. Sarup, B., Hommeltoft, S. I., Sylvest-Johansen, M., and Søgaard-Andersen, P., in: Proceedings of the DGMK-Conference "Catalysis on Solid Acids and Bases", Berlin, 175, 1996.

Chapter 3

A detailed investigation of the mechanism of iso-butane/n-butene alkylation on zeolite based catalysts

Abstract

Different samples of the large pore zeolite X in its acidic form were explored as catalysts for the iso-butane/butene alkylation reaction. The materials were characterized by IR spectra of adsorbed pyridine, ammonia-TPD, SEM, XRD, AAS and ^{27}Al NMR and tested in a continuously operated stirred tank reactor under industrially relevant conditions. A high ratio of Brønsted to Lewis acid sites and a high concentration of strong Brønsted acid sites ensure a high hydride transfer activity and therefore are mandatory for long catalyst life. Iso-butane self-alkylation activity is higher in catalysts with a high ratio of Brønsted to Lewis acid sites. The influence of the reaction temperature, the olefin space velocity and the paraffin/olefin ratio were evaluated. The catalytic performance is very sensitive with respect to the reaction temperature. The optimum reaction temperature was 75°C concurrent with a maximum in self-alkylation activity. The lifetimes were found to be correlated linearly with residence time, while the feed paraffin/olefin ratio and the space velocity had only minor effects on the total productivity of the zeolite based catalysts.

3.1 Introduction

The importance of iso-butane/butene alkylation in the refining industry as a source of clean high-octane gasoline is greater than ever (1, 2). Until now, industrial processes are based on sulfuric and hydrofluoric acid as catalysts. Processes utilizing solid acid catalysts have not been successfully implemented because of the rapid deactivation of the solid catalysts. As all solid acids suffer from this drawback, numerous efforts have been made to overcome this problem (3, 4).

A variety of different materials has been tested as solid alkylation catalysts. Among oxidic materials, large pore zeolites, which are non-corrosive, non-toxic, and rather inexpensive, have the highest concentration of acid sites with sufficient strength. Furthermore, well-proven ways of regeneration methods are available. Among the zeolites explored so far, materials based on faujasites and zeolite BEA showed the best performance. While BEA has a lower limit in its Si/Al ratio of about 9, faujasites can be synthesized with ratios down to 1. As a consequence of this, zeolites Y and X potentially have higher Brønsted acid site concentrations than other materials. Because of the dependence of the total turnover number on the Brønsted acid site concentration (see ref (5)), this is expected to lead to longer catalyst lifetimes.

Several studies have been devoted to the use of these materials. However, since a considerable amount of the literature describes experiments in fixed bed or batch reactors under conditions of ill-defined catalyst activity and rapid catalyst deactivation, the correlation between the physicochemical properties of the material and the reaction conditions on the one and the catalytic performance on the other side has remained ambiguous. In particular, the role of the catalyst acidity, i.e., the strength and concentration of Brønsted- respectively Lewis-acid sites, remains unclear.

It has been proposed, that only very strong Brønsted acid sites are active in alkylation (6). Other authors suggest that Brønsted sites with intermediate strength are catalytically active (7), while there is agreement that weak Brønsted centers only catalyze oligomerization. Furthermore, the influence of Lewis centers such as extra-framework aluminum (EFAL) species resulting from the (sometimes deliberate) dealumination of the zeolite framework is not fully understood. The presence of such sites could lead to an increase in the strength of some Brønsted acid sites, but might also neutralize Brønsted acid sites (8). In addition, Lewis acid sites have been proposed to enhance the rate of deactivation by catalyzing

dehydrogenation, which leads in turn to unsaturated carbenium ions (9) and by increasing the butene concentration close to the Brønsted acid sites (5).

Also the influence of important process parameters such as reaction temperature, paraffin/olefin ratio and olefin space velocity needs further examination. De Jong *et al.* (10) developed a basic kinetic model to describe the influence of the paraffin/olefin ratio and the olefin space velocity on the lifetime of selected catalysts. Extended catalyst lifetimes were achieved by using a continuous stirred tank reactor, which (assisted by low olefin space velocities and high paraffin/olefin ratios) assured a low olefin concentration throughout the reactor. The authors reported oligomerization to be two orders of magnitude faster than hydride transfer, while Simpson *et al.* (11) using a plug-flow reactor with very dilute feed suggested even three orders of magnitude difference in the two reaction rates. In liquid phase, the reaction was found to be severely diffusion limited. Moreover, the authors suggested that hydride transfer is sterically more demanding than olefin addition. Taylor and Sherwood (12) developed an alternate kinetic model to estimate the lifetime of the catalyst in dependence of several process parameters, including the reaction temperature. It was concluded that all changes in experimental conditions, which increase the concentration of unreacted alkenes, decrease the catalyst lifetime and product quality. The optimum reaction temperature was claimed to balance low butene conversion at low temperature and high oligomerization activity at high temperature.

In this work, a variety of modified acidic faujasite samples was examined to establish correlations between the physicochemical properties and the process conditions on the one hand and the alkylation mechanism on the other. These findings are related to the observations with zeolite BEA, which have been reported earlier (see e.g., ref. (5)).

3.2 Experimental

3.2.1 Material synthesis

The parent material for most of the materials prepared in this study is Na-X obtained from Chemische Werke Bad Köstritz (Si/Al = 1.2). It was brought into the acidic form by aqueous exchange with 0.2M lanthanum nitrate solution and in some experiments by additional aqueous exchange with ammonium nitrate solution in various concentrations. The liquid-to-solid ratios in these experiments were usually approximately 10 ml/g. The temperature during exchange was kept at 70°C and the exchange time was two hours. This

procedure was typically repeated 2-3 times. After washing the resulting material with doubly distilled water until it was nitrate-free and drying at 100°C, the samples were calcined either in flowing air or under static air conditions with a slow temperature ramp up to 450°C. One sample was calcined in vacuum at 10^{-2} mbar. To further lower the sodium content of the zeolites, an additional ion-exchange step followed by washing, drying and calcining was carried out.

To exclude biased conclusions based on low-quality starting materials, other Na-X parent materials were also screened. The results were essentially the same. In addition, other La-sources were used, also without significant effects. For comparison, also a Na-Y (CBV100 from Zeolyst, Si/Al = 2.5) was exchanged with La^{3+} and NH_4^+ ions and a Na-H-USY (CBV400 from Zeolyst, Si/Al = 2.5, framework Si/Al ≈ 5), which was exchanged with NH_4^+ to give a H-USY.

3.2.2 Catalyst characterization

The ion-exchanged materials were characterized by SEM, XRD, ^{29}Si-NMR and ^{27}Al-NMR. AAS was used to determine the Si/Al ratio and the Na^+ concentration, usually expressed as the molar ratio of residual Na^+ per Al^{3+}. For measuring the acidity, two different kinds of adsorption/desorption experiments were carried out, i.e., TPD of ammonia in a vacuum setup with a mass spectrometer detector to estimate the total number of acid sites and sorption of pyridine monitored by IR spectroscopy. For the latter the sample was pressed into a self-supporting wafer, which was placed into a sorption cell, where it was activated in vacuum for 1 hr at 450°C. Then, the sample was cooled down to 100°C and pyridine at a partial pressure of 10^{-2} mbar was introduced into the system. After saturation of all acid sites, the sample was outgassed for 1 hr at 100°C followed by a linear increase of 10 K/min to 450°C and maintaining that temperature for 1 hour. Subsequently, the cell was cooled down again to 100°C. Spectra of the sample were taken before adsorption of pyridine at 100°C, after outgassing at 100°C and 450°C. From this set of spectra, the ratio of Brønsted (as evidenced by the band of pyridinium ions at 1540 cm^{-1}) to Lewis acid sites (the band of coordinately bound pyridine at 1450 cm^{-1}) was calculated for T = 100°C (B/L_{100}) and T = 450°C (B/L_{450}). Ratios of extinction coefficients were taken from ref. (13).

3.2.3 *Catalytic experiments*

The alkylation of iso-butane with 2-butene was performed in a stirred tank reactor operated in continuous mode. The liquefied gases were received from Messer with a purity of 99.95% (iso-butane) and 99.5% (cis-2-butene). The sample (typically 4 – 5 g) was activated *in situ* within the alkylation reactor at 170°C for 16 h in flowing nitrogen. After cooling down to the reaction temperature, typically 75°C, the reactor was filled with liquid iso-butane at a pressure of 32 bar. The reaction was started by admitting a butene-iso-butane mixture with a paraffin-to-olefin (P/O) ratio of 6.7 and an olefin space velocity (OSV) of 0.2 g_{butene} / ($g_{catalyst}$ hr). In order to investigate the influence of the reaction temperature on the alkylation mechanism, a study was performed on an exemplary catalyst at temperatures varying from 40°C to 130°C. On the same catalyst also the influence of the P/O ratio and the OSV was examined, with parameters between 6.7 and 18.1 (P/O ratio) and from 0.17 h^{-1} to 0.80 h^{-1} (OSV). These conditions (with the exception of the temperature) are in the range at which the commercial processes typically operate.

The product from the reactor was expanded and passed through a six-port-valve with a sample loop, the contents of which were injected automatically into an HP 6830 gas chromatograph equipped with a FID-detector and a 35 m DB-1 column. Downstream of the six-port-valve, the product stream was condensed into a cold trap cooled with a dry ice/isopropanol mixture. The product was collected over the whole time on stream and was weighed and analyzed chromatographically to give the integral product composition. The results were compared with the mathematical integration of the differential data points gathered during the run, with the differences being less than 10%.

When the reaction is started, the reactor contains only iso-butane. With the introduction of the iso-butane/butene mixture and the subsequent (near-) complete conversion of butene, the reactor content steadily changes its composition to an iso-butane/products mixture, with an increasing fraction of products. With the knowledge of the theoretical butene build-up curve derived from the mass balance (and its experimental verification) conversions and yields were calculated. At complete butene conversion the theoretical maximum yield is 2.04 $g_{product}/g_{butene}$, assuming a 1:1 stoichiometry of iso-butane alkylation with butene.

3.3 Results

3.3.1 Physicochemical characterization

A wide variety of samples was prepared *via* La^{3+} and NH_4^+ exchange steps followed by calcination in flowing or static air. A summary of some important physicochemical properties is compiled in Table 3-1. With two calcination steps zeolite X could be brought to a sodium level lower than 0.5%. Using only one calcination step, but performing multiple ammonium-exchange steps, resulted in a poorer exchange level. The benefit of employing a repeated exchange-calcination procedure has been described earlier (14). Additionally, the author reported that zeolite X was easier to exchange than zeolite Y. The same was observed here, seen in the lower exchange levels achieved with zeolite Y compared to zeolite X.

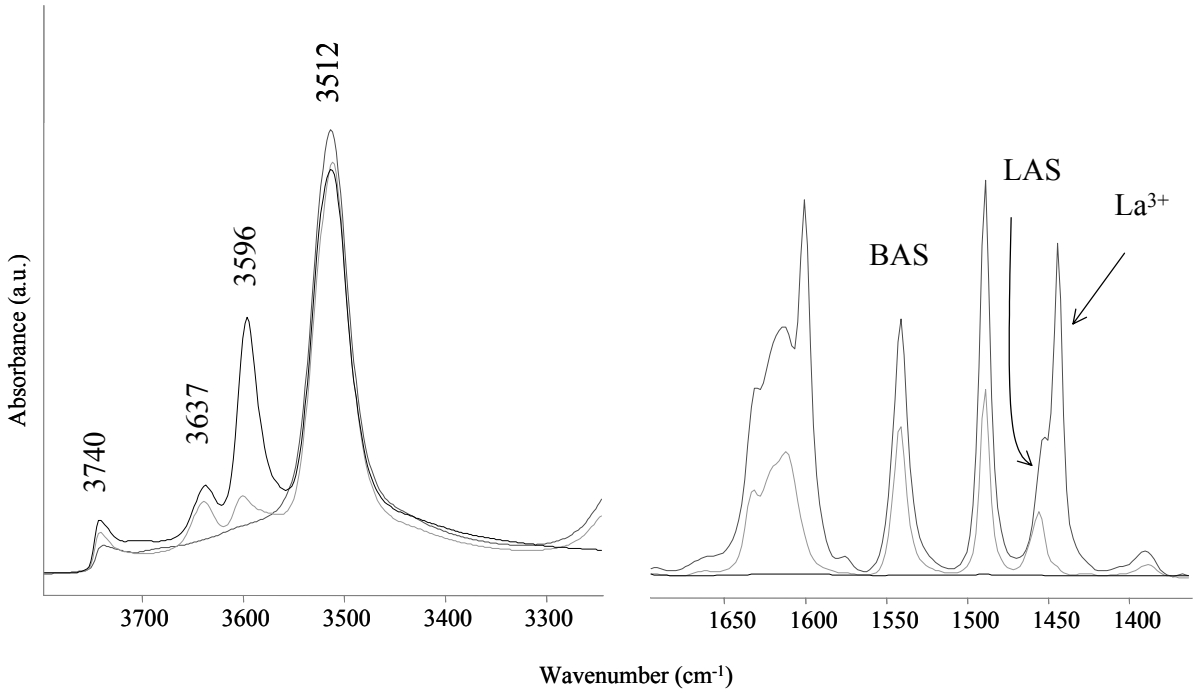

Figure 3-1: IR-spectra of La-X-e of activated sample (black line); sample with pyridine adsorbed at 100°C (dark gray line); sample after degassing at 450°C (light gray line). All spectra were taken at 100°C.

Pyridine sorption experiments revealed that zeolite X has a significantly higher fraction of strong Brønsted acid sites than zeolite Y. This leads to comparable B/L_{100}, but to considerably different B/L_{450} values, which are much higher for the X-samples.

Table 3-1: Modification procedure and selected physicochemical properties of the tested samples. The Na/Al ratio was measured by AAS, Brønsted and Lewis acid site ratios were measured by pyridine adsorption/desorption monitored by IR-spectroscopy.

Sample	Procedure	Na/Al mol/mol	strong BAS	strong LAS	B/L 100°C	B/L 450°C
La-X-a	2x La^{3+} + calc. + 2x 1M NH_4^+ + calc.	0.7%	33%	47%	1.8	1.3
La-X-b	2x La^{3+} + calc. + 2x 1M NH_4^+ + La^{3+} + calc.	0.0%	38%	44%	2.3	2.0
La-X-c	2x La^{3+} + calc. + 3x La^{3+} + calc.	0.0%	37%	50%	3.5	2.5
La-X-d	10x NH_4^+ 1M + 3x La^{3+} + calc. 400°C	1.7%	35%	62%	2.4	1.3
La-X-e	2x La^{3+} + calc. + 4x La^{3+} + calc.	0.5%	55%	65%	3.5	2.9
La-X-f	La-X e (without calc.) + 0.025M NH_4^+ + calc.		46%	55%	3.0	2.5
La-X-g	La-X e (without calc.) + 0.050M NH_4^+ + calc.	0.0%	37%	53%	3.5	2.4
La-X-h	La-X e (without calc.) + 0.075M NH_4^+ + calc.	0.0%	41%	50%	3.3	2.8
La-X-i	2x La^{3+} + calc. + 3x La^{3+} + calc.	0.5%	44%	55%	3.2	2.6
La-X-j	2x La^{3+} + vac.calc. + 3x La^{3+} + vac.calc.	0.0%	31%	38%	2.8	2.3
La-X-k	2x La^{3+} + calc. + 2x 0.5M NH_4^+ + La^{3+} + calc.	0.8%	44%	64%	2.3	1.6
La-X-l	2x La^{3+} + calc. + 2x 0.5M NH_4^+ + La^{3+} + calc.	0.2%	31%	50%	2.5	1.6
La-X-m	2x La^{3+} + calc. + La^{3+} + calc.	1.0%	30%	68%	2.2	1.0
La-X-n	2x La^{3+} + calc. + La^{3+} + 0.05M NH_4^++ calc.	1.7%	24%	43%	1.3	0.7
La-X-o	2x La^{3+} + calc. + La^{3+} + calc.	0.7%	27%	53%	1.7	0.9
La-X-p	3x La^{3+} + calc. + 3x 1M NH_4^+ + La^{3+} + calc.	0.0%	30%	56%	2.2	1.2
La-Y-a	2x La^{3+} + calc. + 2x 1M NH_4^+ + La^{3+} + calc.	6.5%	13%	62%	2.5	0.5
La-Y-b	2x La^{3+} + calc. + 3x 1M NH_4^+ + calc.	4.5%	18%	44%	1.9	0.8
La-Y-c	2x La^{3+} + calc. + 4x La^{3+} + calc.	13.4%	4%	56%	3.6	0.3
La-Y-d	La-Y c + 3x 1M NH_4^+ + calc.	0.9%	8%	49%	2.0	0.3
H-USY	7x 1M NH_4^+ + calc.	2.4%	27%	42%	1.3	0.8

Next to the bands at 1540cm^{-1} and 1450cm^{-1}, also a band at ca. 1445cm^{-1} was detected. This band has been attributed to Na^{+} or La^{3+} metal ions, which both act as weak Lewis acid sites, as concluded from the complete desorption of pyridine from these sites at 450°C. Figure 3-1 displays a typical spectrum of a La-X sample before (a) and after pyridine adsorption (b) at 100°C and after desorption at 450°C (measured after cooling down at 100°C, c). In the hydroxyl region four bands were observed, i.e., (i) the silanol band at 3740cm^{-1}, (ii) the band at 3637cm^{-1} (acidic hydroxyl group), (iii) the band at 3595cm^{-1} (acidic hydroxyl group) and the band characteristic for the non-acidic Lanthanum hydroxyl group at 3512cm^{-1}. Upon adsorption of pyridine, all OH bands except those for La-OH disappeared. After desorption to 450°C the weakly acidic silanol band and the 3637cm^{-1} band completely reappeared, while a substantial fraction of the hydroxyls characterized by the band at 3595cm^{-1} retained pyridine.

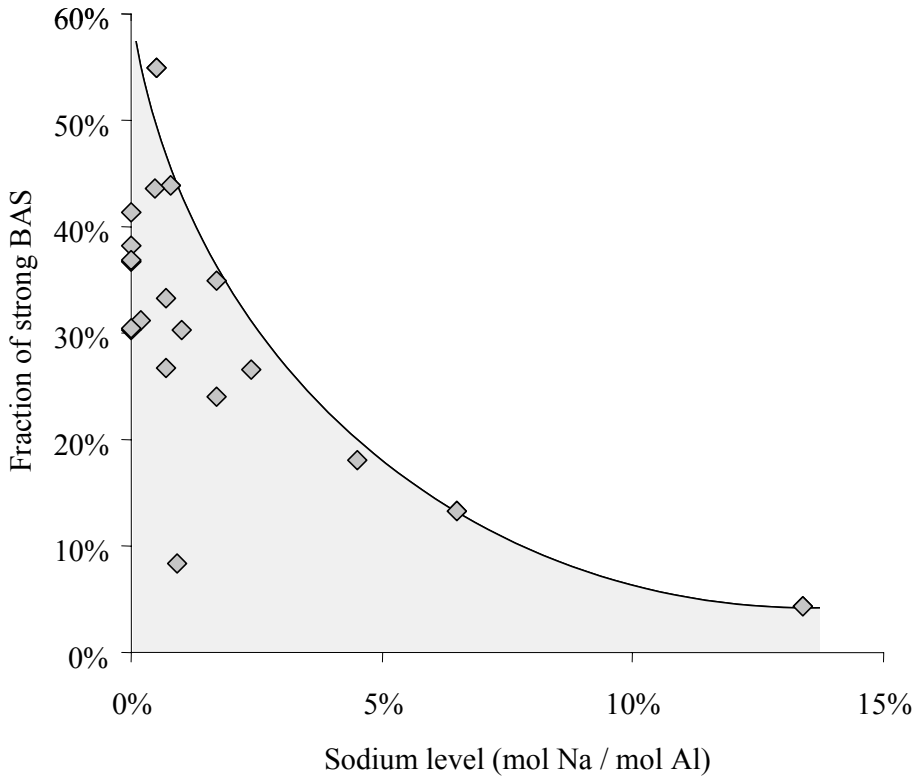

Figure 3-2: Fraction of strong Brønsted acid sites as a function of the sodium level in the individual zeolites.

The influence of the exchange degree on the acidity can be seen in Figure 3-2. With

decreasing Na^+ concentration, the fraction of strong Brønsted acid sites (expectedly) increased. The graph suggests that the concentration of Na^+ determines an upper limit for the distribution of site strengths of the Brønsted acid sites. Localized weakening of acid sites by neighboring Na^+ ions is suggested by the pronounced scattering of points under the curve. Obviously, the presence of Na^+ ions exhibits a strong poisoning effect on neighboring acid sites. This is typical for zeolites with some concentration of extra lattice alumina as has been pointed out by Haag *et al.* (15). Note that pronounced sodium poisoning in faujasites was also observed by Fritz and Lunsford (16).

The overall acid site concentration as measured with NH_3-TPD (not shown in Table 3-1) was between 0.6 – 0.8 mmol/g for all the La-X samples. The values for the Y-zeolites were slightly higher, around 1 mmol/g.

SEM was used to analyze the crystal size. The zeolite X samples showed an average crystal size between 1 and 2 μm, the zeolite Y samples between 0.5 and 1 μm.

^{27}Al-MAS-NMR discerned for all the measured samples three different aluminum species. Besides the signal at approx. 50-60 ppm representing tetrahedrally coordinated Al, and the signal at 0 ppm for octahedral Al, also a broad signal between 40 and 10 ppm was detected. For the La-X samples, this was the most prominent signal, accounting for about 70% of the total signal area. The assignment of this signal is not straightforward. It has been reported to represent distorted tetrahedral framework Al in both La-free (17) and La-containing (18, 19) samples, but it could also indicate a second type of poorly ordered extraframework Al (20) and pentacoordinated Al (19). ^{29}Si-MAS-NMR was used to characterize La-X-g, La-X-k and La-X-p and the parent Na-X. The Si(*n*Al) signals (*n* represents the number of aluminum atoms in the second coordination sphere of the silicon atom) with the La-X samples were high-field shifted compared to the signals in Na-X. In La-X the chemical shifts were -88.9, -93.1, -96.7, -102.1 and -105.5 ppm for Si(*n*Al) atoms with n = 4, 3, 2, 1 and 0, respectively. The corresponding chemical shifts for Na-X were –84.0, -88.4, -93.6, -98.4 and –102.1 ppm. This upward shift is attributed to a local strain of framework SiO_4 tetrahedra caused by neighboring large La-cations (18). Si/Al ratios were calculated from the signal areas. For the parent Na-X the Si/Al ratio was determined to be 1.18, which is in good agreement with the elemental analysis. La-X-g had a Si/Al ratio of 1.10, La-X-k 1.18 and La-X-p 1.28. Although these values seem rather low compared to the sodium form, they increase with increasing B/L ratio (see Table 3-1) reflecting the increasing

degree of dealumination. The Si/Al ratios of the La-containing materials may be underestimated due to an overlap of the La-distorted Si(4Al) signal (-88.9 ppm) with the non-distorted Si(3Al) signal (-88.4 ppm) as was suggested by Gaare and Akporiaye for La exchanged X and Y zeolites (21).

3.3.2 Activity and selectivity in alkylation of iso-butane with n-butene

The alkylation reaction was performed with the samples of Table 3-1, employing a reaction temperature of 75°C, an olefin space velocity of 0.2 g_{butene} / ($g_{catalyst}$ hr), and a P/O ratio of 6.7. The lifetimes achieved varied from 3 – 12 hrs.

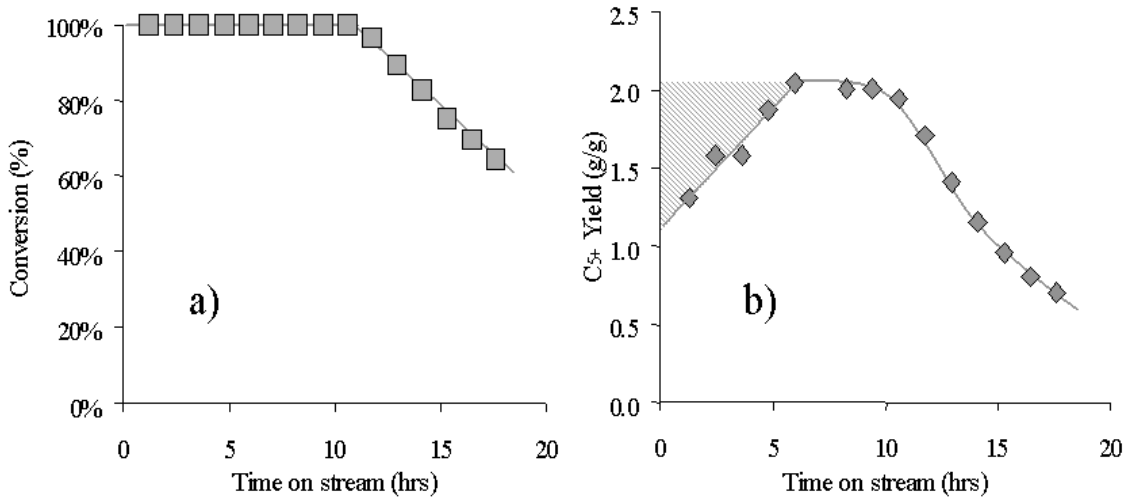

Figure 3-3: Alkylation performance of catalyst La-X-e. a) Butene conversion as a function of time on stream; b) C_{5+} product yield as a function of time on stream. T = 75°C, OSV = 0.18 h^{-1}, P/O ratio = 6.7. The shaded area represents the buildup of hydrocarbons on the zeolite surface.

Before we describe the differences among the tested materials, a typical case is described in detail. Figure 3-3 compiles the conversion (a) and the yield (b) of La-X-e. The lifetime, defined as the time of the (near-) complete butene conversion, was approximately 11 hrs. Then, the conversion sharply dropped to values below 60%. The yield steadily increased for the first 5 hrs TOS, reaching the theoretical maximum and staying nearly constant for the next 5 hrs. With the decrease in conversion, also the yield decreased to values below 1 g/g. The slow increase in yield for the first hours on stream is attributed to a build up of hydrocarbons in the catalyst pores, especially on the acid sites. The integrated area between

the curve and the theoretical maximum amounts to an average 2,3 – 2,7 butene molecules per acid site. This suggests that on each site on average a C_{10} hydrocarbon is adsorbed.

Figure 3-4 (a) displays the selectivities to the three main product fractions, *i.e.,* the hydrocarbons with 5 to 7 carbon atoms, the octane fraction and the fraction with 9 and more carbon atoms as function of time on stream. Additionally, the selectivity to n-butane is shown, which was produced in substantial amounts in the beginning. The main products were iso-octanes with an initial selectivity of 85 wt.%, which decreased with time on stream to a value of approximately 60 wt.%. The selectivity to the cracked products (C_5-C_7) passed through a maximum of approximately 18 wt.% at 9 hrs TOS. The heavy alkylation products (C_{9+}) had a constant low selectivity during the first 5 hrs, after which the selectivity increased to values above 30 wt.%. The n-butane selectivity monotonously declined from a start value of approximately 8 wt.%.

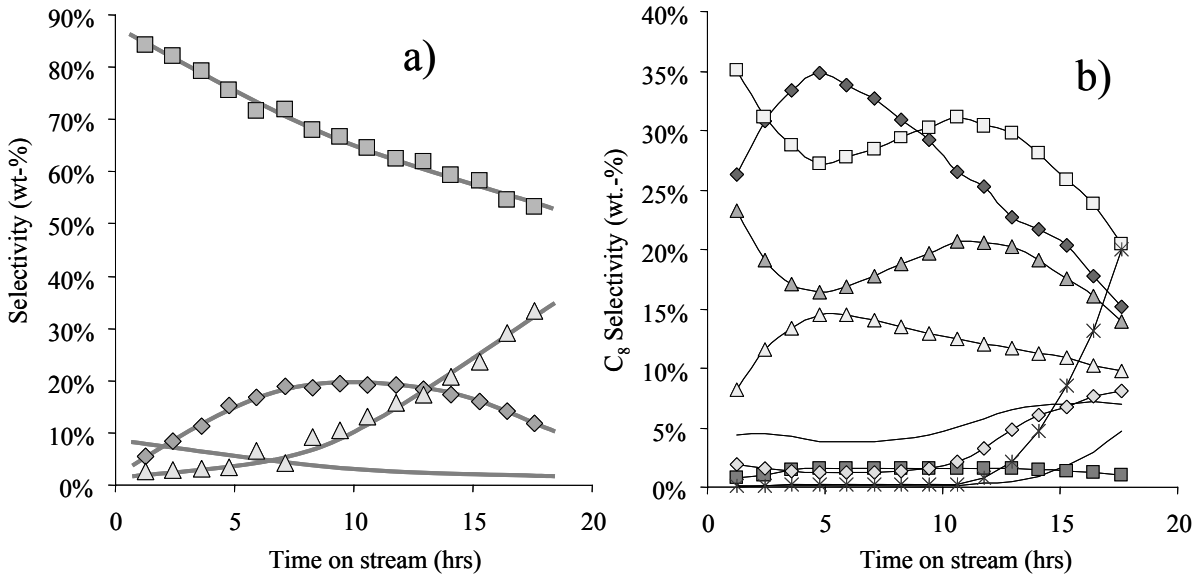

Figure 3-4: Alkylation performance of catalyst La-X-e. a) Product group selectivities with time on stream (n-butane, ◆ C_5 – C_7 products, ■ C_8 products, △ C_{9+} products); b) selectivities in the C_8 fraction with time on stream (—◆— 2,2,4-TMP, —■— 2,4-DMH, —△— 2,5-DMH/2,2,3-TMP, —▲— 2,3,4-TMP, —□— 2,3,3-TMP, —— 2,3-DMH, —— 4-MHp/3,4-DMH, —◇— 3,4-DMH, —✳— Octenes). T = 75°C, OSV = 0.18 h^{-1}, P/O ratio = 6.7.

The selectivity in the C_8-region is shown in Figure 3-4 (b). The main components were the trimethylpentanes 2,2,4-TMP, 2,3,3-TMP and 2,3,4-TMP, which made up together more

than 80 wt.% of the total C_8 fraction. The characteristic increase in 2,2,4-TMP selectivity during the first hours TOS and the subsequent decline was seen with all La containing samples of zeolite X. The fourth TMP, 2,2,3-TMP, which is the primary product of the alkylation of iso-butane with 2-butene, could not be separated from 2,5-DMH. Their combined selectivity showed the same TOS-behavior as 2,2,4-TMP, with values between 7 and 14 wt.% of the C_8 fraction. The others, 2,3-DMH, 2,5-DMH and 3,4-DMH had selectivities below 5 wt.% during the time of complete butene conversion. When the conversion started to drop, the selectivity to 3,4-DMH increased and octenes were observed in the product stream. Then, the octenes rapidly became the dominant product indicating a switch in the reaction from alkylation to dimerization.

The results compiled in Figures 3-3 and 3-4 clearly demonstrate the problems associated with the use of a tubular/plug flow reactor. Using a plug flow reactor, a marked concentration gradient in olefins and products exists over the length of the catalyst bed, so that at a certain time on stream catalyst particles at different positions in the bed will catalyze different reactions. Consequently, the product at the reactor exit will be a mixture of products of different deactivation stages and the catalyst particles at the top of the active zone will experience a much higher olefin concentration than the particles in a backmixed reactor under identical macroscopic operating conditions. In consequence, this will lead to a more rapid decrease in the lifetime of the catalyst particles at the top of the active catalyst bed. After some time on stream, these deactivated catalyst particles will produce octenes, which will subsequently react further downstream in a zone containing still fully active sites producing heavy-end alkylation products. These will either desorb as such or undergo further cracking. With the continuously operated stirred tank reactor, ideally, all particles are in contact with the same fluid at the same time on stream. Therefore, all particles show the same state of deactivation and experience a much lower severity with respect to the olefin concentration. Furthermore, the product from a CSTR will contain much more of the primary products, the trimethylpentanes, while with a PFR generally more oligomerization/cracking products are formed. To produce a high quality alkylate in a plug-flow reactor very high P/O ratios and low OSV have to be used, in this way slowing down the deactivation process, but not preventing the coexistence of catalyst particles with a broad distribution of deactivation states.

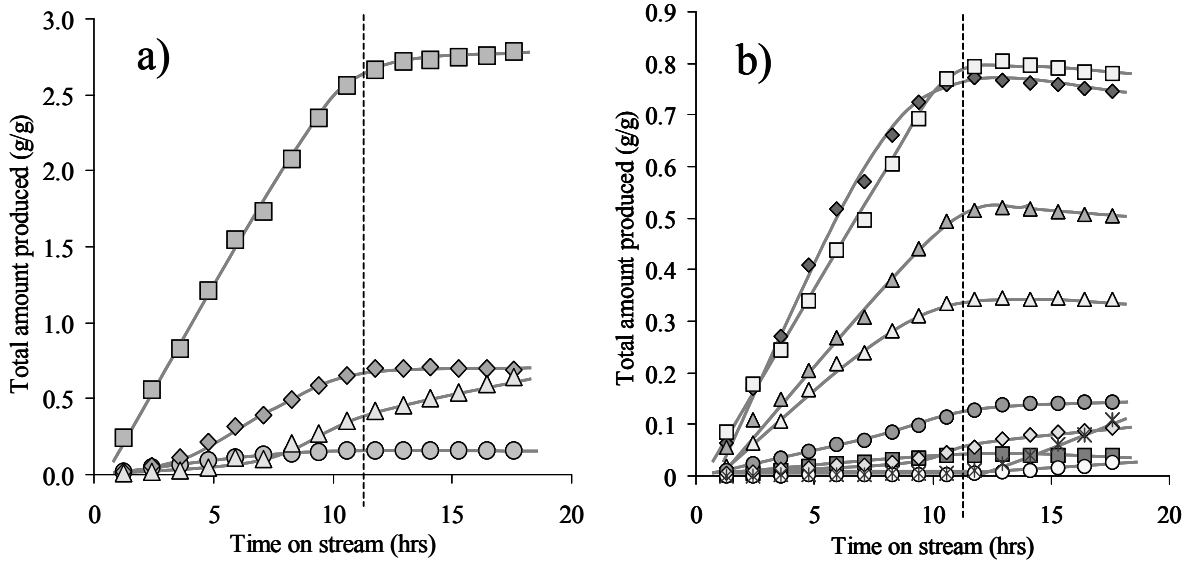

Figure 3-5: Alkylation performance of catalyst La-X-e. a) Total amount produced of the different product groups with time on stream (○ n-butane, ◇ C_5 – C_7 products, □ C_8 products, △ C_{9+} products); b) total amounts produced of the individual C_8 products with time on stream (—◆— 2,2,4-TMP, —□— 2,4-DMH, —△— 2,5-DMH/2,2,3-TMP, —▲— 2,3,4-TMP, —□— 2,3,3-TMP, —●— 2,3-DMH, —○— 4-MHp/3,4-DMH, —◇— 3,4-DMH, —✳— Octenes). T = 75°C, P/O ratio = 6.7, OSV = 0.18 h^{-1}. The dashed line represents the end of the lifetime of the catalyst.

Thus, the CSTR allows for a more detailed data treatment, when examining the total amount of individual compounds produced with TOS. In Figure 3-5 (a) this is shown for the different product groups; Figure 3-5 (b) displays the total production of individual octanes (normalized against the catalyst mass) with TOS. The dashed line represents the end of the catalyst lifetime. As can be seen, the production of the trimethylpentanes was nearly constant over the catalyst lifetime with a sudden stop when the catalyst deactivates. The cracking activity also ceased completely at this point. The only compounds, which were produced after the conversion started dropping, were 3,4-DMH, octenes, and some of the heavier hydrocarbons. Whether these compounds are alkanes or alkenes is unclear at this point. It is noteworthy that the production of n-butane slowed down some hours earlier than that of the other products. The slight decrease in the produced mass of the trimethylpentanes during the last stage of the reaction suggests that these alkane molecules are consumed under these reaction conditions with a small rate.

3.3.3 Influence of the acidity

After the detailed description of a typical case, the relationship between the acidity of the individual catalyst samples and their performance in the alkylation is addressed. All examined materials were active and selective alkylation catalysts. In general, zeolite X samples showed longer lifetimes than zeolite Y samples.

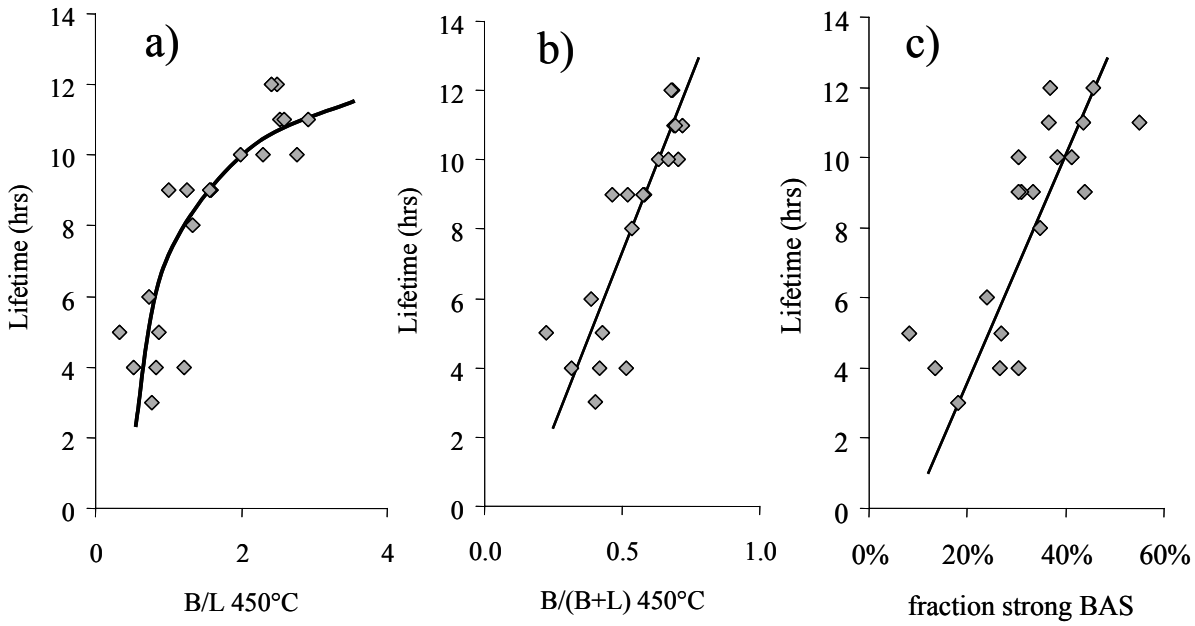

Figure 3-6: Details of the acidity-lifetime correlations. a) Catalytic lifetime of the individual samples as a function of the Brønsted/Lewis ratio measured at 450°C; b) catalytic lifetime of the individual samples as a function of the Brønsted/(Brønsted + Lewis) ratio measured at 450°C; c) catalytic lifetimes as a function of the fraction of strong Brønsted centers. All catalytic measurements were performed at T = 75°C, OSV = 0.18 h^{-1}, P/O ratio = 6.7.

The acidity of zeolites has extensive and intensive components. The IR spectra of sorbed pyridine allow estimating the concentration of Brønsted and Lewis acid sites and their relative strength. From this, the ratios of Brønsted to Lewis acid sites at specific (outgassing) temperatures representing different strengths of the acid sites can be estimated. A strong correlation between the Brønsted/Lewis ratios measured at 450°C was found (see Figure 3-6 (a).) With increasing ratios of Brønsted to Lewis acid sites, the catalyst lifetimes increased. The correlation is directly proportional to the fraction of Brønsted acid sites among all acid sites (B/(B+L) ratio, see Figure 3-6 (b)). Interestingly, the absolute number of Brønsted or of

Lewis acid sites showed no correlation against the catalyst lifetimes. A moderately strong relationship was found for the concentration of strong Brønsted acid sites with the lifetimes (Figure 3-6 c)). The concentration of strong Lewis acid sites alone did not directly influence the alkylation performance.

Samples with varying lifetimes also showed varying selectivities. As these samples pass through different stages of deactivation at different absolute times on stream, the integral selectivities of alkylate produced until the end of the catalyst lifetime is used in this study. Note that this differs markedly from the practice in other reports, where either data at very short TOS are compared or even selectivities at a later time-on-stream with varying conversion levels. The products compared are virtually free of olefins and represent the yield along the usable lifetime.

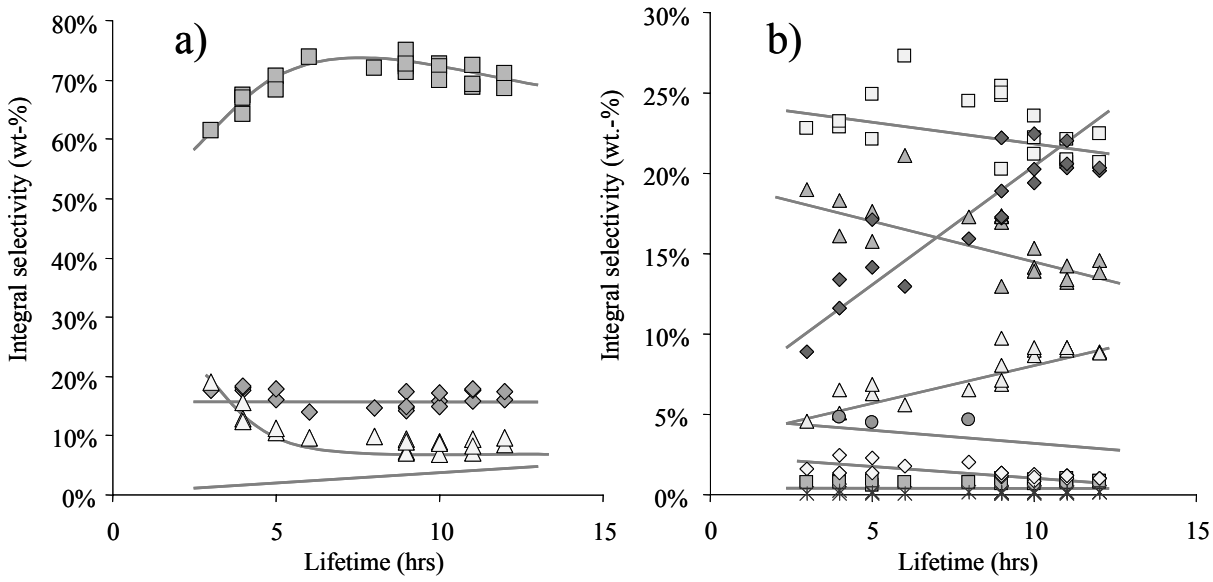

Figure 3-7: Changes in selectivities with the lifetimes of the individual samples. a) Integral selectivities to the different product groups as a function of the lifetimes of the individual samples (n-butane, ◆ C_5 – C_7 products, ■ C_8 products, △ C_{9+} products); b) Integral selectivities to the individual C_8 products as a function of the lifetimes of the individual samples (—◆— 2,2,4-TMP, —□— 2,4-DMH, —△— 2,5-DMH/2,2,3-TMP, —▲— 2,3,4-TMP, —□— 2,3,3-TMP, —— 2,3-DMH, —— 4-MHp/3,4-DMH, —◇— 3,4-DMH, —✳— Octenes). Each data point represents a single experiment. T = 75°C, OSV = 0.18 h^{-1}, P/O ratio = 6.7.

In Figure 3-7 (a), the dependence of the integral selectivities to the different product

groups on the lifetimes is shown. Each data point represents one individual alkylation experiment. For all samples, the isooctane fraction dominated the products. With increasing lifetime the C_8-selectivity increased from 60 to 75 wt.% and slightly decreased again with catalysts of long lifetimes. The selectivity to cracking was independent of the lifetime with about 17 wt.%. Most importantly, a steep decline in the selectivity to the heavy-end products was seen with increasing lifetime from 20 down to 8 wt.%. The selectivity to n-butane increased linearly with the lifetime from 1.6 wt.% to nearly three times as much, 4.7 wt.%. Note that the total amount of n-butane produced with the long living catalysts was more than four times higher than the number of acid sites in the sample.

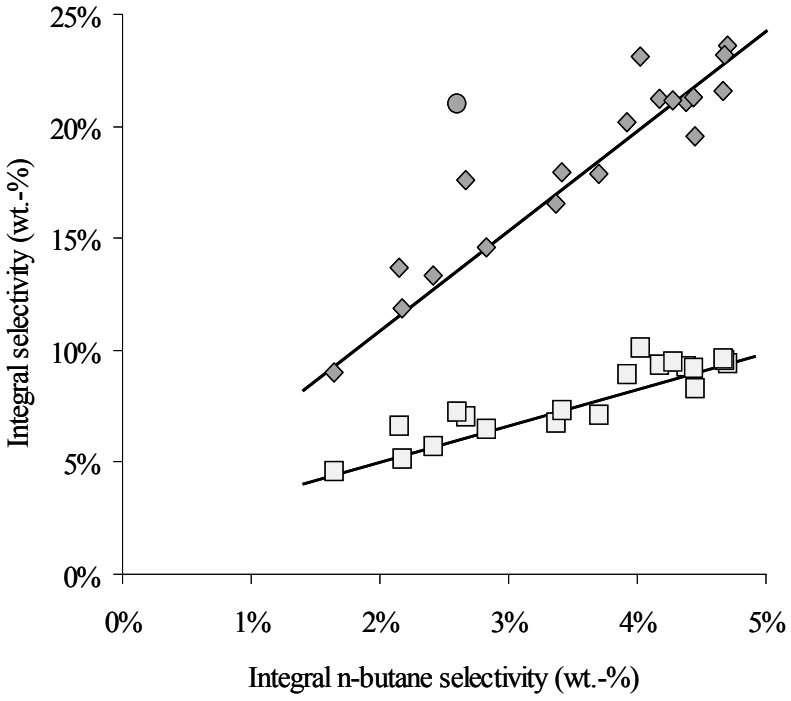

Figure 3-8: The integral selectivities to 2,2,4-TMP (◆) and 2,5-DMH/2,2,3-TMP (□) as a function of the integral n-butane selectivity. The round symbol ( ) represents the 2,2,4-TMP selectivity measured with H-USY. T = 75°C, OSV = 0.18 h^{-1}, P/O ratio = 6.7.

Figure 3-7 (b) displays the integral selectivities in the C_8-fraction. But unlike Figure 3-4 (b), the selectivity is based on the total product and not on the C_8-fraction alone. This representation was used here, as it shows the relative rates of production for the individual compounds. With increasing lifetime, only the rates for 2,2,4-TMP and 2,2,3-TMP + 2,5-DMH increased, while 2,3,4-TMP and 2,3-DMH decreased. The selectivities to the other

products did not change significantly. Thus, 2,2,4-TMP and 2,2,3-TMP + 2,5-DMH are concluded to be at large responsible for the increase in selectivity to the octane-fraction as shown in Figure 3-7 (a).

Figure 3-8 demonstrates the linear interdependence between n-butane on the one hand and 2,2,4-TMP and 2,2,3-TMP + 2,5-DMH on the other. H-USY was found to deviate from this trend (marked in Figure 3-8 with circular symbols). Here, the 2,2,4-TMP selectivity was higher than expected from the general trend, whereas the n-butane and 2,2,3-TMP + 2,5-DMH selectivity did not diverge.

3.3.4 Influence of the reaction temperature

La-X-k was used as a typical catalyst to explore the influence of the reaction temperature. The temperature was varied from 40°C to 130°C, keeping the other conditions (P/O ratio = 6.7, OSV = 0.2 g_{butene} / ($g_{catalyst}$ hr)) constant. Figure 3-9 displays the lifetime in dependence of the reaction temperature. The curve exhibits a surprisingly sharp maximum at 75°C. A difference of only 35°C downward and 55°C upwards was sufficient to reduce the lifetime to a fourth.

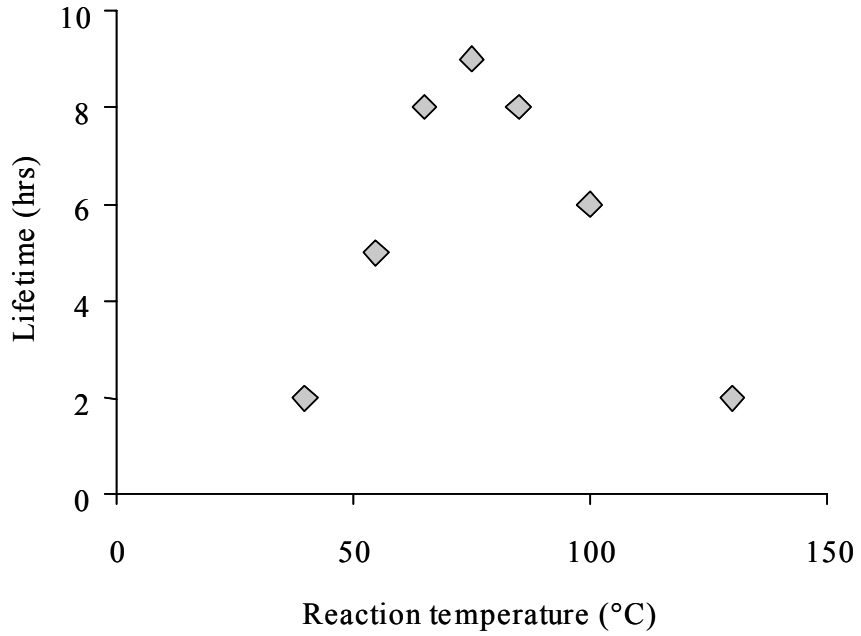

Figure 3-9: Lifetime of catalyst La-X-k as a function of the reaction temperature. OSV = 0.18 hrs^{-1}, P/O ratio = 6.7

Also the selectivities drastically changed with the temperature, as can be seen in Figure 3-10. The selectivities are presented in the same manner as in Figure 3-7. Figure 3-10 (a) shows the decline in the isooctane-selectivity with rising temperature, which was compensated by an increase in the cracking selectivity and at high temperatures also in the C_{9+} selectivity. The selectivity to n-butane increased by a factor of three to about 5 wt.% and then slightly dropped again. Figure 3-10 (b) shows that the drastic decline in C_8-selectivity was caused by a steadily decreasing 2,3,4-TMP and 2,3,3-TMP selectivity, which was partly compensated by an increase in the 2,2,4-TMP selectivity. The 2,2,4-TMP selectivity passed a maximum between 75° and 100°C. The production of all dimethylhexanes increased with the reaction temperature.

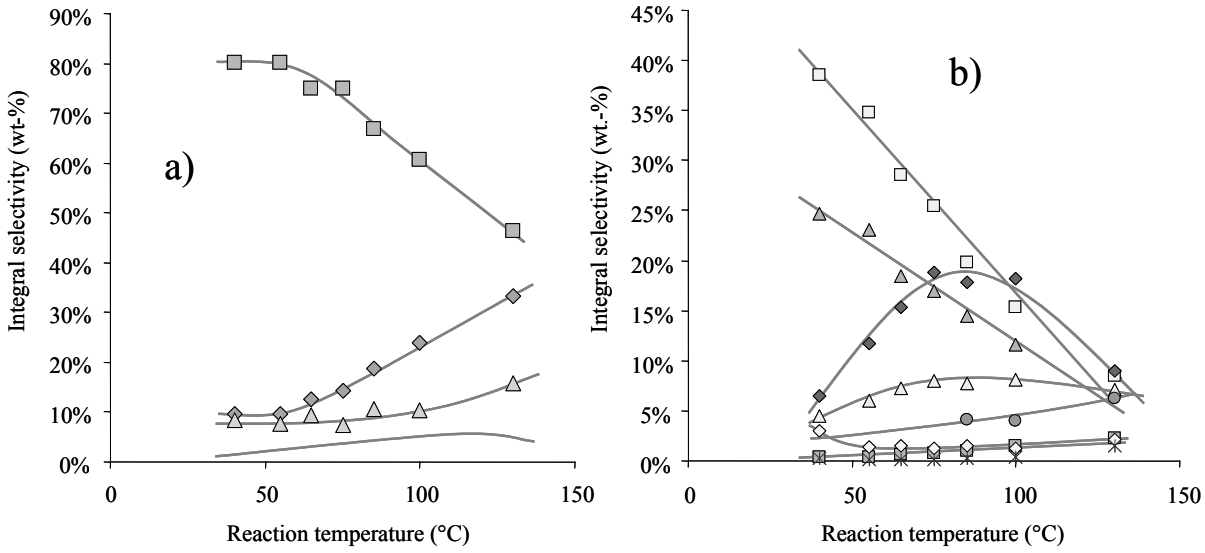

Figure 3-10: Changes in selectivities measured with La-X-k as a function of the reaction temperature. Integral selectivities to the different product groups *vs.* reaction temperature (n-butane, ◆ $C_5 - C_7$ products, ■ C_8 products, △ C_{9+} products); b) Integral selectivities to the individual C_8 products *vs.* reaction temperature (—◆— 2,2,4-TMP, —■— 2,4-DMH, —△— 2,5-DMH/2,2,3-TMP, —▲— 2,3,4-TMP, —□— 2,3,3-TMP, —— 2,3-DMH, —— 4-MHp/3,4-DMH, —◇— 3,4-DMH, —✳— Octenes). OSV = 0.18 hrs^{-1}, P/O ratio = 6.7.

3.3.5 Influence of olefin space velocity and paraffin/olefin ratio

The catalyst La-X-k, which was used for studying the influence of varying temperatures,

was also used in a study on the influence of the OSV and P/O ratio. The OSV was raised from 0.17 h^{-1} to 0.38 h^{-1} and 0.79 h^{-1}. The lifetime was found to be linear with the reciprocal of the OSV, i.e., the residence time (see Figure 3-11 (a)). In other words, the integral yields did not change significantly with varying space velocity. The same amount of alkylate was produced in shorter time. Increasing the OSV did also not lead to significant changes in the selectivities to the different product groups except for a slight decrease in the n-butane selectivity and a concomitant slight increase in the C_{9+} selectivity, as shown in Figure 3-11 (b). Within the C_8-region, the selectivities to 2,2,4-TMP and 2,2,3-TMP + 2,5-DMH decreased, while all other octane-selectivities increased (Figure 3-11 (c)).

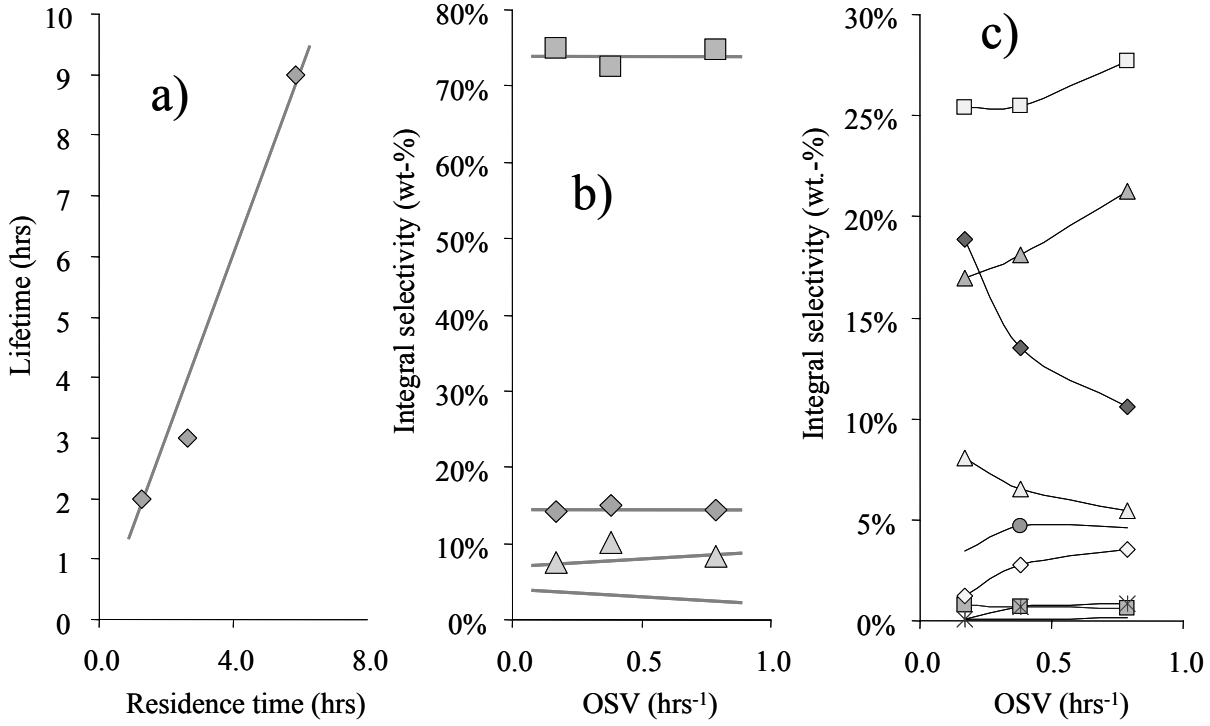

Figure 3-11: Influence of the olefin space velocity on the alkylation performance measured with catalyst La-X-k. a) Lifetime vs. residence time; b) integral product group selectivities as a function of the olefin space velocity (n-butane, ◆ C_5 – C_7 products, ■ C_8 products, △ C_{9+} products); c) integral selectivities for the individual octanes as a function of the olefin space velocity (—◆— 2,2,4-TMP, —■— 2,4-DMH, —△— 2,5-DMH/2,2,3-TMP, —▲— 2,3,4-TMP, —□— 2,3,3-TMP, —— 2,3-DMH, —— 4-MHp/3,4-DMH, —◇— 3,4-DMH, —✳— Octenes). T = 75°C, P/O ratio = 6.7.

The same sample was additionally tested with a paraffin/olefin feed ratio of 18.1 at an

olefin space velocity of 0.17 h^{-1} and 0.66 h^{-1}. Despite the much higher ratio, the lifetime increased only from 9 h to 11 h, when employing an OSV of 0.17 h^{-1}. A slight increase in the C_8-selectivity was seen, while the selectivities to the cracking and the heavy-end products decreased. The n-butane selectivity was somewhat higher. In the octane fraction, the selectivities to 2,2,4-TMP and 2,2,3-TMP + 2,5-DMH decreased with a concurrent increase in the other C_8-selectivities. When increasing the OSV to 0.66 h^{-1} with a P/O ratio of 18.1, the same effects were seen as with the lower P/O ratio of 6.7, i.e., essentially equal integral yields, a further decrease in the 2,2,4-TMP selectivity and no significant changes in the product group selectivities. Figure 3-12 illustrates the changes in the n-butane and the 2,2,4-TMP selectivities with the different P/O ratio and OSV values. At higher P/O ratios, the effects seemed to be less pronounced.

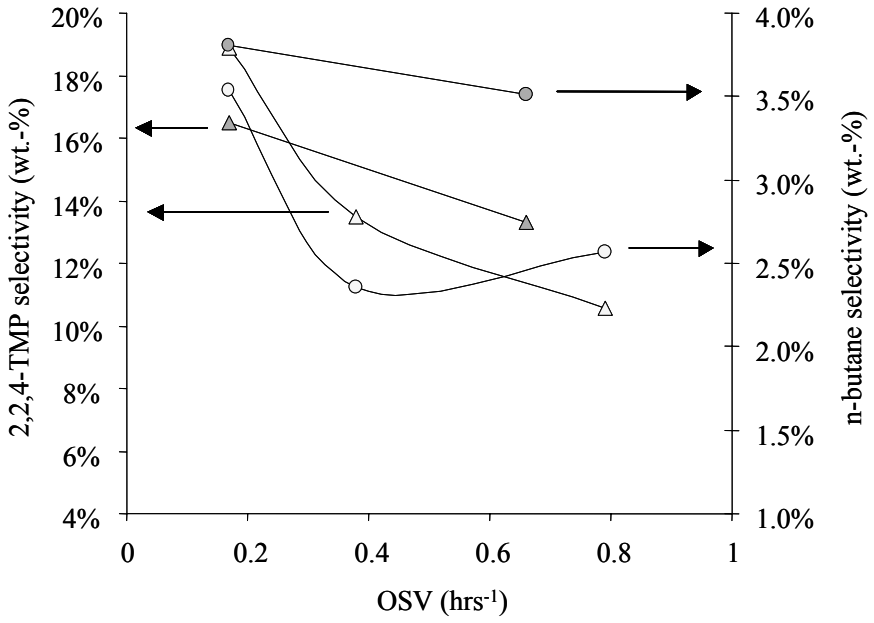

Figure 3-12: Influence of the olefin space velocity and the paraffin/olefin ratio on the integral selectivities to 2,2,4-trimethylpentane (—△— P/O ratio = 6.7, —▲— P/O ratio = 18.1) and n-butane (—— P/O ratio = 6.7, —— P/O ratio = 18.1) measured with catalyst La-X-k.

3.3.6 Reactions with partly deactivated catalyst

The influence of already deactivated catalyst particles in a still active surrounding was examined in a series of experiments employing La-X-k as catalyst. For this, fresh catalyst

was mixed with a fraction of deactivated catalyst. This mixture was activated as usual in the reactor and tested under the standard conditions, i.e., T = 75°C, OSV = 0.18 h^{-1} and P/O ratio = 6.7. Mixtures with 20, 40, 60 and 100 wt.% of deactivated catalyst were tested. The lifetimes as a function of the fraction of the fresh catalyst in the mixture are shown in Figure 3-13. Assuming the already deactivated fraction to be completely inert, the remaining active part simply experiences a higher space velocity.

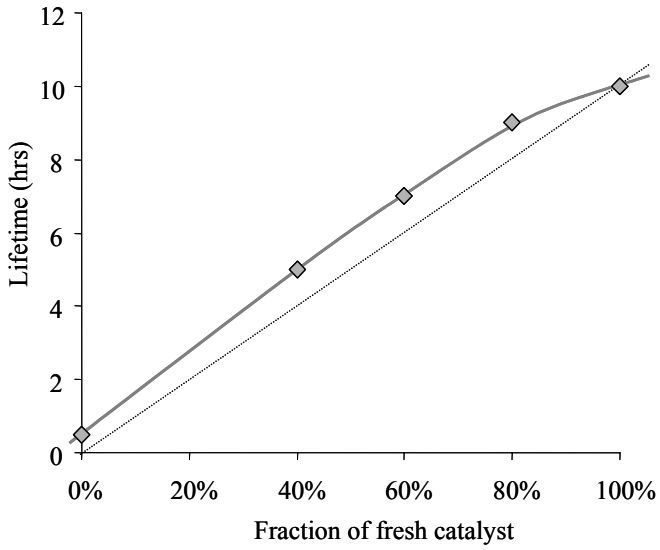

Figure 3-13: Lifetime of catalyst La-X-k with different amounts of added deactivated catalyst as a function of the fraction of fresh catalyst. T = 75°C, OSV = 0.18 h^{-1}, P/O ratio = 6.7. The dotted line represents the theoretical linear behavior.

The accordingly calculated lifetimes are represented by the dotted line in Figure 3-13. The measured results exceeded the calculated lifetimes by 0.5 – 1 h. Even fully deactivated catalyst shows after the *in situ* activation a certain – although low – activity. The integral selectivities in dependence of the fraction of fresh catalyst are depicted in Figure 3-14. It can be seen, that relatively more heavy-end products were produced with decreasing amounts of fresh catalyst, whereas the production of cracked products and n-butane slightly decreased. The C_8-selectivity ran through a flat maximum. Within the C_8-fraction, the selectivity to 2,2,4-TMP strongly increased from ca. 7 wt.% to ca. 23 wt.%. 2,2,3-TMP + 2,5-DMH also monotonously increased with increasing fraction of fresh catalyst. When increasing the amount of deactivated catalyst from 60% to 100% drastic increases in heavy-end, DMH and

octene selectivities were seen.

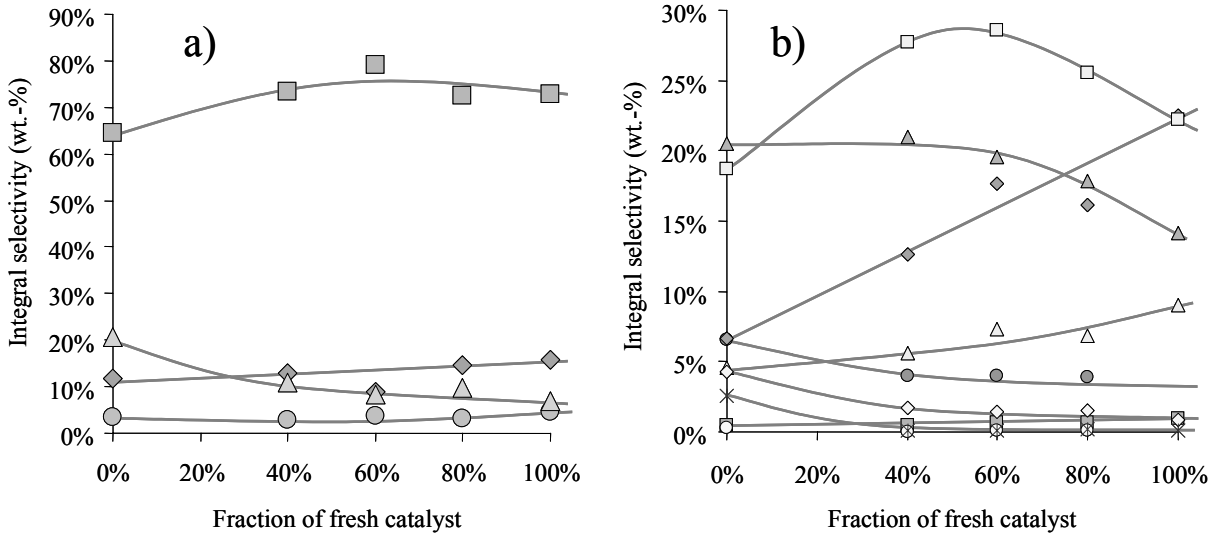

Figure 3-14: Alkylation performance of catalyst La-X-k with different amounts of added deactivated catalyst. a) Product group selectivities as a function of the fraction of fresh catalyst (○ n-butane, ◆ $C_5 - C_7$ products, □ C_8 products, △ C_{9+} products); b) Selectivities within the C_8-fraction as a function of the fraction of fresh catalyst (—◆— 2,2,4-TMP, —□— 2,4-DMH, —△— 2,5-DMH/2,2,3-TMP, —△— 2,3,4-TMP, —□— 2,3,3-TMP, —●— 2,3-DMH, —○— 4-MHp/3,4-DMH, —◇— 3,4-DMH, —✳— Octenes). OSV = 0.18 hrs^{-1}, P/O ratio = 6.7, T = 75°C.

3.4 Discussion

3.4.1 Reactions influencing the product distribution

Figure 3-15 displays the basic alkylation mechanism as adapted from Schmerling (22, 23). The product distribution is governed by the relative rates of the three individual steps, i.e., olefin addition, isomerization and hydride transfer. The antagonistic pair of reactions, i.e., olefin addition – hydride transfer determines the selectivity to single and multiple alkylation.

A high ratio of hydride transfer *vs.* olefin addition retards the build up of long hydrocarbon chains, which finally block the acid sites. Olefin addition is a much more facile reaction than hydride transfer. A high ratio can still be achieved by employing a high P/O ratio in the feed, a high back mixing in the reactor (using CSTR type reactors), by ensuring a low diffusion hindrance of the products out of the pores and by maximizing the hydride

transfer rate as such. The reaction pair isomerization – hydride transfer determines the preference for primary or equilibrium products. A fast hydride transfer shortens the time for isomerization of the adsorbed carbocations through hydride- and methyl-shifts, in this way reducing the formation of thermodynamically favored products. 2,2,3-TMP is the primary product of alkylation with 2-butene. In all runs presented here, the integral selectivity was quite low, never exceeding 10 wt.%. Speculatively, this is attributed to the steric difficulties to achieve hydride transfer, as the carbenium ion is protected by an iso-butyl and an ethyl group, while all other TMP isomers have one methyl group adjacent to the carbon that forms the alkoxy bond to the catalyst.

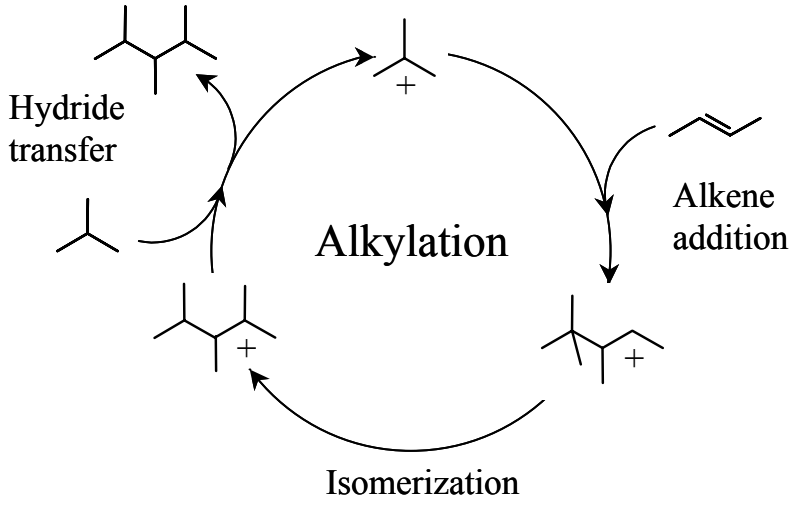

Figure 3-15: Simplified alkylation cycle including the three key reaction steps.

Cracking through β-scission accounts for the C_5-C_7 products and the products with carbon atom numbers, which are not multiples of four. Cracking is concluded to occur on the same acid sites as alkylation. Olefinic fragments from cracking are found only in traces. As long as the hydride transfer activity is sufficiently high, they are quantitatively readsorbed. Therefore, cracking of a C_{12}-carbenium ion leads to one C_5-C_7 carbenium ion (alkoxy group) and one corresponding olefin that will be added to another carbenium ion. Both can desorb *via* hydride transfer from iso-butane as alkanes. Cracking most likely also accounts for some of the produced octanes. However, for the experiments at 75°C, a correlation between individual octane selectivities and the cracking selectivity (which was scattered over a narrow range of 12 – 18 wt.%) could not be established.

Weak Brønsted acid sites catalyze dimerization (24). The more demanding reactions cracking and hydride transfer do not proceed on these sites. Therefore, octenes are produced that adsorb or react with alkoxy groups and enhance so the rate of deactivation. Consequently, the lower the concentration of weak acid sites, the higher the effective hydride transfer rate will be and the longer the catalyst will be active. This is reflected in the correlation between the fraction of strong Brønsted acid sites and the lifetime of the catalyst, which is shown in Figure 3-6 (c).

3.4.2 *Influence of Na^+ exchange level*

The influence of residual sodium cations in the zeolite structure is complex. In addition to neutralizing the framework charge without creating Brønsted acidity, sodium seems to weaken neighboring Brønsted acid sites. Thus, it is important to remove Na^+ cations from the zeolite. However, as can be seen in Figure 3-2, the Na^+ concentration is not the only parameter influencing the strength of the Brønsted acid sites. The severity of the calcination also affects the acidity distribution. It seems to be vital in the case of aluminum-rich zeolites such as X or Y to ensure an efficient water removal during the calcination. However, these materials are very susceptible towards dealumination, which leads to the transformation of Brønsted into Lewis acid sites. Although the Lewis acid sites do not catalyze the hydride transfer, they sorb olefins and, in this way (through the adsorption/desorption equilibrium), increase the olefin concentration near the Brønsted acid sites. This increases the probability of further olefin addition, which leads to accelerated deactivation. Thus, it is not only important to have a high number of strong Brønsted acid sites, but also at the same time as few Lewis acid sites as possible.

3.4.3 *Reactions leading to heavy-end products*

After a significant time of constant activity, the hydride transfer activity stopped surprisingly abrupt, as shown in Figure 3-5. Most saturated compounds (with the exception of 3,4-DMH) ceased being produced at this point. This suggests a parallel progress of the deactivation with respect to all active sites in the reactor, a feature, which is unique for CSTR-type reactors. On the individual site, this means that the hydride transfer comes to a sudden stop, rather than slowing down. The cracking activity stops also simultaneously.

Oligomerization (including dimerization) is the only proceeding reaction. This confirms the existence of two different active sites in zeolites during alkylation, i.e., strong sites catalyzing (multiple-) alkylation and cracking and weak sites catalyzing oligomerization. The C_{9+} products originate from multiple alkylation on the stronger sites and oligomerization on the weaker sites. When the strong sites are deactivated, multiple alkylation ceases, while oligomerization on the weaker sites still proceeds. This is reflected in the changing slope of the C_{9+} curve in Figure 3-5. Deactivation can be caused either by site blocking of the true alkylation sites, or by pore blocking. The latter would imply that an important fraction of the oligomerization sites is located on the outer surface of the zeolite particles.

3.4.4 *"Self-alkylation" and its importance for alkylation*

Following the most basic reaction scheme, the reactor contains only iso-butane at the beginning of the reaction. With the introduction of the iso-butane/2-butene mixture, 2-butene adsorbs on the Brønsted sites and forms secondary butoxy-groups. To these 2-butene can be added to form a 3,4-dimethylhexyloxy group, which desorbs *via* hydride transfer as a DMH, leaving a tertiary butoxy-group on the acid site. Figure 3-4 shows that this occurs to some extent, because the initial 3,4-DMH selectivity is slightly higher than after a few hours TOS. The sec.-butoxy group can also directly undergo a hydride transfer. This will free n-butane and leave a tertiary butoxy-group. As n-butane is not a primary product of β-scission of an alkoxy group, the only way of producing it is this initiating reaction step.

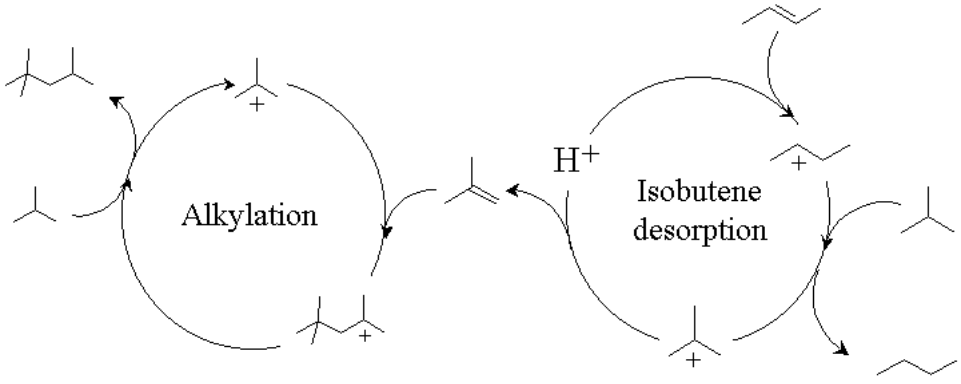

Figure 3-16: "Self alkylation" cycle, depicting the two steps iso-butene desorption and subsequent addition of iso-butene to an isobutyl ion to give after hydride transfer 2,2,4-trimethylpentane.

Assuming that butenes do not desorb from the acid sites, this can only happen once per acid site. Consequently, the total amount of n-butane produced should not exceed the number of acid sites. Surprisingly, with the long-living samples, more than four times the amount of n-butane was found. The most straightforward mechanism to account for the pronounced formation of n-butane is the decomposition of the iso-butoxy group into iso-butene and a free Brønsted acid site. This reaction sequence has been denoted "self-alkylation" (11, 25-27). "Self-alkylation" is of importance in hydrofluoric acid catalyzed processes (4). The importance of this mechanism depends on the feed alkene and the reaction temperature. Its activity was found to increase with the molecular weight and increased branching of the feed alkene (28). Generally, sulfuric acid is less active for self-alkylation than hydrofluoric acid. The corresponding catalytic cycle is shown in Figure 3-16. Note, however, that in contrast to published opinion in the literature (26, 29) the present results allow concluding that dehydrogenation is not involved in "self-alkylation".

The increasing selectivity to n-butane with increasing catalyst lifetime suggests that this route is most pronounced with catalysts fulfilling one criterion for long catalyst life (see Figure 3-7). Assuming that the rate of desorption of iso-butene is (as a first approximation) independent of the catalyst modifications performed in this study, the production of n-butane solely depends on the hydride transfer rate relative to the olefin addition rate. With higher rates of hydride transfer, more n-butane will be produced. As explained above, higher rates of hydride transfer lead to longer catalyst lifetimes, which explains the correlation between lifetime and n-butane selectivity. The increase in the 2,2,3-TMP + 2,5-DMH selectivity parallel to the n-butane selectivity (see Figure 3-8) may also be explained by the increasing hydride transfer activity with increasing lifetime. 2,2,3-Trimethylpentyl alkoxide, which is the primary product of the addition of 2-butene to a tertiary butoxide, has less time to isomerize before it receives a hydride and desorbs as 2,2,3-TMP.

The steep increase in 2,2,4-TMP selectivity with the n-butane selectivity (also shown in Figure 3-8) can be explained by the chemistry iso-butene undergoes subsequent to desorption. After iso-butene is formed in this cycle, it will be added immediately (olefins are not detected in reaction mixtures with active catalysts) to another alkoxy group. If this is a tertiary butoxy group, it leads to a 2,2,4-trimethylpentyl. After hydride transfer, 2,2,4-TMP desorbs. Note that this iso-octane is thermodynamically favored, so it tends to isomerize only

slowly. It is interesting to note that Li *et al.*, while working with sulfuric acid as alkylation catalyst, found higher 2,2,4-TMP and 2,2,3-TMP selectivities when increasing the strength of the acid. The effect was seen with all butene isomers (30). This observation is in line with our results giving higher 2,2,4-TMP and 2,2,3-TMP selectivities with higher concentrations of strong Brønsted acid sites. It suggests that the same mechanistic principles are operative independent of the chosen acid. Simpson *et al.* found 2,2,4-TMP to be the main octane-isomer when performing iso-butane/propene and iso-butane/2-pentene alkylation on a H-USY (11). This allows concluding that when using alkenes other than butenes TMPs are mainly produced *via* the "self-alkylation" route with minor contributions from cracking products.

However, because in the present experiments even for catalysts with low lifetimes the selectivities to 2,2,4-TMP never fell below 9 wt.%, not all 2,2,4-TMP originated from "self-alkylation", but also from conventional alkylation followed by isomerization. From our earlier work with H-BEA and from the results of other groups it is known that H-BEA gives very high 2,2,4-TMP selectivities, sometimes as high as 50 wt.% (5, 31, 32). The n-butane selectivity with BEA based catalysts never exceeded 2 wt.%. This led us to conclude that the high selectivity to 2,2,4-TMP in this case is due to the contribution of the conventional alkylation/isomerization route.

2,2,4-TMP has the highest thermodynamic stability among TMPs with relative concentrations amounting to 50 wt.%. A high concentration of 2,2,4-TMP produced *via* the alkylation/isomerization route, therefore, points either to long residence times of the TMPs on the catalyst surface (slower hydride transfer) or to very high isomerization rates leading preferentially to the thermodynamically most stable isomer.

We speculate at this point that the slower hydride transfer is caused by the higher Si/Al ratio of zeolite BEA compared to La-FAU. Such a conclusion would be in line with findings in cracking experiments, which gave higher hydride transfer rates for zeolites with lower framework Si/Al ratios (33). Conceptually, a more stable bond between the oxygen of the zeolite and the carbon atom of the alkoxy group should be formed for zeolites with higher concentration of aluminum in the lattice and lower acid strength. The fact that it is found experimentally to be easier to remove alkoxy groups by hydride transfer that should be more stable strongly suggests that the formation of the new alkoxy group is of higher importance than the stability of the leaving group.

The H-USY sample of this study gave a moderate lifetime with a correspondingly moderate n-butane selectivity, but a significantly higher 2,2,4-TMP selectivity (the circular symbol in Figure 3-8). Similar to H-BEA, the higher framework Si/Al ratio (Si/Al ≈ 5, as compared to 1.2 in the La-X samples) within the ultrastable FAU may contribute to this deviating behavior. Moreover, it is the only one of the tested samples without La^{3+}-ions, the influence of which on the individual reaction rates is not known.

The influence of the pore topology on the selectivities to the individual TMP isomers has been emphasized earlier (see for example Yoo *et al.* (34, 35)). Diffusion and electrostatic effects induced by the pore structure certainly play a role and may be responsible in part for the high 2,2,4-TMP selectivity with H-BEA. However, within the range of catalysts examined in this study, 2,2,4-TMP selectivities between 9 and 24 wt.% were measured; all samples were of the same pore topology. This clearly evidences that the pore topology is not the dominating factor, but only one of several. Moreover, it may be premature to interpret reaction data, which is based on one sample only.

3.4.5 Influence of the reaction temperature

The influence of the reaction temperature on the alkylation reaction is well documented for liquid acids. Within certain limits, lowering the temperature increases the alkylate quality in terms of selectivity to trimethylpentanes. Corma *et al.* examined sulfated zirconia as a non-zeolitic solid acid alkylation catalyst in the temperature range –10 to 50°C. With increasing reaction temperature, the authors found a constantly declining octane and a sharply increasing cracking selectivity. The heavy-end selectivity went through a minimum at intermediate temperatures (36). Zeolites operate at much higher temperatures. For H-BEA, a maximum in the TMP production was found at a reaction temperature of 75°C, at which also the lifetime was highest. At low temperatures C_{9+} products and at high temperatures cracked products dominated (31). Tests with H-USY between 40°C and 90°C led to an optimum in lifetime at ca. 65°C while the TMP-selectivity constantly declined with reaction temperature (12).

With the catalysts used in this study, a surprisingly strong dependency of the lifetime and the selectivities on the reaction temperature was observed. The product quality was best (highest C_8 and highest TMP selectivity) at low temperatures, the lifetime, however, was highest at intermediate temperatures around 75°C. With increasing temperature, the selectivity to cracking and above 100°C also to heavy-end products increased (see Figure 3-

10). Cracking *via* β-scission did not lead to significant formation of propane or propene under the chosen conditions. The smallest cracking product observed was isopentane (isobutane will be formed as well, but cannot be distinguished from the feed). Therefore, as cracking of a C_8 molecule would lead to the formation of propene or propane, the precursor has to be at least a C_{12} molecule. Consequently, high cracking rates inevitably are coupled with high rates of olefin addition. Within a certain temperature range, cracking may actually slow down the buildup of heavy molecules in the catalyst pores.

In contrast to H-BEA and sulfated zirconia mentioned above, the heavy-end selectivity found within the product was low at low reaction temperatures. The much smaller crystals of zeolite H-BEA (primary particles of about 0.1 µm) and the larger pores of sulfated zirconia might allow more heavy molecules to leave the pore system and thus give higher heavy-end selectivities at low temperatures. Unfortunately, the amount of hydrocarbon retained in the zeolite (between 10 – 20 wt.% of the catalyst) was – compared to the total amount of product formed – too low to be accurately accounted for in the mass balance. Typically, the deposits should comprise 2-5 wt.% of the integral product.

The low lifetimes at low reaction temperatures (see Figure 3-9) most likely were a consequence of the severely hindered diffusion of the heavier molecules at low temperatures. The catalysts deactivated by pore blocking. At high reaction temperatures, where diffusion is less problematic, the catalyst also rapidly deactivated. Here, the catalyst deactivates by highly unsaturated compounds, which block the acid site rather than the pore. With increasing reaction temperature, the deposits in deactivated catalysts have been found to be increasingly hydrogen deficient. These compounds are most likely produced through multiple desorption/hydride transfer steps and are strongly bound to the acid sites. Detailed results on the characterization of the deposits used in this study are presented in chapter 4 (37).

The selectivity to dimethylhexanes gradually increases with the reaction temperature. It has been proposed that dimethylhexanes are produced to a major part *via* cracking of heavier compounds (38). Thus, when increasing the reaction temperature, alongside the increasing cracking selectivity also more dimethylhexanes are produced. The decreasing production of trimethylpentanes is a consequence of the higher rates of the secondary reactions, cracking and olefin addition. Before the TMP-precursors can desorb *via* hydride transfer they are alkylated again. The selectivities to n-butane, 2,2,4-TMP and 2,2,3-TMP + 2,5-DMH pass through a maximum, indicating that the “self alkylation” activity has a temperature optimum

around 75°C. This suggests that the conditions favoring "self alkylation" activity also favor long catalyst lifetime. This has been confirmed by using smaller alkenes than butene. By doing so, the TMPs produced should originate mainly from "self alkylation". With propene and ethene on H-BEA, Nivarthy *et al.* (39) found a maximum in the octane selectivity also at ca. 75°C indicating that a facilitation of the difficult step, the hydride transfer, is crucial for successful operation.

3.4.6 *Influence of the olefin space velocity*

The constant productivity of the catalysts with varying OSV is of high importance for the practical application of the catalyst. It suggests that isomerization and hydride transfer are fast compared to the olefin addition under the practical conditions investigated. In a more rigorous treatment, it suggests that the olefin addition is rate limiting under the experimental conditions probed. There may be, however, a critical OSV, at which insufficient rates of hydride transfer will lead to the preferential formation of higher hydrocarbons *via* multiple alkylation. The decreasing selectivities to n-butane, 2,2,4-TMP and 2,2,3-TMP + 2,5-DMH with increasing OSV (see Figure 3-11) suggest that the fraction of iso-butene desorbing and acting as alkylating agent has decreased, however. With the higher throughput of butenes the probability that the butoxy-groups can decompose before being alkylated is reduced, decreasing in this way the importance of the "self alkylation" route.

The results of the experiments with added deactivated catalyst (shown in Figure 3-13 and 14) connect the findings of the study with catalysts of different acid site distributions and the findings of the OSV study. The individual acid sites in the fresh catalyst fraction experience a higher OSV and give accordingly changing C_8 selectivities. The deactivated catalyst fraction, however, is not completely inert, but produces a low quality alkylate most likely with a high amount of dimerizate. The unsaturated products will readsorb and contribute to the increased heavy-end formation. These experiments nicely simulate the situation in catalysts containing both weak and strong Brønsted acid sites. Weak acid sites would act like the deactivated fraction and the strong sites like the fresh fraction. The lower the amount of strong acid sites in a given sample, the higher the OSV these sites experience with the abovementioned consequences. In reality, we expect a continuum of acid strengths to exist within zeolites. Nevertheless, the general conclusions remain valid.

The P/O ratio is also of high importance for the practical implementation. In addition to

potential inhomogeneities at the feed entrance, higher P/O ratios lead to a lower product concentration in the CSTR. It dilutes the reactor contents with iso-butane. This can have two effects on the reaction mechanism: (i) The increased iso-butane concentration leads to higher rates of hydride transfer, and (ii) a smaller fraction of products might reenter the cycle. Whether the second effect is significant is not unequivocally settled at this point. However, the slightly negative slopes of the integral yields of some products after the onset of catalyst deactivation in Figure 3-5b) might point into this direction. Similarly, the slight increase in the C_8-selectivity with increasing P/O ratio can be speculated to be related to the lower readsorption of products. The lower selectivity to octenes at high P/O ratio (0.3 wt.% at P/O ratio = 18.1, OSV = 0.66 hrs^{-1} as compared to 0.7 wt.% at P/O ratio = 6.7, OSV = 0.38 hrs^{-1}) supports the conclusion of the higher efficiency of the hydride transfer. These small effects appear in summation to lead to the moderate increase in the lifetime from 9 hrs to 11 hrs with the higher P/O ratio. It is interesting to note that an increase by a factor of two for raising the P/O ratio from 15 to 30 has been reported in the literature for H-BEA (10). This suggests that zeolite X is more robust with respect to variations in the operating conditions and can be used at lower P/O ratios than other materials.

3.5 Conclusions

The avoidance of structural damage occurring during the modification procedure is the key factor for suitable faujasitic alkylation catalyst. It ensures a high B/L ratio, which minimizes the olefin concentration close to the Brønsted acid sites. In this way, hydride transfer will be favored over olefin addition. Care has to be taken to remove Na^+ quantitatively, because it weakens neighboring Brønsted acid sites. These weak sites mainly catalyze oligomerization. Maximizing the concentration of strong Brønsted acid sites, thus, reduces oligomerization significantly. Two mechanistic pathways lead to the formation of heavy-end compounds and ultimately to catalyst deactivation, i.e., multiple alkylation on the stronger sites and oligomerization on the weaker. Both routes can be minimized through optimizing ion exchange and calcination.

"Self-alkylation" activity is linked to the acid strength of the catalyst. It is, therefore, most likely an indicator rather than a prerequisite of a suitable catalyst. Brønsted acid sites with a strength required for alkylation permit also self-alkylation. Unfortunately, the higher production of n-butane lowers somewhat the octane-yield. In this respect, the behavior of

faujasitic catalysts resembles that of hydrofluoric acid.

Alkylation is a very temperature-sensitive reaction. The optimum in lifetime is not necessarily the optimum in alkylate quality. A compromise has to be found between a sufficiently fast diffusion of bulky products and acceptable ratios of hydride transfer and olefin addition rates. Cracking might be of help to slow down the build up of the coke precursors.

Within the range tested here, the integral yields did not change significantly with the OSV. The P/O ratio influenced the performance only moderately. These results show that the best of the tested materials are robust alkylation catalysts and can be used under severe conditions without major drawbacks in alkylate quality.

3.6 Acknowledgments

The author wishes to thank Dr Breuninger of Süd-Chemie AG for providing several of the examined samples. Financial support from Süd-Chemie AG is gratefully acknowledged.

3.7 References

1. Stell, J., *Oil Gas J.* **99 (52)**, 74 (2001).
2. Anonymous, *Oil Gas J.* **98 (9)** (2000).
3. Weitkamp, J. and Traa, Y., *in* "Handbook of Heterogeneous Catalysis" (G. Ertl, H. Knözinger, and J. Weitkamp, Eds.), Vol. 4, p. 2039. VCH, Weinheim, 1997.
4. Corma, A. and Martinez, A., *Catal. Rev.-Sci. Eng.* **35**, 483 (1993).
5. Nivarthy, G. S., Seshan, K., and Lercher, J. A., *Microp. & Mesop. Mater.* **22**, 379 (1998).
6. Stöcker, M., Mostad, H., Karlsson, A., Junggreen, H., and Hustad, B., *Catal. Lett.* **40**, 51 (1996).
7. Diaz-Mendoza, F. A., Pernett-Bolano, L., and Cardona-Martinez, N., *Thermochim. Acta* **312**, 47 (1998).
8. Corma, A., Martinez, A., Arroyo, P. A., Monteiro, J. L. F., and Sousa-Aguiar, E. F., *Appl. Catal. A* **142**, 139 (1996).
9. Flego, C., Kiricsi, I., Parker Jr., W. O., and Clerici, M. G., *Appl. Catal. A* **124**, 107 (1995).

10. de Jong, K. P., Mesters, C. M. A. M., Peferoen, D. G. R., van Brugge, P. T. M., and de Groot, C., *Chem. Eng. Sci.* **51**, 2053 (1996).
11. Simpson, M. F., Wei, J., and Sundaresan, S., *Ind. Eng. Chem. Res.* **35**, 3861 (1996).
12. Taylor, R. and Sherwood Jr., D. E., *Appl. Catal. A* **155**, 195 (1997).
13. Borade, R. B. and Clearfield, A., *J. Phys. Chem.* **96**, 6729 (1992).
14. Lindsley, J. F., U.S. Patent 4,125,591 (1978).
15. Haag, W. O., *Stud. Surf. Sci. Catal.* **84**, 1375 (1994).
16. Fritz, P. O. and Lunsford, J. H., *J. Catal.* **118**, 85 (1989).
17. Wouters, B. H., Chen, T. H., and Grobet, P. J., in: Proceedings of the 13th International Zeolite Conference, Montpellier, 344, 2001.
18. Weihe, M., Hunger, M., Breuninger, M., Karge, H. G., and Weitkamp, J., *J. Catal.* **198**, 256 (2001).
19. van Bokhoven, J. A., Roest, A. L., Koningsberger, D. C., Miller, J. T., Nachtegaal, G. H., and Kentgens, A. P. M., *J. Phys. Chem. B* **104**, 6743 (2000).
20. Kuehl, G. H. and Timken, H. K. C., *Microp. Mesop. Mater.* **35-36**, 521 (2000).
21. Gaare, K. and Akporiaye, D., *J. Phys. Chem. B* **101**, 48 (1997).
22. Schmerling, L., *J. Am. Chem. Soc.* **67**, 1778 (1945).
23. Schmerling, L., *J. Am. Chem. Soc.* **68**, 275 (1946).
24. Mostad, H. B., Stöcker, M., Karlsson, A., and Rørvik, T., *Appl. Catal. A* **144**, 305 (1996).
25. Corma, A., Martinez, A., and Martinez, C., *J. Catal.* **146**, 185 (1994).
26. Cardona, F., Gnep, N. S., Guisnet, M., Szabo, G., and Nascimento, P., *Appl. Catal. A* **128**, 243 (1995).
27. Pater, J., Cardona, F., Canaff, C., Gnep, N. S., Szabo, G., and Guisnet, M., *Ind. Eng. Chem. Res.* **38**, 3822 (1999).
28. Hofmann, J. E., *J. Org. Chem.* **29**, 1497 (1964).
29. Guisnet, M. and Gnep, N. S., *Appl. Catal. A* **146**, 33 (1996).
30. Li, K. W., Eckert, R. E., and Albright, L. F., *Ind. Eng. Chem. Process Des. Develop.* **9**, 441 (1970).
31. Nivarthy, G. S., He, Y., Seshan, K., and Lercher, J. A., *J. Catal.* **176**, 192 (1998).
32. Corma, A., Gomez, V., and Martinez, A., *Appl. Catal. A* **119**, 83 (1994).
33. Cumming, K. A. and Wojciechowski, B. W., *Catal. Rev.-Sci. Eng.* **38**, 101 (1996).

34. Yoo, K., Burckle, E. C., and Smirniotis, P. G., *Catal. Lett.* **74**, 85 (2001).
35. Yoo, K., Burckle, E. C., and Smirniotis, P. G., *J. Catal.* **211**, 6 (2002).
36. Corma, A., Martinez, A., and Martinez, C., *J. Catal.* **149**, 52 (1994).
37. Feller, A., Barth, J. O., Guzman, A., Zuazo, I., and Lercher, J. A., *see chapter 4*, (2002).
38. Lee, L. and Harriott, P., *Ind. Eng. Chem. Process Des. Develop.* **16**, 282 (1977).
39. Nivarthy, G. S., Feller, A., Seshan, K., and Lercher, J. A., *Microp. Mesop. Mater.* **35-36**, 75 (2000).

Chapter 4

Deactivation pathways in zeolite catalyzed isobutane/butene alkylation

Abstract

The deactivation of rare-earth exchanged zeolite X as catalysts in isobutane/2-butene alkylation between 40°C and 130°C was studied. The deactivated samples and the isolated deposits were analyzed by a range of techniques, including for the first time (matrix assisted) laser desorption/ionization time-of-flight mass spectroscopy (MALDI-TOF MS, LDI-TOF MS). The compounds found in the deactivated zeolites are, in addition to large alkanes and alkenes, highly unsaturated and highly branched species containing cyclic structures, which are increasingly aromatic as the reaction temperature increased. The deposits in part interact strongly with the acid sites and block the sites for further alkylation reactions. Their structure and route of formation resembles that of conjunct polymers formed in liquid acid catalyzed alkylation.

4.1 Introduction

Acidic large-pore zeolites are active and selective isobutane/butene alkylation catalysts (1, 2). Their industrial application is constrained by rapid deactivation with time on stream. The main factor determining the fate of the catalyst is its hydride transfer activity. The higher the ratio of the rate of hydride transfer *vs.* the rate of oligomerization, the more of the trimethylpentanes will be produced and the more the deactivation will be slowed down. Two strategies help to maximize hydride transfer rates: (i) Careful appropriate synthesis and modification procedures of the zeolites will minimize structural damage and ensure a high concentration of strong Brønsted acid sites, which effectively catalyze hydride transfer reactions. (ii) The use of well-stirred tank reactors operated at very high conversions allows having a minimum local concentration of olefins, while maintaining high space velocities. This minimizes oligomerization activity, which is responsible for a low product quality and premature catalyst deactivation.

Nevertheless, even under these conditions, deactivation of the catalyst occurs and it has to be frequently regenerated. The patent literature suggests that multiple regenerations (as many as several hundred) are needed for processes based on solid catalysts to be competitive with existing processes based on H_2SO_4 and HF (3).

Thus, the understanding of the deactivation mechanism is important for prolonging the active single-cycle lifetime and for designing an efficient regeneration method. Only a small number of publications have been devoted to the characterization of carbonaceous deposits in zeolite catalyzed isobutane/butene alkylation. The characterization techniques that were employed range from ^{13}C-NMR (4-7), ^{1}H-NMR (8), mass spectrometry (also in combination with gas chromatography) (8-10), IR-spectroscopy (6, 8, 11, 12) and UV/VIS (6, 13). These methods were applied to the deactivated catalyst as a whole or to the extracted coke alone.

Coke extraction from zeolitic catalysts typically is done by a complete dissolution of the zeolite in aqueous hydrofluoric acid after which the coke is extracted with an organic solvent, e.g., hexane or methylene chloride. The carbonaceous compounds are claimed to survive this treatment unaltered (14).

(Matrix-assisted) laser desorption/ionization time-of-flight mass spectroscopy, MALDI-TOF and LDI-TOF MS, have been successfully applied as powerful techniques for the determination of the mass of polymers (15) and biomolecules (16). Both methods utilize the energy of a laser beam for desorbing and ionizing sample molecules, which are subsequently

analyzed in a time-of-flight mass spectrometer. In LDI-TOF, the sample itself is desorbed and ionized by the laser beam or post-ionized either by another laser or with an electron beam (17). In MALDI-TOF on the other hand, a matrix, typically an aromatic acid, is mixed with the sample. The matrix absorbs the laser power, is vaporized and carries with it analyte molecules into the gas-phase, where they can be ionized by protonation or cation addition or by charge transfer from the formed matrix ions. The different ionization mechanisms are discussed in ref. (18). The primary advantage of the laser desorption/ionization is the relatively low energy input, which minimizes fragmentation. Thus, the measured mass spectrum directly represents the molecular weight distribution of the analyzed mixture. In turn, however, this eliminates all structural information.

Recently, these methods have been successfully applied to the characterization of technical waxes (19), high-molecular weight alkanes in crude oil (20) and low molecular weight hydrocarbon oligomers (21), all containing mainly aliphatic and naphtenic compounds with masses below 1000 Da. In principle, these mixtures should not be fundamentally different from the deposits formed on the catalysts during alkylation. For this reason, we developed these mass spectrometry methods for and applied it to deactivated catalysts and on the free deposits.

In this chapter, we seek to deepen the understanding of the deactivation mechanism. Analysis of reaction data obtained in a CSTR is combined with information on the deposits formed during the reaction and on the behavior of the deposits under thermal treatment. A variety of characterization techniques on the deactivated catalyst and on the extracted coke is used.

4.2 Experimental

4.2.1 Catalyst preparation

The parent material was Na-X obtained from Chemische Werke Bad Köstritz (Si/Al = 1.2). It was brought into the acidic form by aqueous exchange with 0.2M lanthanum nitrate solution. The liquid-to-solid ratios in the exchange steps were usually approximately 10 ml/g. The temperature during exchange was kept at 70°C and the exchange time was two hours. This procedure was typically repeated 2-3 times. After washing the resulting material with doubly distilled water until it was nitrate-free and drying at 100°C, the samples were calcined in flowing air with a slow temperature ramp up to 450°C. To lower the sodium content of the

zeolites further, this ion-exchange procedure including washing, drying and calcining was repeated. The sample denoted La-H-X, was additionally exchanged with ammonium nitrate solution (0.5M) in this second step. The sample exclusively exchanged with La-ions was named La-X. For comparison, a sample of zeolite H-BEA (H-BEA 25 from Süd-Chemie, Si/Al = 12) was employed without further modification.

4.2.2 Catalyst characterization

The ion-exchanged materials were characterized by a range of different methods. With nitrogen adsorption at 77 K surface area and pore volume were estimated. Prior to adsorption, the samples were activated in vacuum at 400°C for 10 hrs. The crystallite size and morphology was analyzed with SEM. AAS was used to determine the Si/Al ratio and the Na^+ concentration. For measuring the acidity, two different kinds of adsorption/desorption experiments were carried out, i.e., TPD of ammonia in a vacuum-setup with a mass spectrometer detector to estimate the total number of acid sites (at an adsorption temperature of 100°C) and sorption of pyridine monitored by IR spectroscopy. For the latter the sample was pressed into a self-supporting wafer, which was placed into a sorption cell, where it was activated in vacuum (10^{-5} mbar) for 1 hr at 450°C. Then, the sample was cooled down to 100°C and pyridine at a partial pressure of 10^{-2} mbar was introduced into the system. After saturation of all the acid sites, the sample was outgassed for 1 hr at 100°C followed by a temperature ramp of 10 K/min to 450°C with a dwell time of 1 hour. Subsequently, the cell was cooled down again to 100°C. Spectra of the sample were taken before adsorption of pyridine, after outgassing and after desorption to 450°C. All spectra were taken at 100°C. From this set of spectra, the ratio of Brønsted acid sites (as evidenced by the band of pyridinium ions at 1540 cm^{-1}) to Lewis acid sites (the band of coordinately bound pyridine at 1450 cm^{-1}) at 100°C, and at 450°C is calculated. The ratios of the extinction coefficients for Brønsted and Lewis bound pyridine were taken from ref. (22).

4.2.3 Coke characterization

Coke was analyzed while on the catalyst surface and after dissolution of the surrounding zeolite. Coked catalyst samples were characterized by nitrogen adsorption at 77K, after a vacuum treatment for 10 hrs at 120°C to remove weakly bound compounds. These samples were compared to fresh zeolite samples pretreated in the same way. IR-spectroscopy was

used to characterize the hydrocarbon deposits by the individual bands that could be assigned to certain functional groups. Mass spectrometry was employed for monitoring the desorbing products during temperature-programmed desorption experiments of deactivated catalysts. Matrix-assisted laser desorption/ionization time-of-flight mass spectrometry (MALDI-TOF-MS) was used on the deactivated catalysts to obtain the molecular weight distribution of the hydrocarbon deposits. A solution of 1% trifluoroacetic acid in acetonitrile was prepared. 10 mg of the deactivated catalyst were suspended in 100µl of this solution. Another 100µl of this solution were saturated with dihydroxybenzoic acid. The two parts were mixed and 0.5µl of the resulting suspension were deposited on the sample holder. After air-drying the drop, the sample holder was introduced into the ion source of the mass spectrometer. MALDI-TOF-mass spectra were recorded using a Bruker Biflex III MALDI-TOF mass spectrometer equipped with a N_2 laser (ν = 337 nm) operating at a pulse rate of 3 Hz. The ions were accelerated with pulsed ion extraction after a delay of 50 ns by a voltage of 28.5 kV. The analyzer was operated in reflectron mode, and the ions were detected using a microchannel plate detector. The mass spectrometer was calibrated prior to measurement with a polystyrene standard of appropriate molecular mass. The same instrument was also used in laser desorption/ionization mass spectrometry (LDI-MS). Here, the sample was suspended in water and put on the target without matrix. The experiments were conducted using the same settings as in the MALDI measurements. Supplementary experiments were performed with silver tetrafluoroborate ($AgBF_4$) added to the samples. This was supposed to lead to silver-cationization of otherwise difficult to ionize alkanes.

For some measurements, the deposits had to be separated from the zeolite. This was done by a complete dissolution of the deactivated zeolite in a 40% hydrofluoric acid solution at room temperature. Unreacted HF was evaporated and the remainder was mixed with water and hexane and treated in ultrasound for 30 min. The brown colored hydrocarbon phase contained the deposits and was used for further analysis. The coke solution was characterized by UV/VIS upon further dilution with hexane in the wavelength region 190 nm to 500 nm to obtain information on the olefinic and/or aromatic nature of the compounds. The deposits were also analyzed by ^{1}H-NMR at 360 MHz on a Bruker AM 360 spectrometer. After evaporation of the hexane solvent, the remaining tar-like polymer was re-dissolved in $CDCl_3$. Traces of $CHCl_3$ in the solvent were used as an internal standard for calibrating the chemical shift (δ $CHCl_3$ = 7.24 ppm from TMS). GC-MS was used to obtain information on the

number and on the structure of the individual compounds. LDI mass spectra of the deposits (with and without addition of $AgBF_4$) were taken and compared with mass spectra of the deactivated zeolites.

4.2.4 Catalytic experiments

The alkylation of isobutane with 2-butene was performed in a stirred tank reactor operated in continuous mode. The liquefied gases were received from Messer with a purity of 99.95% (isobutane) and 99.5% (cis-2-butene, the main impurity being trans-2-butene). Impurities in the feed cannot be completely ruled out to contribute to the catalyst deactivation. However, all known organic contaminants (diolefins, organic sulfur and oxygen containing compounds) were below the detection limit of our GC analysis. An estimation of the required concentration for a significant contribution of such a contaminant to catalyst deactivation would be about 50-100 times higher than the detection limit.

The catalyst sample (typically 4 – 5 g) was activated *in situ* within the alkylation reactor at 170°C for 16 h in flowing nitrogen. After cooling down to the reaction temperature, typically 75°C, the reactor was filled with liquid isobutane at a pressure of 32 bar. The reaction was started by admitting a butene-isobutane mixture with a molar paraffin-to-olefin (P/O) ratio of 6.7 and an olefin space velocity (OSV) of 0.2 g_{butene} / ($g_{catalyst}$ hr). Note that these numbers are comparable to industrially employed parameters. To study the influence of the reaction temperature on the deactivation process, a series of runs was performed at temperatures ranging from 40 to 130°C.

The reactor was equipped with a sample valve, which allowed the removal of small amounts (ca. 20 mg) of catalyst on-line during the reaction. This mass loss was negligible for the overall run, being about 0.2 – 0.25% of the total catalyst inventory. Thus, during one reaction several samples could be withdrawn and analyzed for the progress of deactivation with time-on-stream.

The product from the reactor was expanded and passed through a six-port-valve with a sample loop, the contents of which was injected automatically into an HP 6830 gas chromatograph equipped with a FID-detector and a 35 m DB-1 column. Downstream of the six-port-valve, the product stream was condensed into a cold trap cooled with a dry ice/isopropanol mixture. The product was collected over the whole time on stream and was weighed and analyzed chromatographically to give the integral product composition. The

product was analyzed by UV/VIS and ^{1}H-NMR. Additionally, an elemental analysis (by complete combustion) was performed on the product for obtaining the overall H/C ratio.

4.3 Results and interpretation

4.3.1 Physicochemical characterization

The most important physicochemical properties of the investigated catalysts are summarized in Table 4-1. The Na^{+} content of all the samples was below 0.1 wt.-%. The crystal size of the faujasitic materials was between 1 and 2 µm, H-BEA sample had primary particles of about 0.1µm, most of which were agglomerated to bigger aggregates.

Table 4-1: Physicochemical properties of the fresh catalysts

Sample	Total acid site concentration [1]	Brønsted/Lewis acid site ratio [2]		Micropore volume [3]	BET Surface area [3]
	mmol/g	100°C	450°C	ml/g	m^2/g
La-X	0.67	3.5	2.9	0.16	505
La-H-X	0.55	2.3	1.6	0.16	518
H-BEA	0.50	0.9	0.2	0.07	566

[1] Measured by adsorption of ammonia at 100°C

[2] Measured by adsorption/desorption of pyridine monitored by IR

[3] Measured by adsorption of nitrogen after activation at 400°C in vacuum for 10 hrs

4.3.2 Alkylation experiments

The three samples varied significantly in their alkylation performance. At a reaction temperature of 75°C and employing an OSV of 0.2 g butene/(g catalyst hr) and a P/O ratio of 6.7, the time of complete butene conversion (termed catalyst lifetime) was 12 hrs for La-X, 9 hrs for La-H-X and only 3 hrs for H-BEA. These differences can be attributed to the acidity distribution of the individual samples. La-X with the highest ratio of Brønsted to Lewis acid sites at both 100°C and 450°C is superior to La-H-X and H-BEA with their correspondingly lower ratios. La-H-X was additionally tested at a range of different reaction temperatures between 40°C and 130°C. The lifetime was found to be optimal at 75°C, while higher selectivities to trimethylpentanes were achieved at lower temperatures. With all samples, the

yield of products steadily increased with TOS, before it reached the theoretical limit of 2.04 g product / g olefin. When the conversion started dropping, also the yield declined. The results of these experiments are summarized in Table 4-2. The reported selectivities are based on the total amount of products that was produced until the activity to alkylation ceased. The implications of the acidity and the reaction temperature on the alkylation performance have been discussed in detail in chapter 3 (23).

Table 4-2: Lifetimes and integral selectivities measured in the different alkylation experiments at an isobutane/2-butene ratio of 6.7 and 2-butene space velocity of 0.2 g/(g hr).

Sample	Reaction temperature	Lifetime	Product group selectivities			
			C_5-C_7	TMP	DMH	C_{9+}
	°C	Hrs	Wt.-%			
La-X	75	12	18.3	57.8	14.1	9.8
H-BEA	75	3	16.0	57.4	12.2	14.3
La-H-X	40	2	9.8	71.5	10.1	8.6
	75	9	14.7	64.2	13.4	7.7
	100	6	25.3	49.1	14.7	10.9
	130	2	35.0	29.9	18.6	16.4

4.3.3 Characterization of the deactivated catalysts

Samples of the deactivated catalysts La-X and H-BEA were analyzed by IR-spectroscopy. Spectra were taken at 100°C after outgassing at 100°C in vacuum for 2 hrs. The spectra of the two deactivated catalysts are compared in Figure 4-1. Both samples showed the typical bands for sorbed hydrocarbons. The bands at 2960 and 2930 cm^{-1} are characteristic of the asymmetric stretching vibrations of the CH_3 and the CH_2 group, respectively. The different intensities of these two bands in the two samples indicate a higher degree of branching of the hydrocarbons present on La-X. The bands at 1465 and 1380 cm^{-1} are attributed to the asymmetric and symmetric CH_3 deformation vibration. The band at 1640 cm^{-1} is assigned to the stretching mode of a C=C double bond. The samples were exposed to atmospheric conditions after removing them from the reactor. Thus, it cannot be completely

ruled out, that the band at 1640 cm^{-1} is partly caused by the deformation vibration of adsorbed water, usually found between 1630 and 1610 cm^{-1}. With La-X a weak band at 1536 cm^{-1}, and with H-BEA two stronger bands at 1531 and 1505 cm^{-1} are observed. Hydrocarbon bands in this region were assigned to alkenyl cations in both liquid acids (24, 25) and zeolites (26, 27). However, also partly oxidized species such as carboxyl groups absorb around 1600 and 1530 cm^{-1}. Bands characteristic of aromatic molecules were not detected. Let us now consider the bands of the hydroxy groups. With La-X, all bands of acidic hydroxy groups including the SiOH band are completely missing and only the band at 3520 cm^{-1} characteristic of the non-acidic La-OH band was observed. In contrast with H-BEA a fraction of the silanol (3740 cm^{-1}) and the acidic hydroxyl-band (3605 cm^{-1}) is visible and, hence, not covered by hydrocarbons.

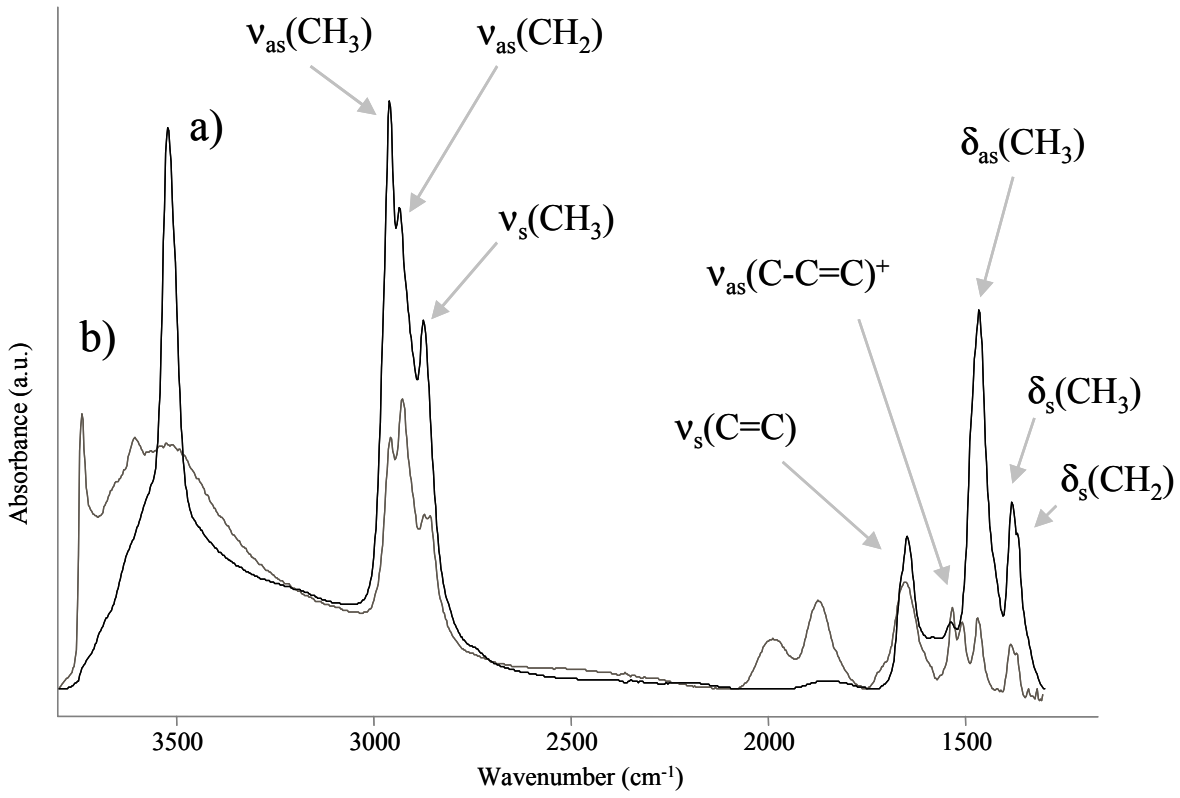

Figure 4-1: Spectra of deactivated catalysts (alkylation at 75°C) after evacuating for 2 hrs at 100°C with assignment of hydrocarbon bands. a) La-X (black line), b) H-BEA (gray line)

A sample of deactivated La-X was used to study the behavior of the hydrocarbon deposits during thermal treatment. After outgassing at 100°C, the temperature was raised with 10 K/min to 450°C. A mass spectrometer connected to the IR-cell recorded the desorbing

species. Figure 4-2 shows the IR-spectra taken before and after the thermal treatment in comparison with the fresh sample and the evolution of the bands during the temperature increase. All hydrocarbon bands decrease in intensity with increasing temperature. This decrease is accompanied by the appearance of a new band at 1580 cm^{-1}, which is tentatively assigned to condensed ring aromatic structures (14) or structural vibrations of polycyclic aromatic compounds (28). A weak band at 3070 cm^{-1} characteristic of the C-H stretching vibration of aromatic compounds supports this assignment. Only weak bands were observed between 3000 and 2700 cm^{-1} after thermal treatment. In the region between 1700 and 1300 cm^{-1} the CH_3 bending vibrations were markedly reduced in intensity. The intensity and shape of the hydroxyl bands of the sample after the thermal treatment were similar to those of the fresh sample.

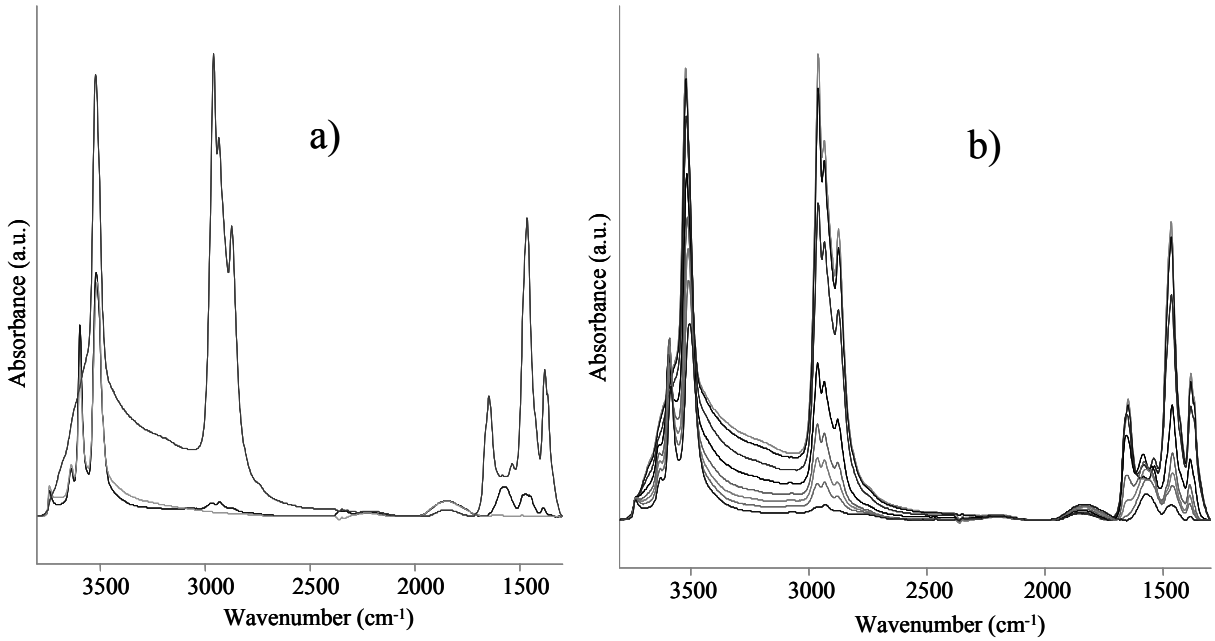

Figure 4-2: Thermal treatment of deactivated La-X recorded with IR. a) Comparison between fresh sample, deactivated sample after outgassing at 100°C and after heating to 450°C, b) Changes during heating to 450°C. Spectra were taken every 50°C, starting from 100°C.

The species desorbing during the thermal treatment can be grouped into two categories, i.e., alkanes and alkenes that desorbed between 100 and 280°C, and the high temperature desorption of aromatic compounds starting at 250°C. Fragments characteristic of the different types of molecules desorbing from the zeolite surface are compiled in Figure 4-3. The masses

83 and 85 represent alkene and alkane fragments. Mass 119 represents aromatic compounds with one benzene ring (substituted with alkyl side-chains) and mass 115 represents bi-cyclic aromatics, which desorb at temperatures above 300°C.

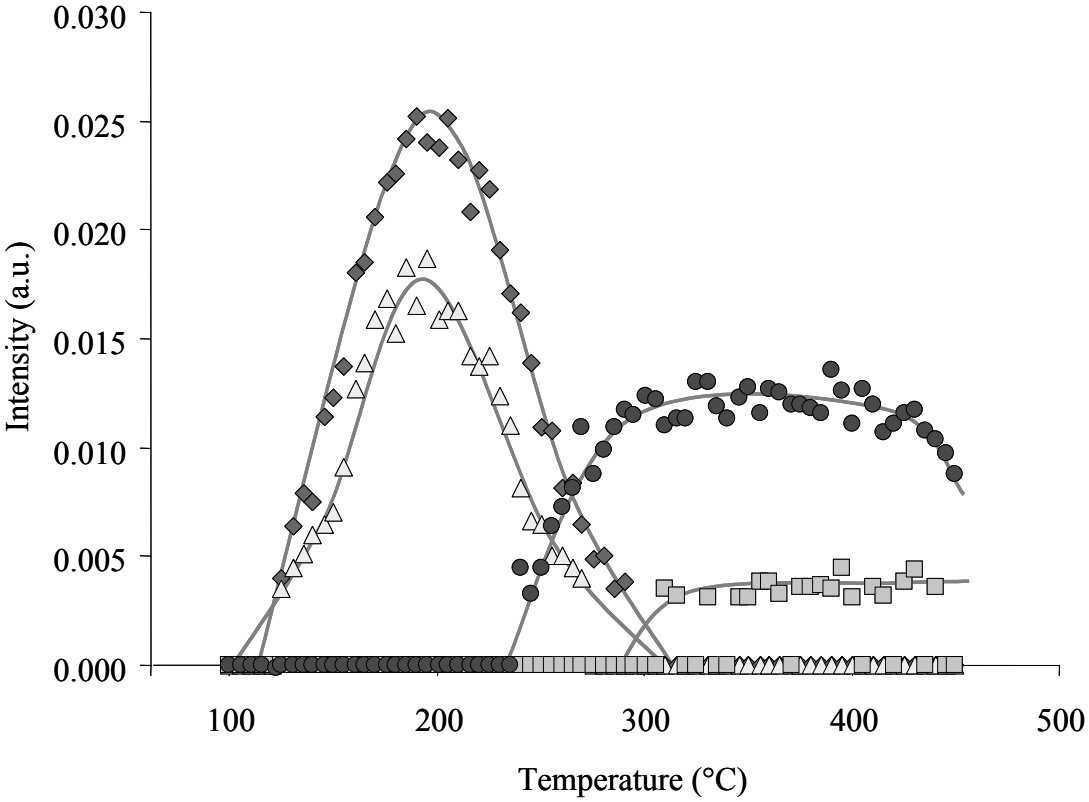

Figure 4-3: Temperature programmed desorption of hydrocarbons from deactivated La-X. ◆ Mass 83, △ Mass 85, □ Mass 115, Mass 119

The alkylation reaction was also simulated in an IR flow-cell. The sample was activated at 450°C in the cell in a stream of helium before a flow of a gaseous mixture of isobutane/2-butene (P/O = 6.7) was passed over the catalyst at 75°C. Immediately, the acidic hydroxyl-bands disappeared and the bands typical for hydrocarbons evolved. Although the flow was maintained for 75 minutes, the hydrocarbon band intensities reached a plateau after the first 10 minutes. Next, the sample was flushed with He for 180 minutes at 100°C. The spectrum after outgassing is compared with the spectrum of the deactivated La-X in Figure 4-4. The most notable differences between the two spectra are related to the fact that (i) the silanol band is still visible in the spectrum of the sample exposed to the alkylation reagents in the IR reactor and (ii) the bands in the 1500-1540 cm^{-1} region are missing in this spectrum.

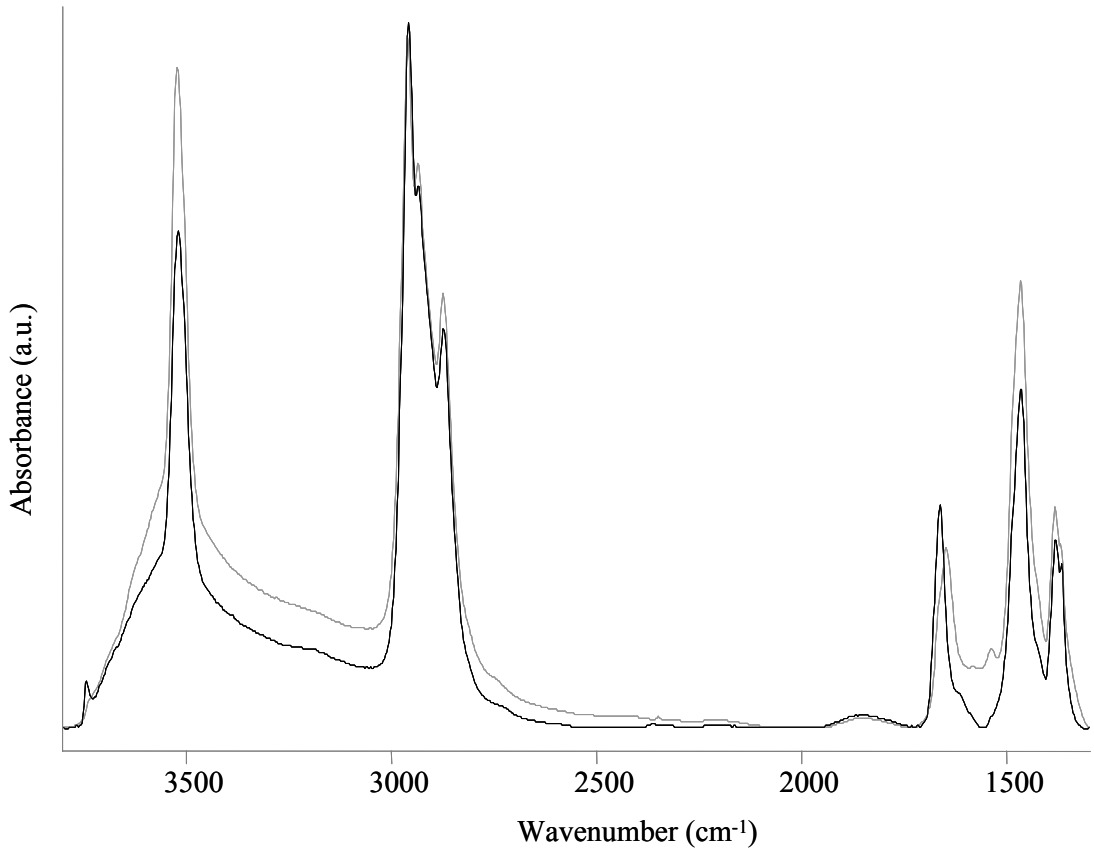

Figure 4-4: Comparison of the spectrum of deactivated La-X (gray) with the spectrum of simulated alkylation on La-X (black).

The remaining acidity of deactivated zeolites La-X and H-BEA was analyzed with pyridine adsorption at 100°C in the IR-cell. Prior to adsorption, the samples were outgassed at 100°C in vacuum for 2 hrs. In Figure 4-5, difference spectra of adsorbed pyridine on the fresh zeolites in comparison to the deactivated zeolites are shown. In both samples, pyridine could access a large fraction of the originally present Brønsted acid sites and a smaller fraction of the Lewis acid sites. Additionally, the hydrocarbon bands at 1650, 1530, 1505 and 1470 cm^{-1} were reduced in intensity after pyridine adsorption.

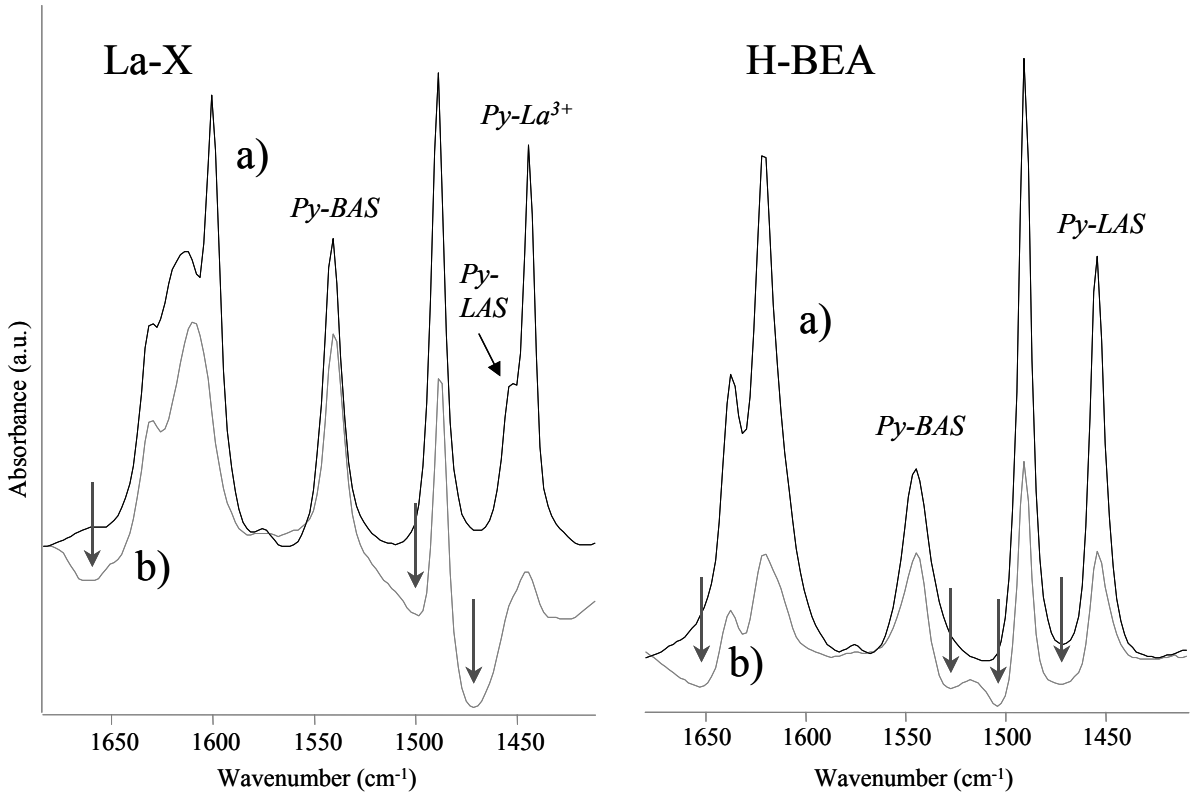

Figure 4-5: Difference spectra of adsorbed pyridine on La-X and H-BEA in a) fresh and b) deactivated state at 100°C. The arrows indicate the positions of the hydrocarbon bands, which were reduced in intensity upon adsorption of pyridine.

The deactivated zeolites La-X and H-BEA were also analyzed by nitrogen adsorption. Here, the fresh and used samples were pretreated at 120°C for 10 hrs in vacuum. Especially with the hydrophilic La-X, this is too low to completely remove the strongly sorbed water from the fresh sample, but most of the micropore area is accessible for nitrogen. After pretreatment at 400°C, a micropore volume of 0.16 ml/g was measured (see Table 4-1), and after pretreatment at 120°C a micropore volume of only 0.09 ml/g. The results are displayed in Figure 4-6. The micropores of the deactivated materials were completely blocked. Only a small fraction of the macro- and mesopores were accessible for N_2. It should be emphasized that although outgassing was done at a slightly higher temperature and for a longer time, N_2 (in contrast to pyridine) did not access the micropores.

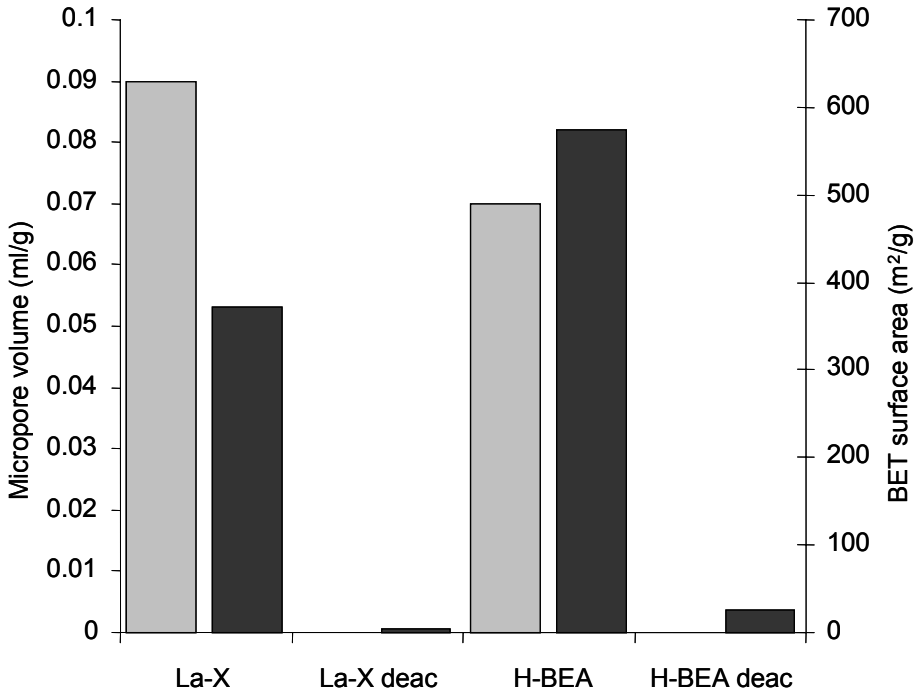

Figure 4-6: Nitrogen adsorption at 77 K on La-X and H-BEA, both in fresh and deactivated state. ☐ Micropore volume (left axis), ■ BET surface area (right axis).

4.3.4 Characterization of the recovered deposits

The recovered deposits gained from La-H-X alkylated at different temperatures were analyzed with UV/VIS spectroscopy. The results are compiled in Figure 4-7. Due to the unknown concentration and extinction coefficients of the individual compounds, the results are discussed only in qualitative terms. All spectra show a broad complex absorbance between 200 nm and 450 nm with three components at 200-205 nm, 235 nm, 250-260 nm and 310-320 nm. The energies strongly suggest the presence of π-electron systems in the deposits.

π-Electron systems of pure hydrocarbons, which absorb in this range, belong to single and conjugated double bonds or to C=C bonds in aromatic molecules. The breadth of the absorbance band suggests a high number of different but related species. The deposits recovered from the catalyst tested at 130°C, however, differed distinctively from the others. The absorbance at 235 nm, which is present in the other spectra only as a small shoulder, is the most prominent peak in the spectrum of the deposit from the reaction at 130°C.

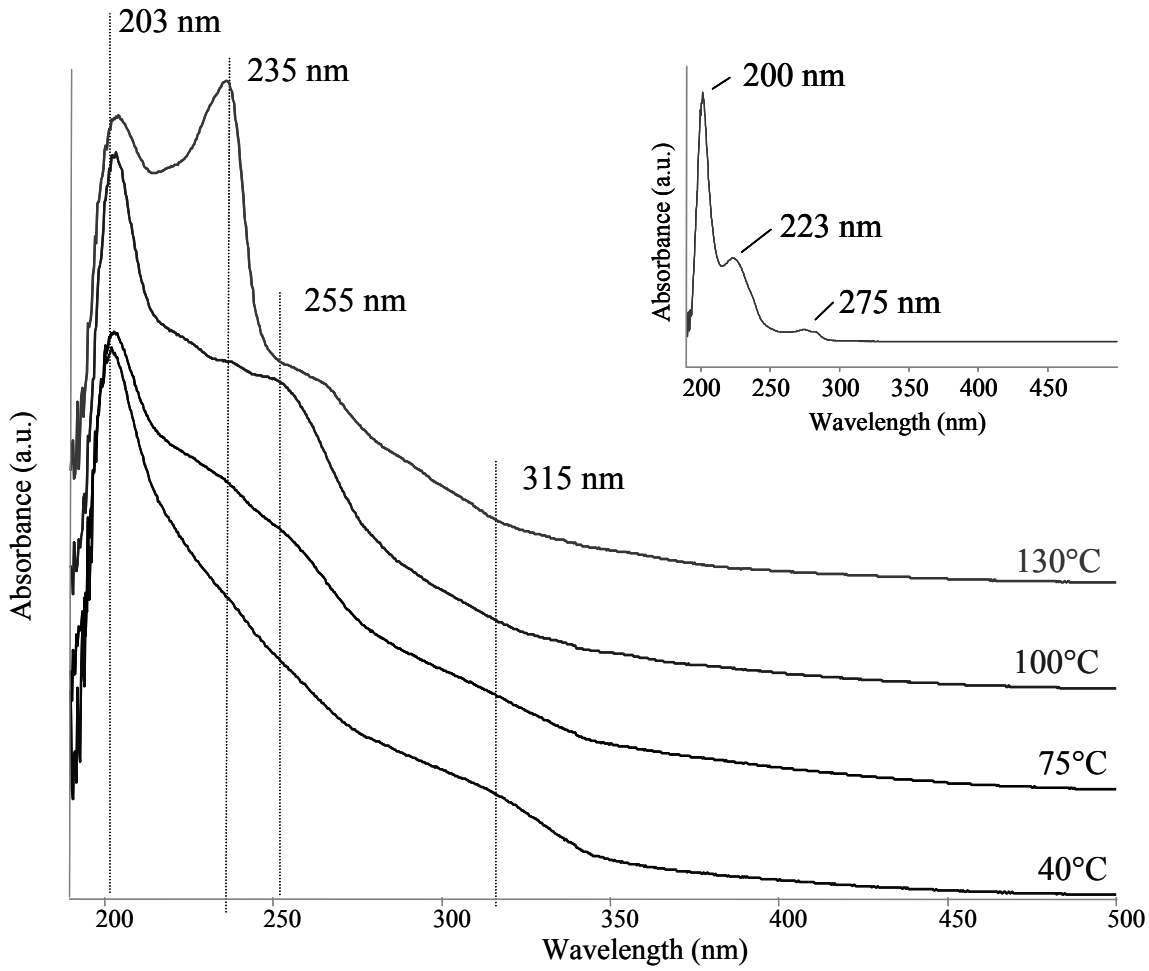

Figure 4-7: UV/VIS spectra of recovered deposits dissolved in hexane gained from alkylation runs of La-H-X at different reaction temperatures. Inset shows the UV/VIS spectrum of the heavy-end fraction of the alkylation product collected during the first 4 hrs TOS of a catalytic run with La-X.

Shown as an inset in Figure 4-7 is the UV/VIS spectrum of the heavy-end fraction of alkylate collected over the first 4 hrs time-on-stream with La-X as catalyst. During this period, the catalyst exhibited 100% butene conversion. Typically, only very small amounts of alkenes (especially octenes) are found in the products during the initial reaction phase. The integral selectivity of alkenes in the C_5-C_8 fraction is in the order of 0.2 wt.-%. Information on the concentration of unsaturated compounds in the C_{9+} fraction is not available. The UV/VIS spectrum revealed the presence of unsaturated and/or aromatic species. The spectrum shows sharper bands than that of the deposits suggesting a lower number of different compounds. Additionally, the product does not absorb at wavelengths above 300 nm.

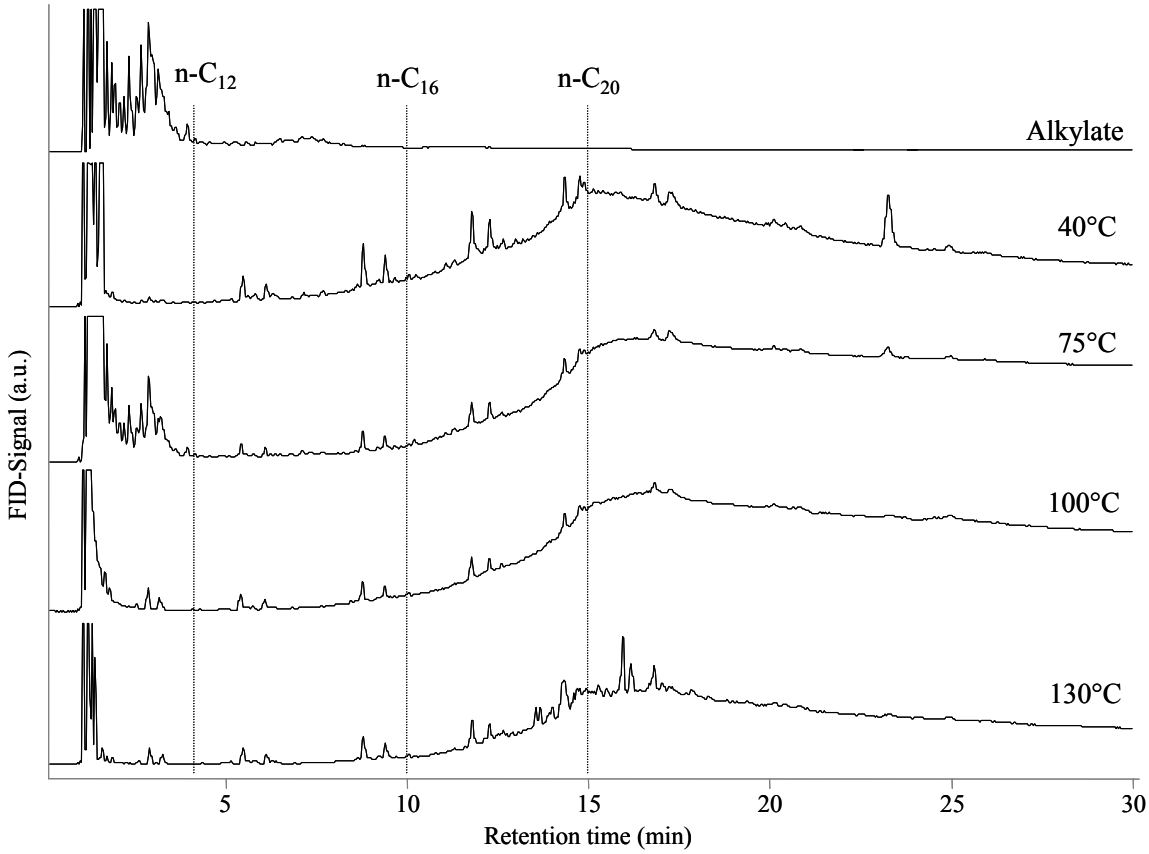

Figure 4-8: Chromatograms of the deposits recovered from La-H-X after alkylation at 40, 75, 100 and 130°C in comparison to the heavy-end fraction of the alkylation product from the run at 75°C. The dashed lines represent the retention times of dodecane, hexadecane and eicosan, respectively. GC program: 5min at 200°C, 10°C/min to 300°C, 15min at 300°C

The deposits were also analyzed by gas chromatography. In Figure 4-8 the chromatograms of certain deposits and a typical alkylate are compared. It can be seen that the deposits are similar in composition. The chromatogram of the deposit formed at 130°C exhibits additional peaks, which are not found in the other chromatograms. This is in accordance with the UV/VIS spectra, which are also similar except for the deposit formed at 130°C. The heavy-end fraction of the alkylate consists mainly of compounds between C_9 and C_{12}, with a minor amount of compounds up to C_{16}. The deposits contain a considerable fraction of higher boiling compounds and except for the deposit formed at 75°C only small amounts of compounds in the C_9-C_{12} region.

The GC-MS measurements of the deposits established the highly branched nature of the

deposits at all reaction temperatures. In many spectra the mass fragment 57 ($C_4H_9^+$) exhibited the highest peak. Independent of the reaction temperature, the compounds at higher retention times were more and more hydrogen deficient. The number of substituted benzene (evidenced by the mass fragments 77, 91 and 105) and condensed aromatic species (mass fragments 115 and 129, most likely containing no more than 3 rings) was very low in the deposit formed at 40°C, slightly higher in the deposit formed at 75°C and substantially higher in the deposit formed at 130°C. The reverse trend was seen for non-aromatic cyclic compounds containing 5- and/or 6-ring structures (discernible by the mass fragments 121, 123 and 124), which were more abundant in the deposits formed at 40°C and 75°C. Masses up to 490 m/z corresponding to C_{35} molecules were detected in all samples. Iso-alkane and alkene fragments were also detected in all samples, but in most of these spectra no molecular ion-peak was present.

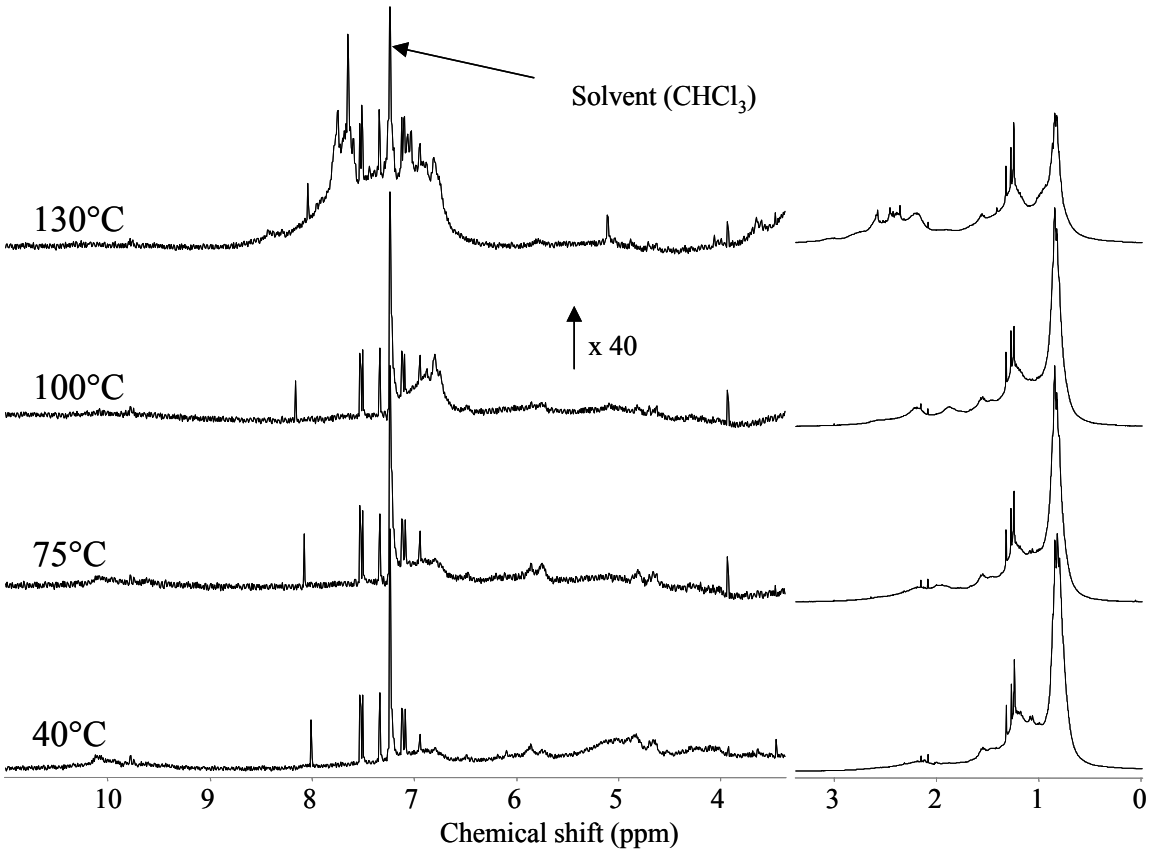

Figure 4-9: ^{1}H-NMR spectra of the deposits recovered from La-H-X after alkylation at 40, 75, 100 and 130°C.

Molecular ion-peaks found in the deposit formed at 40°C mainly belonged to C_nH_{2n-2} type compounds, to a lesser degree also to C_nH_{2n-4} and C_nH_{2n}. The deposit formed at 75°C exhibited C_nH_{2n-2} and C_nH_{2n-4} compounds and at higher retention times also C_nH_{2n-6} and C_nH_{2n-8}. The deposit formed at 130°C contained substances with markedly higher unsaturation, i.e., mainly C_nH_{2n-8}, some C_nH_{2n-6} and at higher retention times also C_nH_{2n-10} and C_nH_{2n-12}. Most of the molecular ion-peaks were found in the C_{18} – C_{30} region for all deposits.

The deposits formed at 40, 75, 100 and 130°C were also analyzed by ^{1}H-NMR spectroscopy. Additionally, two heavy-end fractions of reaction products were analyzed. One was accumulated over the first 4 hrs time-on-stream, the other over the whole reaction time including the deactivation phase. The NMR spectra of the deposits are displayed in Figure 4-9, those of the products in Figure 4-10.

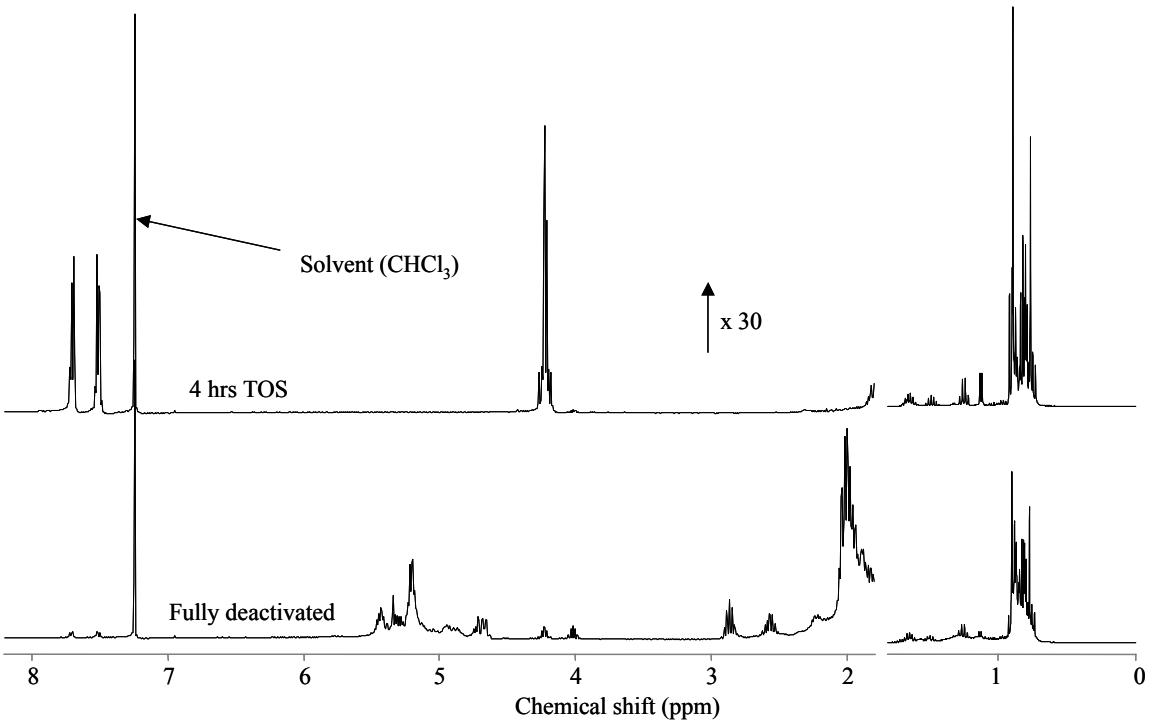

Figure 4-10: ^{1}H-NMR spectra of the heavy-end fractions of alkylates collected over the first 4 hrs TOS and after complete deactivation.

The peaks in each spectrum can be grouped to distinguish protons in different positions. This is only an approximate classification, because some of the functional groups overlap in

their chemical shifts, depending on the surrounding groups. The signal between 0 and 1.1 ppm, which was most abundant in all spectra, corresponds to protons in CH_3 groups in α position to saturated C atoms. Its contribution to the overall signal was significantly higher in the alkylate samples than in the deposits. Thus, we conclude that the degree of branching was higher in the product than in the deposits. The degree of branching in the product at early TOS was higher than that of the product collected during the whole run including deactivation. The degree of branching in the deposits also continuously decreased with increasing reaction temperature (the fraction of CH_3 protons decreased from 61% at 40°C to 33% at 130°C).

Signals between 1.1 and 1.4 ppm correspond to protons in CH_2 groups. No marked changes were seen in this group among the deposits (19 – 21%), whereas the product collected at early TOS showed only half the amount than the product collected during the whole run (6% and 14%). Signals between 1.4 and 1.7 ppm correspond to protons in CH groups in α position to saturated C atoms. With reaction temperature and reaction time the importance of this group increased (from 7% to 14% in the deposits and from 7% to 9% in the products).

Signals between 1.7 and 3.5 ppm represent protons in CH_3, CH_2 and CH groups in α position to unsaturated or aromatic carbon atoms. Due to the broad distribution of chemical shifts for these kinds of protons, a further classification within this range was not attempted. The number of protons in the deposits in this range increased steeply with reaction temperature (from 10% at 40°C to 30% at 130°C). Its contribution to the total number of protons in the products was much smaller (0.1% and 0.9%).

Protons of olefinic groups are found between 4 and 6.6 ppm. The deposits exhibited ill-resolved peaks in this range. Around 1.5% of all the protons in the deposits formed between 40 and 100°C were located at olefinic carbon atoms. The deposit formed at 130°C contained markedly less, only about 0.4%. The product collected during the complete run showed a broad absorption between 4.5 and 5.5 ppm. The product collected during the early reaction stage exhibited one sharp signal at 4.2 ppm. This peak most likely does not represent olefinic protons as will be discussed below.

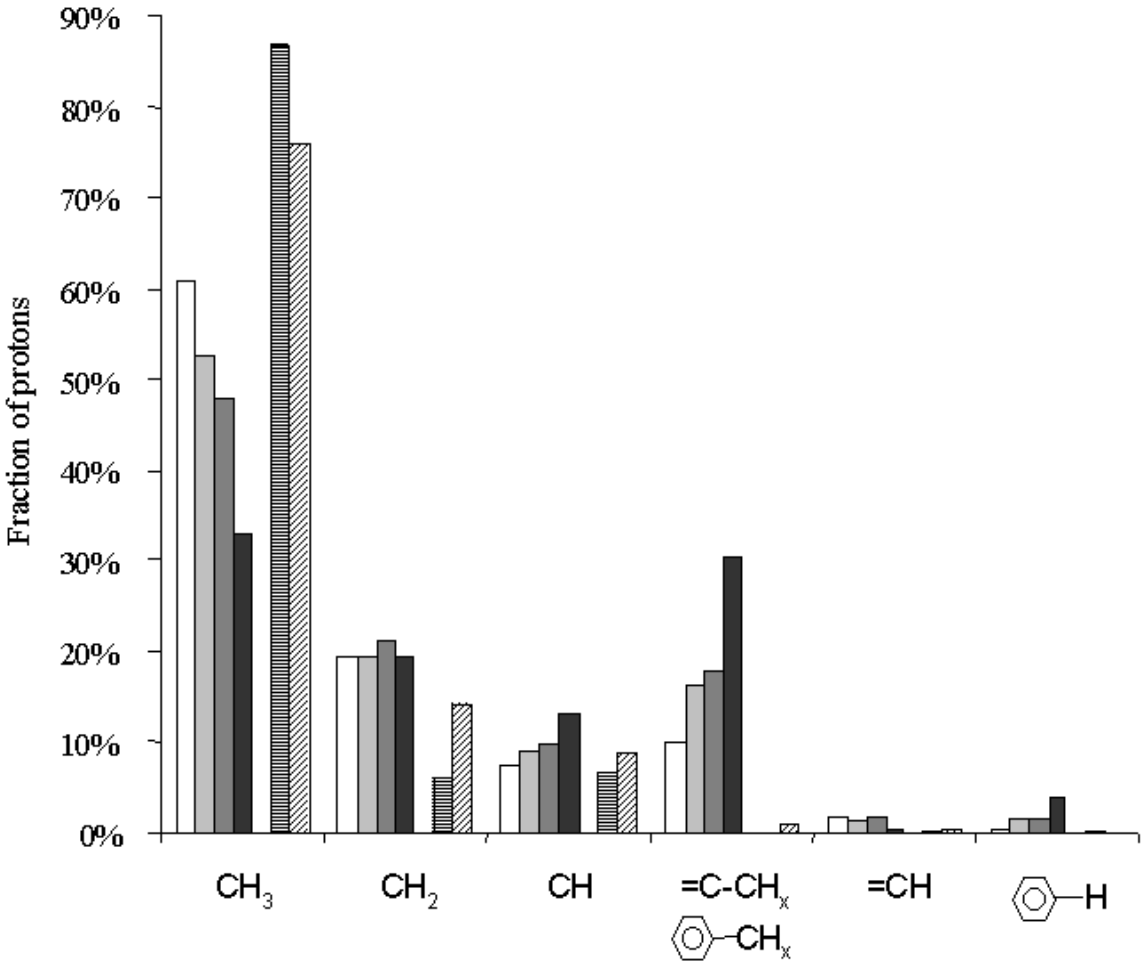

Figure 4-11: Fraction of protons in the individual positions obtained by the integration of the NMR-spectra in Figure 4- and Figure 4-. ☐ 40°C, ▒ 75°C, ▒ 100°C, ■ 130°C, ▤ product after 4 hrs TOS, ▨ product after complete deactivation.

Aromatic protons absorb in the range 6.6 to 9 ppm. All deposits showed signals in this range, but the amount steeply increased with increasing reaction temperature (from 0.5% at 40°C to 3.9% at 130°C). The products showed two sharp signals at 7.7 and 7.5 ppm, with a higher contribution in the product collected during the early reaction stage (0.2% and 0.04%). The signal at 4.2 ppm is proportional to them and is tentatively described to protons in a CH or CH_2 group connecting two aromatic rings. The lack of signals higher than 8.1 ppm in the spectra of the deposits formed from 40 to 100°C suggests the absence of condensed aromatic molecules with three or more rings. The deposit formed at 130°C might contain a small amount of these compounds. The number of protons in the deposits connected to carbon in α-positions of olefinic or aromatic double bonds is 5-7 times higher than the number of protons

within the double bonds. This demonstrates that these bonds are highly substituted.

Small contributions between 9.5 and 10.5 ppm seen in the low-temperature deposits were assigned to hydrogen in OH- or aldehyde-groups. These could possibly result from oxidation reactions after the deposit had been exposed to air. An overview about the importance of each class of protons in the deposits and products is presented in Figure 4-11.

The elemental analysis of the reaction products gave H/C ratios between 2.12 and 2.15, corroborating the almost pure paraffinic nature of the heavy-end alkylate.

4.3.5 MALDI-TOF mass spectrometry

Deactivated catalysts used in reactions at 40, 75 and 130°C were analyzed by MALDI-TOF MS employing DHB as matrix. The mass spectra are displayed in Figure 4-12. The samples from reactions at 40°C and 75°C resulted in very similar spectra. Both gave a clean Gaussian-curved distribution of masses with peaks in the mass range from 150 to 450 and a maximum between 235 and 291. A repetitive pattern was found within these samples. One prominent peak was always accompanied by a small peak one m/z higher and by a small peak two m/z below. This pattern was repeated every 14 m/z. This is a sign for each set being larger by a CH_2 group than the preceding set. For reasons not yet known, every forth of these sets exhibited a higher intensity than the Gaussian distribution. The main peaks based on the series 179 + 14*n*. Assuming the detected ions to be of the typical $[M + H]^+$ nature (which leads to uneven masses for hydrocarbons), this would correspond to molecules of a general C_nH_{2n-4} (three unsaturations or cycles) or C_nH_{2n-18} (*e.g.,* three condensed aromatic rings with alkyl side chains) formula. The matrix $[M + H]^+$ peak at 155 was nearly completely suppressed, which is typical for readily ionizable analytes (29). It is unlikely that non-aromatic molecules of the C_nH_{2n-4} formula exhibit such a high ionizability. Therefore, the molecules either are of the C_nH_{2n-18} type or contain heteroatoms such as oxygen.

The deactivated catalyst of the reaction at 130°C gave a different spectrum. The mass distribution had a maximum at 212 m/z and then followed the distribution of the other spectra with a second maximum at 268 m/z. The main peaks were based on the 184 + 14*n* series. At higher molecular weights, additional series developed, being 2 and 6 m/z lower than the main series. At molecular weights above 300, these peaks showed higher intensities than the main series. At m/z above 330, series being 4 and 8 m/z lower than the main series were seen. All these peaks represent *even* molecular masses in contrast to the MALDI spectra of the two

other samples. Assuming the detected masses to be radical cations, they represent molecules of the general formula C_nH_{2n-12}, C_nH_{2n-14} (or C_nH_{2n}) and C_nH_{2n-18} (or C_nH_{2n-4}). The C_nH_{2n-12} structures have the same molecular weight as alkanes. The occurrence of alkanes in the mass spectrum can be ruled out, because they cannot be ionized without the help of silver-cations, to which they form adducts (30). Simple olefins also should be difficult to ionize. It is more likely that the detected masses represent the general formulas C_nH_{2n-14} and possibly also C_nH_{2n-18} rather than C_nH_{2n-4}.

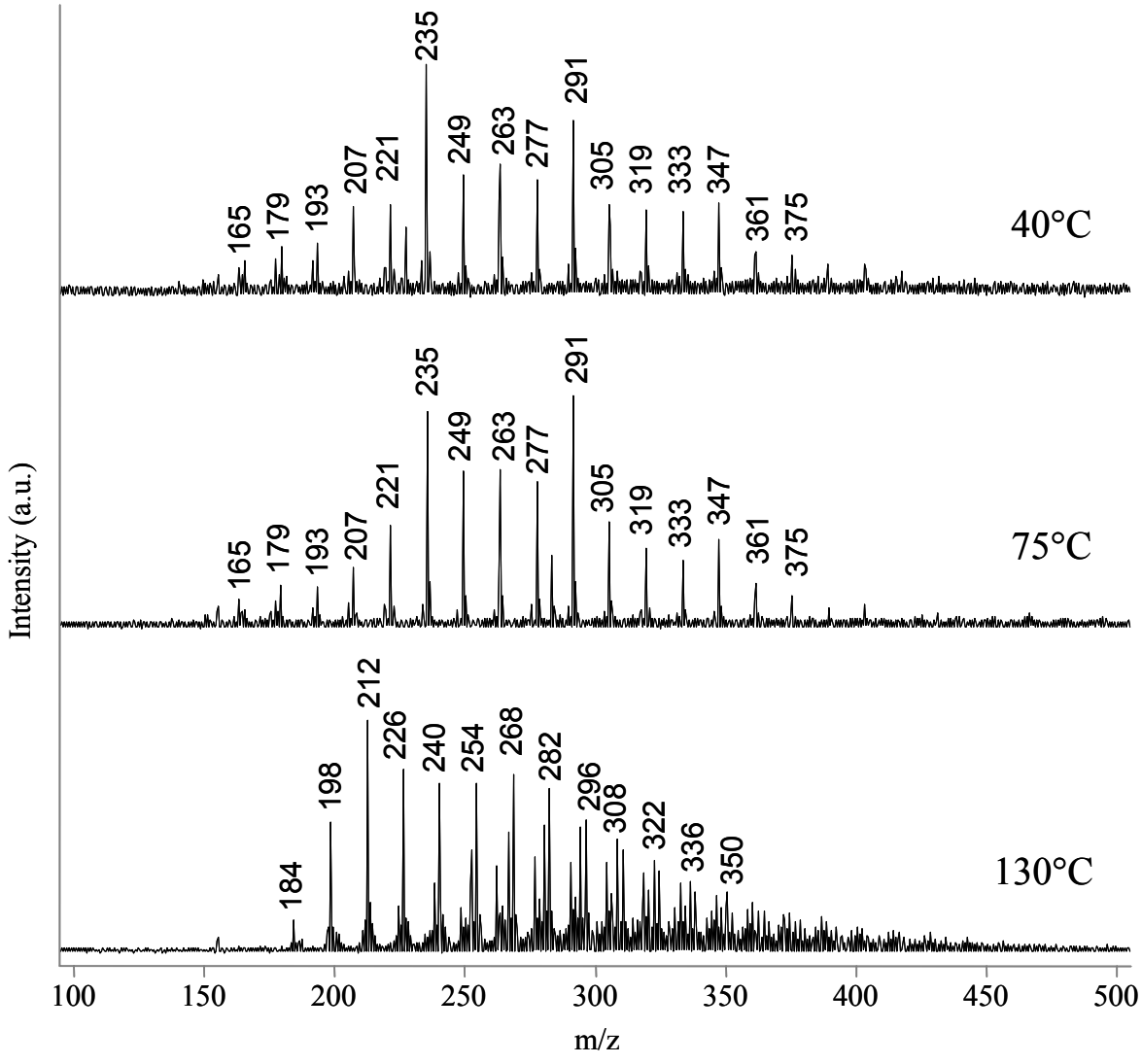

Figure 4-12: MALDI-TOF mass spectra of the deactivated catalysts used in reactions at 40, 75 and 130°C.

The LDI-TOF mass spectra of the deactivated catalysts used in reactions at 40, 75 and 130°C are displayed in Figure 4-13. The mass distributions of the recorded spectra resembled the distributions measured by MALDI-TOF MS. They were narrower but centered on a similar maximum. The main peaks in all spectra were *even* masses. In the mass spectra of the catalysts deactivated at 40 and 75°C the main peaks followed the 212 + 14*n* series, with smaller peaks 2 and 4 m/z below. They corresponded to the general formula C_nH_{2n-12}, C_nH_{2n-14} and C_nH_{2n-16} (or C_nH_{2n-2}), respectively.

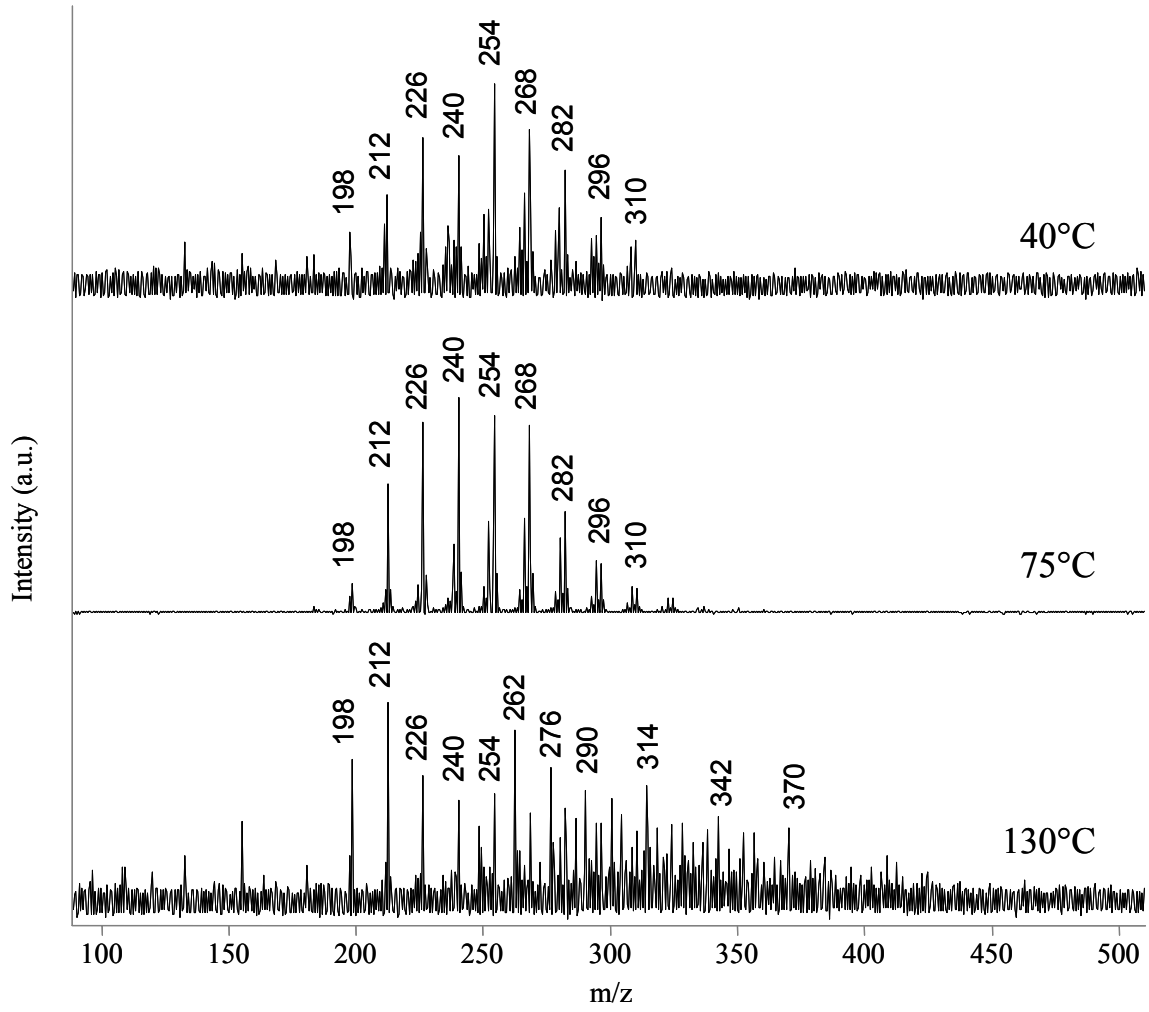

Figure 4-13: LDI-TOF mass spectra of the deactivated catalysts used in reactions at 40, 75 and 130°C.

The LDI-TOF mass spectrum of the catalyst deactivated at 130°C resembled the corresponding MALDI-TOF mass spectrum not only in the shape of the mass distribution

curve but also in the detected masses themselves. Up to 250 m/z, peaks of the C_nH_{2n-12} series dominated as in the MALDI-TOF spectrum and as in the two other LDI spectra. Between 250 and 300 m/z, C_nH_{2n-18} (or C_nH_{2n-4}) were the main peaks, which were replaced by the C_nH_{2n-22} (or C_nH_{2n-8}) series above 300 m/z. This last series was non-existent in the MALDI-TOF mass spectrum and in the other LDI-TOF mass spectra.

Typical MALDI spectra exhibit protonated molecular cations or analyte-cation adducts, the cation typically being Na^+ or K^+. For aliphatic hydrocarbons this should always lead to uneven masses. The molecules desorbing from the low-temperature deactivated catalysts followed this rule, the one deactivated at 130°C did not. Moreover, the MALDI spectrum of the high-temperature deactivated catalyst was similar to the LDI spectra of the deactivated samples. This suggests that the majority of the detected masses were not ionized by the interaction with the matrix, but, like in LDI, ionized by the laser beam. All types of species, except for the oxidation products, found in the low-temperature deposits are also found in the high-temperature deposit. For this reason it is postulated that MALDI selectively ionizes oxygen-containing compounds (polar heteroatom-containing hydrocarbons are much easier to ionize than non-polar pure hydrocarbons), which suppress the formation of other ions. In the absence of a matrix, only molecules with absorption in the region of the wavelength of the laser (λ = 337 nm) can be desorbed and ionized. The compounds are adsorbed on the zeolite surface and at least a fraction of them interacts strongly with the acid sites. It has been shown by Flego *et al*. that adsorbed species in deactivated zeolitic alkylation catalysts give rise to strong UV/VIS absorption bands between 300 and 400 nm assigned to alkenyl cations (6). Unsaturated carbenium ions have been extensively examined by Deno, who measured absorption bands in this range (25, 31). Flego *et al.* did not take into account that also aryl and benzenium cations exhibit absorption maxima between 300 and 400 nm (32). Exhibiting even masses in the LDI spectra, these ions obviously desorb as the radical cations of the corresponding olefinic and aromatic molecules.

LDI mass spectra of the deposits were also taken. This was unsuccessful for the deposits from the reactions at 40 and 75°C, in which ions were not detected. The deposit from the reaction at 130°C readily gave a mass spectrum, resembling the LDI spectrum of the deactivated catalyst. Masses of the formula C_nH_{2n-12}, C_nH_{2n-14} and C_nH_{2n-18} already seen in the deactivated samples were outweighed by masses of the formula C_nH_{2n-8} (or C_nH_{2n-22}) and C_nH_{2n-10} (or C_nH_{2n-24}). These results confirm the hypothesis that by LDI on the low-

temperature deactivated catalysts only unsaturated carbenium ions with sufficient absorption at 337 nm can be detected. None of these are present in the free deposits; therefore, no molecules are desorbed and ionized.

It is unclear at present why the deposit formed at 130°C led to the LDI peaks observed. The UV/VIS spectrum (see Figure 4-) did not show a significantly higher absorption at 337 nm than the other deposits. One possible explanation can be derived from studies by Macha *et al.*, who examined the behavior of several non-polar matrices (anthracene, acenaphthene and similar aromatics with two to four condensed rings and sufficient absorption at 337 nm) and analytes (with low absorption at 337 nm) under MALDI conditions. The matrices were found to ionize the analyte molecules only when the ionization energy of the analyte was lower than the ionization energy of the matrix. In this way, the analyte is ionized by charge transfer from the matrix giving a molecular radical cation (and not by proton addition) (33).

The unusual behavior of the high-temperature deposit is interpreted accordingly. The aromatic fraction of the deposit might contain a sufficiently large amount of molecules acting as matrices for compounds that otherwise would not be ionized due to lack of absorption at 337 nm. The same molecules in the low-temperature deposits with their significantly lower proportion of aromatics cannot be ionized because of the absence of suitable matrices.

Silver salts are frequently used to ionize alkanes and cycloalkanes by forming cation adducts in MALDI and LDI MS (21). The addition of $AgBF_4$ to the deactivated catalysts containing DHB as matrix only led to a considerable decrease in signal intensity without changing peak positions. No silver adducts were detected. Adding $AgBF_4$ to the deactivated catalysts without a further matrix, gave mass spectra, which contained the uneven masses seen in MALDI mode and the even masses observed in LDI mode. Also here no silver adducts were detected. Therefore, it is tentatively concluded that the silver salt or metallic silver (the silver salts readily decompose) acts as a matrix itself.

Fine metal or metal oxide powder has also been successfully employed as matrix for small molecule analysis leading to protonated or alkali-adduct ions (34). The matrix effect is weaker as with DHB, because the formation of “LDI-type ions” is not fully suppressed. The same was observed with the deposits. Mixing the low-temperature deposits with $AgBF_4$ gave the typical “MALDI-type ions” with strongly reduced signal intensity. The high-temperature deposit gave the same spectrum as without silver addition. Again, silver adducts were not detected.

The molecular weight distribution measured with MALDI and LDI MS gave the same maximum at 260 – 270 m/z. The LDI mass spectra were narrower than the MALDI spectra. MALDI gave masses between 150 – 450 m/z, LDI between 190 – 340 m/z and – 420 m/z for the catalyst deactivated at 130°C. The LDI mass spectrum of the deposit formed at 130°C had a distribution between 220 – 510 m/z. The maximum was also shifted to 314 – 328 m/z. Molecules at the lower end of the molecular weight distribution might evaporate in the UHV of the MALDI apparatus when not adsorbed on the zeolite, so that the maximum is seen at higher masses. Moreover, it is not known whether the mass distribution of the deposits changes significantly with the distance from the pore mouth. The laser can only desorb molecules on or close to the outer surface of the zeolite particles.

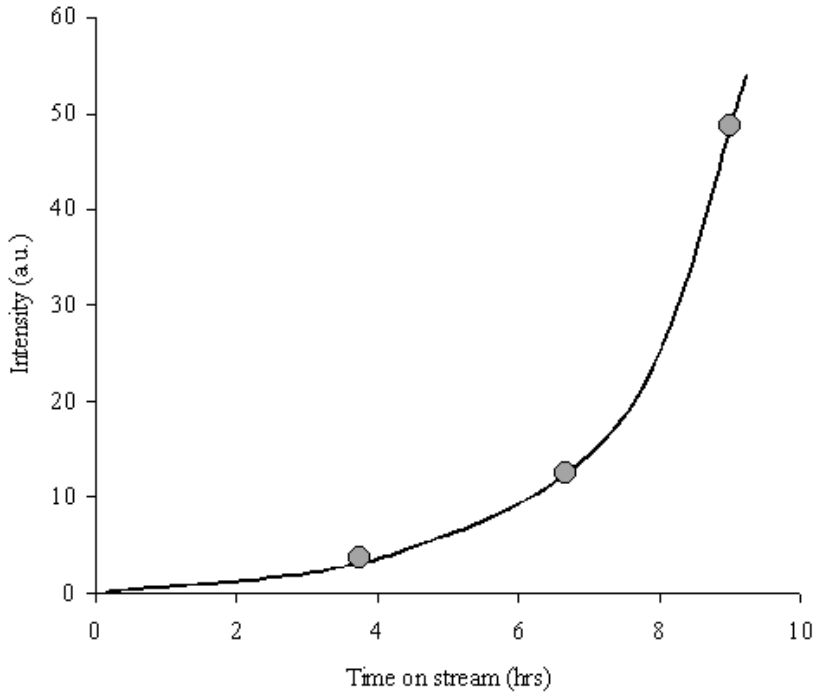

Figure 4-14: Signal intensity of MALDI-TOF mass spectra taken at different time-on-stream during reaction on La-H-X at 75°C.

During reaction on La-H-X at 75°C, catalyst-samples were withdrawn at 3.75 hrs, 6.7 hrs and 9 hrs TOS. These samples were analyzed by MALDI to examine the progress of catalyst deactivation. All three samples exhibited spectra similar to the one shown in Figure 4-12. The mass spectrum taken after 3.75 hrs TOS exhibited a maximum in the mass distribution, which

was approximately 50 m/z lower than the maxima of the spectra taken after 6.7 and 9 hrs TOS. With time-on-stream the signal intensity increased. While there was only a moderate increase up to 6.7 hrs TOS, it steeply increased when the catalyst reached the end of its active lifetime, see Figure 4-14.

4.4 Discussion

4.4.1 Chemical nature of the deposits

While MALDI/LDI (Figure 4-12 and Figure 4-13) gives information on the molecular mass distribution of the molecules in the deposits, NMR (Figure 4-9) and UV/VIS (Figure 4-7) (although to a lesser degree) give information on the structure of the molecules. GC-MS provides useful information on both the mass and the structure. A simple GC analysis (Figure 4-8) gives an estimate on the number (and boiling points) of the individual compounds in the deposit. UV/VIS and LDI clearly proofed that all deposits contained unsaturated species. However, both methods cannot detect saturated hydrocarbons. The significance of the unsaturated compounds can be estimated from NMR and GC-MS. Both these methods revealed an increase in the concentration of unsaturates as well as an increase in the degree of unsaturation with increasing reaction temperature. This increase was gradual at low to moderate temperatures and steep towards high reaction temperatures. However, at all reaction temperatures, the deposit is a complex mixture of alkanes, alkenes, non-aromatic cyclic and aromatic compounds, all of them with alkyl side chains. Polycyclic aromatics were found only at high reaction temperatures. MALDI, LDI and GC-MS gave for low to moderate temperatures a carbon number distribution in the range of C_{12}-C_{35}, with a maximum at about C_{20}. These numbers slightly shifted to higher values at high reaction temperatures.

Our detection of unsaturated species is in line with results obtained *via* mass spectrometry analysis of extracted coke performed by two different research groups (8, 9). C_{15} – C_{20} compounds with 2 – 4 unsaturations/cycles were found in the deposits. After hydrogenation, the general formula suggested a naphtenic structure with one or two five- and six-rings. UV/VIS data obtained by Flego *et al.* also confirmed the unsaturated nature of the deposits (6).

These unsaturated cyclic structures are very similar to the so-called conjunct polymers, which are by-products of sulfuric and hydrofluoric acid catalyzed alkylation reactions. The polymers are dissolved in the acid phase and are responsible for the acid consumption due to

the decrease of the acid strength (35, 36). The conjunct polymers were shown to be cyclic polyolefinic hydrocarbons with a high proportion of heteroannular-conjugated double bonds and numerous side chains (37).

4.4.2 Routes of formation of coke compounds

The deposits in alkylation often have been intuitively related to large saturated species that result from multiple alkylation and oligomerization of butenes and other alkenes formed during the alkylation reaction (4, 5, 7). The results presented here demonstrate that the products retained in the zeolite pores during isobutane/butene alkylation are complex and strongly vary with subtle variations in the reaction conditions. Only a fraction of the detected compounds originates from the typical alkylation reactions. The detected alkanes are products of multiple alkylation, similar to the heavy-end fraction of the reaction products. The molecules are probably too bulky to diffuse out of the pores. Alkenes found in the deposits are concluded to originate from alkoxides bound to the acid sites in the zeolite pores.

All other compounds have to undergo additional reactions. As a start, a large cation produced *via* multiple alkylation or oligomerization has to crack or deprotonate to form a large and branched alkene. This might transfer a hydride to another carbenium ion and, thus, form an alkenyl carbenium ion, which can desorb *via* proton transfer as a diene (Scheme 1). Further hydride transfer leads to a dienylic cation, which easily rearranges into an alkyl-substituted ring (Scheme 2) *via* a 1,5-cyclization and subsequent hydride and methyl shifts. Each step produces next to the ion also a saturated molecule (represented here as isobutane). Therefore, no true dehydrogenation step is involved.

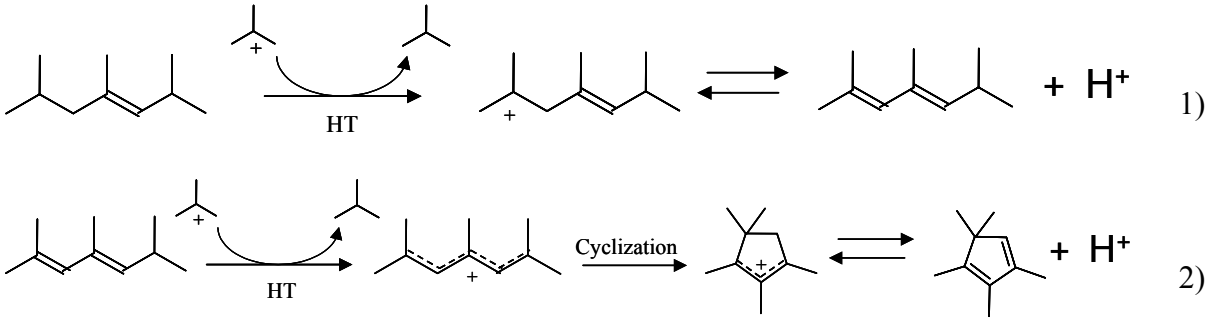

The formed cycloalkenyl carbenium ions, especially the cyclopentenyl cations, are very stable (25, 38) and have been observed as free cations in zeolites (39, 40). The occurrence of enylic cations was established by the IR-bands between 1540 and 1500 cm^{-1}. The same

reaction sequence is operative when absorbing alkenes in concentrated sulfuric acid. The alkenes disproportionate on the one hand into a layer of saturated hydrocarbons, on the other hand into highly unsaturated cyclic compounds dissolved in the acid phase, which turns a dark red color (41, 42).

Gas phase alkylation did not lead to the formation of alkenyl ions. This is seen in the absence of bands in the region 1500 – 1540 cm^{-1} in Figure 4-. We explain this with the lower concentration of reactants in the zeolite pores (gas phase *vs.* liquid phase) and the shorter total time-on-stream, which is backed up by the silanols still being visible in the spectrum of the gas phase alkylation sample. A similar behavior was observed by Kiricsi *et al.* (13). Adsorption of pure butene on La-BEA immediately led to the formation of alkenyl ions, while upon adsorption of a 1-butene/isobutane mixture the formation of alkenyl ions was strongly suppressed. The decelerating effect of isobutane on the deactivation mechanism is twofold: (i) a high concentration of isobutane (achieved by high P/O ratios in the feed stream and by backmixing the reactor contents) slows down the buildup of high molecular weight compounds, which are the precursors of the alkenyl ions. (ii) Isobutane competes in the hydride transfer step with the unsaturated compounds. A higher isobutane concentration will therefore inhibit the formation of enylic cations.

In liquid acids (25) and zeolites (43) at room temperature or below, alkenyl ions are the end product of such carbenium ion reactions. The situation changes at already moderately increased temperatures, as can be seen by the presence of aromatics in the deposits. A further deprotonation/hydride transfer step of a cyclohexenyl cation leads to a benzenium ion. The proton affinity of cyclohexadiene (837 kJ/mol) is significantly higher than the proton affinity of benzene (750 kJ/mol). Thus, a relatively high energy barrier has to be overcome to form the benzenium ion. This should lead to a high temperature-sensitivity for the formation of these ions. A steep increase in aromatic protons with reaction temperature as measured with ^{1}H-NMR confirms this hypothesis (see Figure 4-11). At low reaction temperatures, most ions are of aliphatic and naphtenic nature. Once the temperature is high enough, they are converted to aromatics. At even higher temperatures, polyaromatic compounds would be produced. The same trend is observed during the temperature programmed desorption of the adsorbed deposits (see Figure 4-3). Aromatics leave the zeolite pores only at temperatures above 200°C, condensed aromatics above 300°C. The desorption of aliphatic compounds has ceased completely at these temperatures. Since the deposit contains only a small amount of

aromatics, most of the desorbing products have to be produced *in situ* during the heating process. Performing the alkylation reaction at such high temperatures would give similar deposits as produced during the TPD (4). It has to be emphasized here, that the difference in the nature of the deposits at low and high reaction temperatures is not reflected in the product distribution. Alkylation products leaving the zeolite pores at low temperatures are the same as at high temperatures, although they exhibit considerably different selectivities. This is concluded from the product chromatograms exhibiting the same peaks in all runs. Alkylation at 130°C produces the same compounds as alkylation at 40°C, although the deposits (chromatograms shown in Figure 4-8) are significantly different.

The results presented in this study establish that only a fraction of the adsorbed species resembles the conjunct polymers formed in liquid acid catalyzed alkylation. On the one hand, they contain alkanes and mono-olefins; on the other hand, they contain aromatic fragments. Both are not found within the conjunct polymers. While the former are alkylation and oligomerization products, the appearance of the latter is a consequence of the substantially higher reaction temperature with zeolites.

4.4.3 Interaction of the coke molecules with the acid sites

The question remains how the catalysts deactivate. In principle, two mechanisms are possible. These are pore blocking and site blocking/poisoning. The first mechanism implies that bulky molecules of arbitrary chemical nature grow in the catalyst pores. When these molecules reach a certain critical size, they cannot diffuse out and block the pores by *physical* presence. The second mechanism requires the formation of a strong *chemical* bond between the adsorbate and the active site. To discriminate between the two mechanisms, the deactivated catalysts are analyzed by nitrogen and pyridine adsorption (see Figure 4-5 and Figure 4-6). The minute concentration of mesopores shows that under these conditions the pores are completely full. Nitrogen as a non-polar and non-basic molecule cannot enter the micropore system at all (at the rather low temperature of 77 K, at which the adsorbed molecules are very rigid). Pyridine as a strong base on the other hand can enter and even replace some adsorbed species, as seen in the formation of the pyridinium ion and the negative hydrocarbon bands.

A similar replacement has been described for zeolites coked in m-xylene transformation. Pyridine was found to replace a substantial amount of coke molecules. The authors observed

a concomitant decrease of hydrocarbon bands upon adsorption of pyridine. Bands at 1350, 1505, 1590 and 1600 cm^{-1} wavenumbers were found to decrease or disappear (44).

The theoretical description of this phenomenon was given by Song *et al.*, who studied the 1,3-dimethylcyclopentenyl carbenium ion ($C_7H_{11}^+$) adsorbed on H-ZSM-5. Coadsorption of basic molecules led to a deprotonation of the carbenium ion to form the neutral diene only when the employed base exhibited a proton affinity higher than the deprotonation enthalpy of the ion (45). Only those reactions will be thermodynamically favored, which produce more stable carbenium ions. Pyridine with its very high proton affinity of 930 kJ/mol can replace almost all carbenium ions. Hydride transfer from the most abundant hydride transfer agent isobutane (having a proton affinity of 678 kJ/mol) to a substituted cyclopentenyl ion (a corresponding parent, e.g. 1-methylcyclopentene having a proton affinity of 817 kJ/mol) to give a simple isobutyl ion (or alkoxide) should therefore be highly unfavorable. Thus, once an acid site is occupied by a cycloalkenyl ion, it is lost for the alkylation chemistry.

The steep increase in the MALDI signal intensity at the end of the active catalyst lifetime shown in Figure 4-14 can be interpreted in line with this reasoning: When a significant number of acid sites is deactivated by alkenyl ions the remaining sites experience a higher butene concentration, which speeds up the formation of further alkenyl ions. The deactivation therefore is auto-accelerated. This phenomenon is responsible for the sudden drop in conversion, which is often observed with solid acid alkylation catalysts.

H-BEA exhibited a similar behavior during pyridine and nitrogen adsorption. This material follows the same deactivation route as faujasitic catalysts. Differences arising from a different pore topology may be reflected in the lower CH_3/CH_2 ratio seen in the IR-spectra of the deactivated catalysts, as shown in Figure 4-1. The straight channels in zeolite BEA may not allow the same degree of branching that is possible in the more spacious supercages of faujasites.

Table 4-2 shows that the lifetime of La-H-X runs through a maximum at 75°C. At both low and high reaction temperatures the lifetime is significantly lower. Assuming the irreversible adsorption of alkenyl ions to be the only deactivating route, the lifetime should be highest at low temperatures and constantly decline with increasing temperature, because of the increasingly unsaturated nature of the deposits. To account for the short lifetimes at low reaction temperatures, we attribute this to the strongly hindered diffusion of bulky high molecular weight alkanes. With increasing temperature, diffusion will be facilitated, but the

increasing hydrogen deficiency of the molecules will bind them to the acid sites. Thus, the lifetime exhibits a maximum, at which the diffusion is sufficiently fast and the rate of formation of unsaturated compounds still slow.

Deactivated faujasitic alkylation catalysts typically contain 10 – 20 wt.-% hydrocarbon deposits (4, 8, 46). Assuming an average density for the deposits of 0.9 g/ml and a pore volume of 0.16 ml/g (see Table 4-1), roughly 15 wt.-% coke would fit in the pore system. This suggests that the pores of deactivated catalysts are completely filled. On the other hand, taking an acid site density of 0.6 mmol/g and an average molar mass of 250 g/mol for the molecules adsorbed on the acid sites, also gives a coke loading of ca. 15 wt.-%. It can be concluded from this that almost all hydrocarbons in the zeolite pores are adsorbed on the acid sites, but at the end of the catalyst-lifetime they completely fill the pore-system. Since a substantial fraction of these compounds can be replaced by pyridine, some of them obviously are not too bulky to leave the pores. However, their chemical interaction with the acid sites strongly retains them in the pores. These calculations also rule out the assumption that carbonaceous species might preferentially grow on the outside and simply block the entrance into the pore system.

4.5 Conclusions

During zeolite catalyzed isobutane/butene alkylation, which almost exclusively produces isoalkane products, a highly unsaturated and highly branched polymer is formed. The polymer strongly adsorbs on the acid sites and completely fills the pores at the end of the reaction. With increasing reaction temperature, the deposits are increasingly hydrogen deficient and are of increasingly aromatic nature. The deposits contain compounds, which are similar to the conjunct polymers formed during alkylation with liquid acids. However, zeolitic deposits additionally contain alkanes and aromatics, which are not present in conjunct polymers.

MALDI and LDI both gave spectra when applied on the deactivated catalysts. However, MALDI most likely selectively detected oxidized products. Ions absorbing in the wavelength region of the laser were detected in the LDI experiments. Some of the aromatic molecules present in the deposits might have acted as matrices for other compounds. Silver salt addition did not lead to the formation of silver cation adduction. Instead, silver acted as a matrix. The molecular weight distribution is in good agreement with the distribution measured by GC-

MS. However, the assignment of individual masses to certain types of compounds is still ambiguous. The interpretation of MALDI and LDI spectra should be of lesser complexity when used on catalysts with purely aromatic coke.

4.6 Acknowledgments

The author wishes to thank Süd-Chemie AG for providing several of the examined samples. Financial support from Süd-Chemie AG is gratefully acknowledged**.**

4.7 References

1. Corma, A. and Martinez, A., *Catal. Rev.-Sci. Eng.* **35**, 483 (1993).
2. Weitkamp, J. and Traa, Y., *in* "Handbook of Heterogeneous Catalysis" (G. Ertl, H. Knözinger, and J. Weitkamp, Eds.), Vol. 4, p. 2039. VCH, Weinheim, 1997.
3. van Broekhoven, E. H., Mas Cabre, F. R., Bogaard, P., Klaver, G., and Vonhof, M., U.S. Patent 5,986,158 (1999).
4. Weitkamp, J. and Maixner, S., *Zeolites* **7**, 6 (1987).
5. Stöcker, M., Mostad, H., and Rørvik, T., *Catal. Lett.* **28**, 203 (1994).
6. Flego, C., Kiricsi, I., Parker Jr., W. O., and Clerici, M. G., *Appl. Catal. A* **124**, 107 (1995).
7. Nowak, A. K., Mesters, C. M. A. M., Rigby, A. M., and Schulze, D., *Preprints, Div. Petr. Chem., Am. Chem. Soc.* **41**, 668 (1996).
8. Pater, J., Cardona, F., Canaff, C., Gnep, N. S., Szabo, G., and Guisnet, M., *Ind. Eng. Chem. Res.* **38**, 3822 (1999).
9. Schöllner, R. and Hölzel, H., *Z. Chem.* **15**, 469 (1975).
10. Yoo, K., Burckle, E. C., and Smirniotis, P. G., *Catal. Lett.* **74**, 85 (2001).
11. Diaz-Mendoza, F. A., Pernett-Bolano, L., and Cardona-Martinez, N., *Thermochim. Acta* **312**, 47 (1998).
12. Nivarthy, G. S., He, Y., Seshan, K., and Lercher, J. A., *J. Catal.* **176**, 192 (1998).
13. Kiricsi, I., Flego, C., and Bellussi, G., *Appl. Catal. A* **126**, 401 (1995).
14. Guisnet, M. and Magnoux, P., *Appl. Catal. A* **212**, 83 (2001).
15. Hanton, S. D., *Chem. Rev.* **101**, 527 (2001).
16. Fitzgerald, M. C. and Siuzdak, G., *Chemistry & Biology* **3**, 707 (1996).
17. Yang, M. and Reilly, J. P., *J. Phys. Chem.* **94**, 6299 (1990).

18. Zenobi, R. and Knochenmuss, R., *Mass Spectrom. Rev.* **17**, 337 (1998).
19. Kühn, G., Weidner, S., Just, U., and Hohner, G., *J. Chromatogr. A* **732**, 111 (1996).
20. Dutta, T. K. and Harayama, S., *Anal. Chem.* **73**, 864 (2001).
21. Pruns, J. K., Vietzke, J. P., Strassner, M., Rapp, C., Hintze, U., and König, W. A., *Rapid Commun. Mass Spectrom.* **16**, 208 (2002).
22. Borade, R. B. and Clearfield, A., *J. Phys. Chem.* **96**, 6729 (1992).
23. Feller, A., Guzman, A., Zuazo, I., and Lercher, J. A., *see chapter 3*, (2002).
24. Evans, J. C., *in* "Carbonium Ions" (G. A. Olah and P. R. Schleyer, Eds.), Vol. 1, p. 223. Interscience, New York, 1968.
25. Deno, N. C., *in* "Carbonium Ions" (G. A. Olah and P. R. Schleyer, Eds.), Vol. 2, p. 783. Interscience, New York, 1970.
26. Kiricsi, I. and Förster, H., *J. Chem. Soc. Faraday Trans.* **84**, 491 (1988).
27. Kiricsi, I., Förster, H., Tasi, G., and Nagy, J. B., *Chem. Rev.* **99**, 2085 (1999).
28. Eisenbach, D. and Gallei, E., *J. Catal.* **56**, 377 (1979).
29. Knochenmuss, R., Dubois, F., Dale, M. J., and Zenobi, R., *Rapid Commun. Mass Spectrom.* **10**, 871 (1996).
30. Ehlers, A. W., de Koster, C. G., Meier, R. J., and Lammertsma, K., *J. Phys. Chem. A* **105**, 8691 (2001).
31. Deno, N. C., Bollinger, J., Friedman, N., Hafer, K., Hodge, J. D., and Houser, J. J., *J. Am. Chem. Soc.* **85**, 2998 (1963).
32. Olah, G. A., Pittman, C. U., and Symons, M. C. R., *in* "Carbonium Ions" (G. A. Olah and P. R. Schleyer, Eds.), Vol. 1, p. 153. Interscience, New York, 1968.
33. Macha, S. F., McCarley, T. D., and Limbach, P. A., *Anal. Chim. Acta* **397**, 235 (1999).
34. Kinumi, T., Saisu, T., Takayama, M., and Niwa, H., *J. Mass Spectrom.* **35**, 417 (2000).
35. Albright, L. F., *Chemtech* **June 1998**, 40 (1998).
36. Albright, L. F., Spalding, M. A., Kopser, C. G., and Eckert, R. E., *Ind. Eng. Chem. Res.* **27**, 386 (1988).
37. Miron, L. and Lee, R. J., *J. Chem. Eng. Data* **8**, 150 (1963).
38. Sorensen, T. S., *in* "Carbonium Ions" (G. A. Olah and P. R. Schleyer, Eds.), Vol. 2, p. 807. Interscience, New York, 1970.

39. Nicholas, J. B. and Haw, J. F., *J. Am. Chem. Soc.* **120**, 11804 (1998).
40. Yang, S., Kondo, J. N., and Domen, K., *Catal. Today* **73**, 113 (2002).
41. Deno, N. C., Boyd, D. B., Hodge, J. D., Pittman, C. U., and Turner, J. O., *J. Am. Chem. Soc.* **86**, 1745 (1964).
42. Olah, G. A. and Olah, J. A., *in* "Carbonium Ions" (G. A. Olah and P. R. Schleyer, Eds.), Vol. 2, p. 715. Interscience, New York, 1970.
43. Förster, H. and Kiricsi, I., *Zeolites* **7**, 508 (1987).
44. Cerqueira, H. S., Ayrault, P., Datka, J., and Guisnet, M., *Microp. Mesop. Mater.* **38**, 197 (2000).
45. Song, W., Nicholas, J. B., and Haw, J. F., *J. Am. Chem. Soc.* **123**, 121 (2001).
46. Querini, C. A., *Catal. Today* **62**, 135 (2000).

5 General conclusions

The aim of this work was to examine the mechanism and the routes of deactivation of isobutane/butene alkylation on faujasitic zeolites. It could be shown that hydride transfer from isobutane is a very sensitive step regarding the acid properties of the tested materials. Hydride transfer affects the selectivities to primary and equilibrium products, the self-alkylation activity and most important the lifetime of the catalysts *via* a slowing down of multiple alkylation and oligomerization, the products of which are the precursors of the molecules that finally deactivate the catalyst. Strong acid sites are a prerequisite for high hydride transfer activity. However, super-acidic sites do not seem to be beneficial, as they lead to excessive cracking.

Weak Brønsted acid sites are detrimental for the catalytic performance, because they only catalyze oligomerization, which leads to the formation of coke precursors and hence to faster catalyst deactivation. Lewis acid sites may (in ultra-stable zeolites) increase the strength of neighboring Brønsted acid sites, but they clearly have a negative effect on lifetime and selectivities. They increase the concentration of alkenes at Brønsted acid sites in the vicinity and they may lead to an increased formation of alkenyl ions *via* proton abstraction from alkenes.

It could be shown that the catalysts follow the same deactivation pathway as the liquid acids. A highly unsaturated polymer is built up, which strongly binds to the acid sites in the form of stable carbenium ions, which cannot be removed *via* hydride transfer from isobutane, because the proton affinity of the corresponding free hydrocarbons is much higher than the proton affinity of isobutane. Owing to the microporous nature of zeolites, the rate of deactivation is further increased by a slow diffusion of bulky molecules stemming from multiple alkylation and oligomerization. At low reaction temperatures, these molecules lead to deactivation through pore blocking.

The importance of hydride transfer from compounds other than isobutane, especially from unsaturated molecules, has long been neglected. This class of reactions is responsible for the formation of multiply unsaturated compounds. Although isobutane is available in much higher concentrations, the competing hydride transfer from unsaturated molecules seems to be surprisingly fast and cannot be fully suppressed. The only way to slow down this process is to prevent the build up of the precursor oligomers.

It is, however, possible to remove these compounds after they have been formed. A hydrogenative regeneration, which is the method of choice in all true solid acid catalyzed alkylation process developments, has been shown successful in removing these unsaturated species from the catalyst surface.

All findings taken together, faujasites with a high framework and a low extraframework aluminum concentration are suitable alkylation catalysts. They can be operated under severe conditions without major losses in alkylate quality. The total turnover number per site is higher than that of sulfuric acid. Moreover, regeneration with hydrogen seems a feasible method to extend the catalyst lifetimes in a way that a process development based on faujasites can be competitive with the existing processes.

6 Summary

In this thesis, the isobutane/2-butene alkylation was studied on lanthanum-exchanged zeolite X in a CSTR-type slurry reactor. Catalysts with a high concentration of strong Brønsted acid sites and a high Brønsted to Lewis acid site ratio exhibited higher active catalytic lifetimes than samples with lower ratios. Isobutane self-alkylation activity was also increasing with increasing Brønsted/Lewis ratio. The integral productivity of the catalysts was found to be independent of the butene space velocity. The catalysts deactivated by the buildup of highly unsaturated polymers, which strongly adsorbed on the acid sites and blocked them for further reactions. With increasing reaction temperature, the deposits were increasingly aromatic.

7 Zusammenfassung

Die Isobutan/2-Buten Alkylierung wurde an Lanthan ausgetauschtem Zeolith X in einem Rührkesselreaktorsystem untersucht. Katalysatoren mit hoher Konzentration an starken Brønsted-Säurezentren und hohem Brønsted/Lewis Säurezentrenverhältnis zeigten eine längere katalytische Lebensdauer als Proben mit niedrigem Verhältnis. Die Isobutan Selbstalkylierungsaktivität stieg mit zunehmendem Brønsted/Lewis Verhältnis ebenfalls an. Die integrale Produktausbeute der Katalysatoren war unabhängig von der Buten-Raumgeschwindigkeit. Die Katalysatoren deaktivierten durch den Aufbau von ungesättigten Oligomeren, die fest an den Säurezentren adsorbiert waren und diese für weitere Reaktionen blockierten. Mit zunehmender Reaktionstemperatur stieg die Aromatizität der Katalysatorablagerungen.